

In Vitro Selection, Characterization, and Application of a Sodium-Dependent
DNAzyme and a Metal-Independent Ribozyme

by

Lingzi Ma

A thesis

presented to the University of Waterloo

in fulfilment of the

thesis requirement for the degree of

Doctor of Philosophy

in

Chemistry

Waterloo, Ontario, Canada, 2021

© Lingzi Ma 2021

Examining Committee Membership

The following served on the Examining Committee for this thesis. The decision of the Examining Committee is by majority vote.

External Examiner

Dr. Dipankar Sen

Professor, Department of Molecular Biology & Biochemistry
Simon Fraser University, Burnaby, Canada.

Supervisor

Dr. Juewen Liu

Professor, Department of Chemistry,
University of Waterloo, Waterloo, Canada.

Internal Member

Dr. John Honek

Professor, Department of Chemistry,
University of Waterloo, Waterloo, Canada.

Internal Member

Dr. Thorsten Dieckmann

Associate professor, Department of Chemistry,
University of Waterloo, Waterloo, Canada.

Internal Member

Dr. Richard Manderville

Associate professor, Department of Chemistry,

University of Guelph, Guelph, Canada

Internal- External Examiner Dr. Kesen Ma

Associate professor, Department of Biology,

University of Waterloo, Waterloo, Canada.

Author's Declaration

“This thesis consists of material all of which I authored or co-authored: see Statement of Contributions included in the thesis. This is a true copy of the thesis, including any required final revisions, as accepted by my examiners.

I understand that my thesis may be made electronically available to the public.”

Statement of Contributions

The work presented in this thesis is the result of work performed by the author and several scientific collaborations. Contributions from each scientist and the resulting publications are listed in detail below.

The work in Chapter 2 has been published as: Ma, L.; Liu, J., An *in vitro* selected DNAzyme mutant highly specific for Na⁺ in slightly acidic conditions. *ChemBioChem* **2019**, *20* (4), 537-542. All the work in this chapter was performed by the author.

The work in Chapter 3 has been published as: Ma, L.; Kartik, S.; Liu, B.; Liu, J., From general base to general acid catalysis in a sodium-specific DNAzyme by a guanine-to-adenine mutation. *Nucleic Acids Research* **2019**, *47* (15), 8154-8162. Sanjana Kartik provided assistance on DNAzyme kinetics assays and gel electrophoresis. Biwu Liu provided assistance on mathematical analysis. Other work presented in this chapter was performed by the author.

The work in Chapter 5 has been accepted as: Ma, L.; Huang, Z.; Liu, J., Selection of a self-cleaving ribozyme activated in chemically and thermally denaturing environment. *Chemical Communications* **2021**, *57* (62), 7641-7644. Zhicheng Huang provided assistance on *in vitro* transcription assays and gel electrophoresis. Other work presented in this chapter was performed by the author.

Abstract

Ribozymes and DNAzymes are collectively called catalytic nucleic acids. Compared to protein enzymes, catalytic nucleic acids are programmable in structure, easy to synthesize or modify, and more chemically stable especially for DNA. In particular, many RNA-cleaving DNAzymes display excellent activities and specificities to metal ions, making them attractive for metal ion sensing. In recent years, several Na^+ -dependent DNAzymes have been reported, indicating DNA catalysis without divalent or trivalent metal ions directly involved in the reaction. In Chapter 1, I reviewed the current state-of-the-art of the field, and provided the relevant background information regarding to catalytic nucleic acids.

In Chapter 2, a new Na^+ -dependent DNAzyme, NaH1, was selected under a relatively acidic condition, which turned out to be a variant of a previously reported DNAzyme, NaA43. Compared to other competing monovalent ions, NaH1 also displays an excellent specificity for sodium. At low Na^+ concentrations, the selected DNAzyme exhibited a higher cleavage rate than NaA43 and thus a tighter binding affinity. Thus, the NaH1 DNAzyme was engineered into a fluorescent Na^+ biosensor by labeling a fluorophore/quencher pair. Preliminary work on detecting Na^+ in serum matrix was demonstrated as well. This study provides a useful mutant that works in a slightly acidic environment, which might be useful for sensing Na^+ in acidic intracellular environment.

The NaA43 and NaH1 DNAzymes share the same 16-nt Na^+ -binding motif but differ in one or two nucleotides in a small catalytic loop. Nevertheless, they display an opposite pH-dependency, implicating distinct catalytic mechanisms. In Chapter 3, rational mutation studies demonstrated conserved nucleotide residues in these DNAzymes. The pH-rate profiles using pK_a -

perturbed analogs further revealed their distinct general acid-base mechanisms. Further experiments with 2AP modifications and PS-modified substrates provided more insights into the active site. This is an interesting example where single point mutations shift the mechanism of cleavage from general base to general acid, and it can also explain this Na⁺-dependent DNAzyme scaffold sensitive to a broad range of metal ions and molecules.

The Na⁺-dependent DNAzymes do not require multivalent metal ion for catalysis and can fold into well-defined structures. Thus, they provided an excellent platform for studying the metal ion effect at the cleavage site. In Chapter 4, I used them as models to explore the role of Pb²⁺ in RNA cleavage which has been frequently observed. By examining the Pb²⁺ effect in several representative DNAzymes, the capability of Pb²⁺ to bind specifically to the cleavage site has been demonstrated. Upon binding, the hydrated Pb²⁺ can serve as a poor general acid and facilitate the RNA cleavage. In a special case, Pb²⁺ can facilitate the binding of Ca²⁺ cofactor and significantly enhance the activity of a Ca²⁺-dependent DNAzyme. The mechanism study on Pb²⁺ activity further revealed versatile roles of Pb²⁺ in RNA cleavage which is important for understanding DNAzyme catalysis. This could also provide insights in rational design of catalytic DNA or RNA with desired cleavage activity.

Given the excellent Na⁺-binding selectivity of DNAzymes, a natural question is whether similar ribozymes exist. In the last chapter, I further performed *in vitro* selection to search for Na⁺-dependent self-cleaving ribozymes. Surprisingly, a novel ribozyme was obtained displaying a site-specific cleavage activity under denaturing conditions, such as high temperatures, denaturing solvents, and low salt concentrations. Most importantly, unlike other self-cleaving ribozymes, divalent metal ions do not contribute to the catalysis but suppress its cleavage. Together, I proposed that both denaturants and temperatures facilitate a conformational change favorable to the cleavage

activity. In addition, BLAST was applied in searching its natural analogs among genomes. Interestingly, its conserved motif was founded in several extremophilic bacteria. This work further broadened the horizon of catalytic RNAs functioning under extreme environments, and thus provided another strong support for the RNA world hypothesis.

Acknowledgements

I would like to express my heartfelt gratitude to my supervisor, Dr. Juewen Liu, for his warm-hearted encouragement and invaluable guidance in the past six years. Thank you for providing me research opportunity and creating a positive and enjoyable environment. As a supervisor, he is always patient, humble, precise, and conscientious. I feel lucky to join his group early when I was an undergraduate student, since his passion and commitment to scientific research greatly inspired me. The time I spend in his laboratory will always be one of the most valuable experience in my life. I would also like to express the deepest and sincere appreciation to my committee members: Dr. John Honek, Dr. Thorsten Dieckmann, and Dr. Richard Manderville for their generous advice and time given to evaluate my research project. I would like to thank my external examiner, Dr. Dipankar Sen, and my internal-external examiner, Dr. Kesen Ma, for the time and efforts in attending my Ph.D. thesis oral examination. In addition, I would like to acknowledge Cathy van Esch, Lisa Pokrajac, and Dr. Richard Smith for their kind guidance and support.

My sincere thanks also go to every group member in the Liu lab I have once worked with: Dr. Biwu Liu, Zhicheng Huang, Yuqing Li, Mohamad Zandieh, Dr. Po-Jung Jimmy Huang, Dr. Runjhun Saran, Dr. Wenhui Zhou, Dr. Zijie Zhang, Dr. Yibo Liu, Anand Lopez, Yichen Zhao, Jennifer Moon and many others. Thanks to everyone for bring kindness, inspiration, and positive energy to work and to my daily life. It has been my great honor to work with you all!

I would also like to thank my family and friends especially my mother for always believing in me and encouraging me. Her faith and strength have tremendous influence in shaping me to an independent woman. I am also extremely grateful for the unconditional love and company from

Kyu Bin and my furry friend, Mochi. Last but not least, I would like to thank University of Waterloo, the Natural Sciences and Engineering Research Council (NSERC) of Canada, Canadian Institutes of Health Research (CIHR), and the Department of Chemistry for financial support and all the research equipment.

Dedication

I would like to dedicate this thesis to my family for their love and support.

Table of Contents

Examining Committee Membership	ii
Author's Declaration	iv
Statement of Contributions	v
Abstract.....	vi
Acknowledgements	ix
Dedication	xi
Table of Contents	xii
List of Figures.....	xvi
List of Tables	xxiii
List of Abbreviations	xxiv
Chapter 1. Introduction to Catalytic Nucleic Acids	1
1.1 Chemical structure of nucleic acids	2
1.2 An overview on catalytic nucleic acids	5
1.3 Ribozymes in the early days	6
1.4 Ribozymes for therapeutic applications	9
1.5 RNA-cleaving DNazymes	11
1.5.1 DNazymes for gene-silencing in cells	12
1.5.2 Representative metal-dependent DNazymes	13
1.5.3 <i>In vitro</i> selection for DNazymes.....	15

1.5.4	DNAzymes for metal sensing	17
1.6	Metal ions in DNA catalysis	18
1.6.1	Metal binding sites in nucleic acids	19
1.6.2	Metal ions in RNA cleavage reaction	22
1.6.3	Methods to study metal binding sites	25
1.7	Na⁺-dependent RNA-cleaving DNAzymes	28
1.7.1	The NaA43 DNAzyme	29
1.7.2	Identify the Na ⁺ -binding domain	31
1.7.3	The EtNa DNAzyme	32
1.8	Research focus	33
Chapter 2. An <i>In Vitro</i> Selected DNAzyme Mutant Highly Specific for Na⁺ in Slightly Acidic Conditions		35
2.1	Introduction	35
2.2	Results and discussions	36
2.2.1	<i>In vitro</i> selection	36
2.2.2	Sequence analysis	38
2.2.3	Biochemical characterization	42
2.2.4	A Na ⁺ biosensor	46
2.3	Summary	49
2.4	Materials and methods	50
2.4.1	Oligonucleotides and chemicals	50
2.4.2	<i>In vitro</i> selection	51
2.4.3	Deep sequencing	52
2.4.4	Activity assays	52

2.4.5	Fluorescence-based Na ⁺ sensing.....	53
-------	---	----

**Chapter 3. From General Base to General Acid Catalysis in a Sodium-Specific DNAzyme
by a Guanine-to-Adenine Mutation 55**

3.1	Introduction	55
3.2	Results and discussions	56
3.2.1	The NaA43 and NaH1 DNAzymes	56
3.2.2	Rational evolution from NaA43T to NaH1	58
3.2.3	The A22 in NaH1 is highly conserved	59
3.2.4	pH-rate profiles.....	60
3.2.5	Base analogs further probing catalytic mechanism	63
3.2.6	Phosphorothioate substitution and metal rescue	66
3.3	Summary	70
3.4	Materials and methods.....	71
3.4.1	Oligonucleotides and chemicals	71
3.4.2	Activity assays.....	72
3.4.3	Phosphorothioate substitution.....	73
3.4.4	Fluorescence spectroscopy.	73
3.4.5	Sample preparation for mass spectrometry.....	74

Chapter 4. Explore the Ubiquitous Activity of Lead (II) Ion in RNA-Cleaving DNAzymes75

4.1	Introduction	75
4.2	Results.....	78
4.2.1	Distinct Pb ²⁺ effects on sodium DNAzymes	78
4.2.2	Pb ²⁺ -induced cleavage in the Ce13d DNAzyme.....	81
4.2.3	Pb ²⁺ -enhanced cleavage activity in the EtNa DNAzyme.....	84

4.3	Discussion	89
4.4	Summary	94
4.5	Materials and methods.....	94
4.5.1	Chemicals	94
4.5.2	Activity assays.....	94
	Chapter 5. <i>In Vitro</i> Selection of A Self-Cleaving Ribozyme Activated in Chemically and Thermally Denaturing Environment	96
5.1	Introduction	96
5.2	Results and discussion.....	97
5.2.1	<i>In vitro</i> selection of self-cleaving ribozymes.....	97
5.2.2	Formamide and high temperature enhance cleavage	102
5.2.3	Divalent metal ions inhibit cleavage.....	106
5.2.4	Effect of other solvents.....	108
5.2.5	Searching ribozyme sequence in nature	110
5.3	Summary	112
5.4	Materials and methods.....	113
5.4.1	Oligonucleotides and chemicals	113
5.4.2	<i>In vitro</i> selection	114
5.4.3	Sequencing sample preparation	116
5.4.4	Characterization of cleavage activity.....	116
	References.....	118

List of Figures

Figure 1.1 The chemical structure of nucleotides and five nucleobases including two purines (A, G) and three pyrimidines (C, T, U).....	2
Figure 1.2 Watson-Crick base pairs (A•T and G•C) in DNA and a sugar–phosphate backbone with 5'-to-3' phosphodiester bonds.....	3
Figure 1.3 The unperturbed pK_a values of nucleobases and ionization sites. ¹³	5
Figure 1.4 Comparisons on the number of publications (A) and citations (B) from 1995 to 2020 with “ribozyme” and “DNAzyme” or “deoxyribozyme” as keywords.....	5
Figure 1.5 (A) The peptidyl transferase activity of the ribosomal RNA during a peptide bond formation. (B) The minimal secondary structure of the hammerhead ribozyme containing 13 conserved nucleotides Redrawn from ref 33. (C) The cleavage of a 3', 5'-phosphodiester bond catalyzed by self-cleaving ribozymes.....	8
Figure 1.6 (A) Trans-cleaving ribozymes for gene-silencing. (B) Intracellularly selected hammerhead ribozymes with enhanced cleavage activity in living cells. Spinach is a report RNA that binds with a small molecule, DFHBI, and emits fluorescence. Reprinted with permission from ref 39. (C) Covalent labeling of a fluorophore on RNA by a self-alkylating ribozyme. Redrawn from ref 42. (D) Rational design of an aptazyme for ligand-responsive gene expression.....	10
Figure 1.7 The secondary structures of the (A) GR5, (B) 8-17, (C) 10-23 DNAzymes, and (D) 7-38-32 DNAzyme.	12
Figure 1.8 The secondary structures and metal binding sites of the (A) 39E, (B) Cd16, (C) PSCu10, (D) EtNa, (E) Dy10a, (F) Tm7, (G) Ce13d, (H) NaA43, and (I) Ag10c DNAzymes and their corresponding target meta ions.	15
Figure 1.9 A scheme showing the key steps of <i>in vitro</i> selection for RNA-cleaving DNAzymes starting from a random DNA library.	16

Figure 1.10 Three representative signaling strategies for RNA-cleaving DNAszymes. (A) Cleavage-induced fluorescent signal enhancement in a fluorescence beacon. (B) The disassembly of AuNPs after the cleavage reaction. (C) The conformational change of the 8-17 DNAszyme upon cleavage generates electrochemical signals for Pb^{2+} sensing. 18

Figure 1.11 A hydrated metal ion interacts with a phosphate through (A) diffusion, (B) outer-sphere binding, and (C) inner-sphere binding. Adapted with permission from ref 8. (D) The ion atmosphere around a cross-section of an RNA hairpin. Reprinted with permission from ref 86. A Mg^{2+} ion binds with (E) three guanines through hydrogen bonds or (F) with phosphate groups through inner-sphere coordination. Adapted with permission from ref 8. 20

Figure 1.12 (A) Metal ion-binding sites in nucleobases. (B) The C- Ag^+ -C base pair. (C) The T- Hg^{2+} -T base pair. (D) A G-tetrad stabilized by K^+ coordination. 22

Figure 1.13 Divalent metal ion-induced folding of the 8-17 DNAszyme studied by FRET. Reprinted from ref 102. 23

Figure 1.14 Possible catalytic roles of metal ions playing in an RNA cleavage reaction. 24

Figure 1.15 PS modification on the R_p substrate results in a thio effect by disturbing the interaction between a catalytic Mg^{2+} ion and the *pro-R_p* oxygen. Adapted with the permission from ref 112. 26

Figure 1.16 (A) The secondary (left) and crystal structure (right) of the RNA-cleaving DNAszyme, 8-17, revealing a V-shaped overall folding (PDB: 5XM8). (B) A Pb^{2+} -bound water captured in the catalytic core. (C) A hypothetical mechanism of 8-17 catalysis including a Pb^{2+} -bound water molecule as a general acid and a conserved guanine (G13) as a general base. Adapted with the permission from Ref 114. 27

Figure 1.17 (A) The NaA43 DNAszyme-based intracellular sensing of Na^+ based on the photocaging strategy. (B) Confocal microscopy images of HeLa cells transfected with caged NaA43 complex showing the Na^+ influx upon irradiation. Reprinted with permission from ref 72. 30

Figure 1.18 The folding-based sensing of Na^+ using 2AP-labeled Ce13d DNAszyme and the chemical structure of 2-aminopurine. 32

Figure 2.1 (A) A scheme describing the *in vitro* selection of $\text{Co}(\text{NH}_3)_6^{3+}$ -dependent DNAzymes. (B) The sequence of the initial library containing an N_{50} randomized region with a FAM labeled at the 5' end. (C) Progress of the *in vitro* selection at pH 6.0 showing the cleavage percentage of each round..... 37

Figure 2.2 The secondary structure of NaH1 predicted using Mfold. The rA is at number 9 position..... 40

Figure 2.3 Secondary structures of (A) the Ce13d and (B) the NaA43T DNAzymes (NaA43 with a shortened hairpin). (C)The cis-cleaving version of the selected Na^+ -dependent DNAzyme. (D) The trans-cleaving form of the selected Na^+ -dependent DNAzyme with a shortened hairpin structure..... 42

Figure 2.4 The inhibition effect of $\text{Co}(\text{NH}_3)_6^{3+}$ (10 μM) on the cleavage activity of NaH1 in the presence of 20 mM NaCl..... 43

Figure 2.5 (A) Kinetic profile of the NaH1 DNAzyme with various concentrations of NaCl at pH 6.0. (B) The cleavage rate of NaH1 as a function of Na^+ concentration. 44

Figure 2.6 A comparison of the cleavage rates of the NaH1 and NaA43T DNAzymes with 10 mM NaCl. Note that NaH1 was tested in pH 6.0 MES buffer while NaA43T was in pH 7.0 HEPES buffer. 44

Figure 2.7 The kinetics studies of the NaA43T and NaH1 DNAzymes with 10 mM NaCl at (A) pH 6.0 or (B) pH 7.0. (C) Cleavage yield of NaH1 and NaA43T with 10 mM NaCl at different pH's after 30 min incubation..... 45

Figure 2.8 (A) Gel images showing the cleavage in the presence of monovalent (10 mM), divalent (1 mM) and trivalent (100 μM) ions. (B) Quantification of the NaH1 cleavage yield with 20 different metal ions at pH 6.0 for 1 h. The background cleavage (without metal) was subtracted..... 46

Figure 2.9 (A) Schematic description of the Na^+ DNAzyme sensor design. (B) Sensor signaling kinetics measured with various concentrations of Na^+ . (C) Initial rates of fluorescence increase were quantified between 10 min to 15 min, and plotted as a function of Na^+ concentration..... 47

Figure 2.10 (A) Sensor response in the presence of 1% FBS monitored over 1 h. (B) A linear response between the fluorescence signal and $[\text{Na}^+]$ in 1% FBS..... 49

Figure 2.11 Gel image showing the cleavage of NaH1 in 1%, 2%, or 4% FBS samples (v/v) measured after 30 min incubation. 49

Figure 3.1 The secondary structures of two Na⁺-specific RNA-cleaving DNAzymes named (A) NaA43T and (B) NaH1. The key catalytic motifs are the small loops in red. (C) A general RNA cleavage reaction requires the nucleophilic attack from 2'-OH resulting in the leaving of the 5'-OH group, which can be accelerated by the general acid/base catalysis. 57

Figure 3.2 (A) The cleavage rate of each mutant in the presence of 10 mM NaCl at pH 6 (grey bars) and pH 7 (black bars). (B) List of the DNAzyme sequences used in this study. The A22 residue is highlighted with blue squares..... 59

Figure 3.3 (A) The sequences used in this point mutation study based on NaH1 from G20 to T23. (B) The cleavage rate of each mutant measured with 10 mM NaCl in pH 6 buffer..... 60

Figure 3.4 (A) pH-rate profiles of NaH1 and NaA43T in the presence of 10 mM Na⁺. (B) Chemical structures and pK_a values of adenine, 2-aminopurine (2AP), 2,6-diaminopurine (2,6-diAP), guanine, and hypoxanthine (I). (C) pH-rate profiles of the wild-type NaH1 and its 2,6-diAP-, 2AP- and G-substitutions in the presence of 10 mM NaCl. (D) pH-rate profiles of the wild-type NaA43T and its I- and A-substitutions in the presence of 10 mM NaCl. 61

Figure 3.5 (A) Kinetics of NaH1 and the A22-to-2AP mutant measured in the presence of 10 mM Na⁺ at pH 6. (B) Kinetics of NaA43T and the G23-to-I mutant measured in the presence of 10 mM Na⁺ at pH 7. 64

Figure 3.6 (A) Using 2AP to probe the local environment of the catalytic adenine due to Na⁺ binding. (B) The fluorescence spectrum of the A22-to-2AP mutant after titrating NaCl. (C) The 2AP fluorescence at 370 nm versus the Na⁺ concentration. (D) Fluorescence titration with Na⁺, K⁺ or Li⁺ 65

Figure 3.7 (A) The R_p and S_p phosphorothioate diastereomers at the cleavage junction. (B) The comparison between the normal PO-substrate and the PS-substrates of NaH1 in the presence of 10 mM NaCl with or

without 2 mM Cd ²⁺ . (C) Cleavage activity of NaH1 using PO-, R _p -, or S _p -substrates in the presence of 10 mM NaCl.	67
Figure 3.8 Scheme illustrating the cleavage products including a 2', 3'-cyclic phosphate and a 5'-hydroxyl.	69
Figure 3.9 Mass spectrometry characterization of the NaH1 cleavage product.....	69
Figure 3.10 A model describing the general acid/base mechanism of the NaH1 and NaA43 DNAzymes in the RNA cleavage reaction.	71
Figure 4.1 Secondary structures of two Na ⁺ -dependent DNAzymes including (A) NaA43T and (B) NaH1. (C) Gel images of cleavage results after 1 h incubation in the presence of 10 mM Na ⁺ and various Pb ²⁺ concentrations. (D) The cleavage ratio of NaA43T (black dots) and NaH1 (red triangles) in the presence of 10 mM Na ⁺ and various Pb ²⁺ concentrations.	78
Figure 4.2 (A) A competitive inhibition of NaH1 induced by 50 μM Pb ²⁺ . (B) The inhibition of NaH1 activity by 50 μM Pb ²⁺ was rescued by 100 mM Na ⁺ but not by 10 mM Na ⁺ and 90 mM Li ⁺	80
Figure 4.3 (A) Secondary structure of the Ce13d DNAzyme. (B) The Pb ²⁺ -dependent activity of Ce13d measured with or without 25 mM Na ⁺ . Black circles represent the cleavages of PO-substrates alone as a control. (C) Cleavage rates of Ce13d measured with various concentrations of Pb ²⁺ and 25 mM Na ⁺ . (D) Effect of Na ⁺ concentration on the cleavage yields with 20 μM Pb ²⁺	82
Figure 4.4 (A) Cleavage yields of Ce13d measured in various concentrations of Pb ²⁺ or Ce ³⁺ without Na ⁺ (1 h). (B) The comparison of cleavage% of Ce13d in the presence of 200 μM Pb ²⁺ or 1 mM Mg ²⁺ /Ca ²⁺ without Na ⁺ (1 h).....	83
Figure 4.5 (A) Cleavage rates of 20 μM Pb ²⁺ (25 mM Na ⁺) measured in different pH buffers from pH 6.4 to 7.3. The buffers used here are 20 mM PIPES buffer (40 mM LiCl). (B) The logarithm of rate against pH revealing a linear relationship with a slope of -0.9373.	84
Figure 4.6 (A) Secondary structure of the EtNa DNAzyme. (B) Kinetics study of EtNa in the presence of 100 μM Ca ²⁺ (black), 20 μM Pb ²⁺ (red), or 100 μM Ca ²⁺ and 20 μM Pb ²⁺ (green). (C) Gel images showing	

the cleavage% of EtNa measured at several time points in the presence of 100 $\mu\text{M Ca}^{2+}$, 100 $\mu\text{M Ca}^{2+}$ and 20 $\mu\text{M Pb}^{2+}$, or 500 $\mu\text{M Ca}^{2+}$ and 20 $\mu\text{M Pb}^{2+}$, respectively.....	85
Figure 4.7 Metal ion effects on the EtNa activity in 100 $\mu\text{M Ca}^{2+}$ with the addition of 20 μM divalent (Pb^{2+} , Mg^{2+} , Mn^{2+} , Cu^{2+} , Zn^{2+} , Co^{2+} , Cd^{2+}) or trivalent (Ce^{3+} , Al^{3+}) metal ions.....	86
Figure 4.8 (A) Cleavage rates measured as a function of Ca^{2+} concentrations in the presence of 20 $\mu\text{M Pb}^{2+}$. (B) Cleavage rates increased with increasing Pb^{2+} concentrations in the presence of 500 $\mu\text{M Ca}^{2+}$	87
Figure 4.9 (A) Cleavage rates of EtNa measured in various pH buffers. The reaction was performed in 20 $\mu\text{M Pb}^{2+}$ alone. (B) pH-rate profiles measured in 20 $\mu\text{M Pb}^{2+}$ (blue), 1 mM Ca^{2+} (red), or 100 $\mu\text{M Ca}^{2+}$ and 10 $\mu\text{M Pb}^{2+}$ (green).....	89
Figure 4.10 Comparison of pH dependency of the wild type 8-17 DNAzyme and the G14-AP variant in 200 and 100 $\mu\text{M Pb}^{2+}$, respectively. Reprinted with permission from ref 117.	92
Figure 4.11 A schematic summary of various Pb^{2+} effects in the RNA cleavage reaction catalyzed by nucleic acid enzymes..	93
Figure 5.1 (A) The sense strand of the dsDNA template used to generate RNA library for <i>in vitro</i> selection. (B) The secondary structure of designed 80-nt RNA library containing two random regions N_{20} and N_7 . (C) The <i>cis</i> -cleaving structure of Rn2 sequence. (D) The secondary structure of Rn2 sequence predicted by Mfold (including the primer binding domain).	98
Figure 5.2 The <i>in vitro</i> selection procedure for self-cleaving ribozymes.	99
Figure 5.3 (A) Gel image showing the cleavage products of 1 st and 6 th round after selection step.	100
Figure 5.4 (A) Real-time PCR used to monitor the gradual increase in RNA population in library along with the selection progress. (B) The fractional cycles ($C_{1/2}$) at which reaction fluorescence reaches half of maximal (F_{max}).	100
Figure 5.5 (A) Sequence analysis of Rn2 family by calculating the percentage of each nucleotide among a total of 98 sequences. (B) Comparison of two randomized domains in Rn2, Rn2.1, and Rn2.2 sequences. (C) Gel image showing the cleavage activity of Rn2, Rn2.1 and, Rn2.2..	101

Figure 5.6 (A) The self-cleavage activity of Rn2 measured in various formamide vol% after incubating at 65°C for 5 min. 103

Figure 5.7 (A) The temperature effect on the self-cleavage activity of Rn2 in 50 vol% (~12.5 M) formamide. (B) The cleavage% of Rn2 measured during a slow heating process. Reactions were performed in 50 vol% formamide (25 mM Tris•HCl, pH 7.5, 1 mM EDTA•2Na⁺) and quenched by cooling at -20°C. 105

Figure 5.8 The cleavage% of Rn2 measured in 50% or 80% formamide during a slow heating process. The reaction was gradually heated from 30°C to 90°C. The reaction remained for 20 s at each temperature point. An accumulated cleavage% was measured after being quenched at each temperature point. 106

Figure 5.9 (A) The cleavage% measured at different time points in the presence of 50% and 90% formamide under 65°C. (B) Kinetics of Rn2 cleavage measured in buffer, 50%, or 80% formamide at 53°C. 106

Figure 5.10 The cleavage activity of Rn2 measured in various concentration of (A) divalent and (B) monovalent metal ions. Reactions were performed in 50% formamide at 53°C (for 2 min). (C) Gel images of Rn2 cleavage in various concentrations of Mg²⁺ or Na⁺ 108

Figure 5.11 Solvent effect on the self-cleavage activity of Rn2 (65°C, 5 min). The cleavage% was measured in 50 vol% of formamide, DMSO, ethanol, or methanol, while 10 M urea was used. Buffer used was 50 mM Tris•HCl (pH 7.5), and 1 mM EDTA•2Na⁺ was added in all reactions. 109

Figure 5.12 Nucleotide NCBI-BLAST results showing the alignments of Rn2 motif in complete plasmids (A) or genomes (B) databases of microbes. The N₂₀ region of Rn2 ribozyme was used as the input sequence. 111

Figure 5.13 The phylogenetic tree generated by BLAST in complete genomes database. 112

Figure 5.14 (A) The extended dsDNA template use for *in vitro* transcription with a length of 103 bps. (B) Real-time PCR for optimizing the cDNA volume used in PCR reaction. (C) The optimized cycle# and template length were confirmed with 2% agarose gel in each round of selection. 115

List of Tables

Table 1. Chemical properties of several multivalent metal ions. ^{102, 103}	25
Table 2. The N ₅₀ random region of representative families from the round 6 selection pool comparing with the NaA43 sequence.	39
Table 3. List of all the DNA sequences and modifications used in the <i>in vitro</i> selection experiment.....	51
Table 4. A list of DNA sequences (from 5' to 3') used in chapter 3.....	72
Table 5. A literature summary of all the RNA-cleaving DNAzymes in which the Pb ²⁺ -induced activity was detected in previous studies.	76
Table 6. A summary of EtNa activity in various metal ions.....	90
Table 7. The eight most abundant families (from 5' to 3') after sequence alignment present in the final library. N ₂₀ region is in red, and N ₇ region is in blue.....	102
Table 8. Oligonucleotide sequences used in the <i>in vitro</i> selection experiment.....	113

List of Abbreviations

2,6-diAP	2,6-diaminopurine
2AP	2-aminopurine
A	adenine
APS	ammonium persulphate
ATP	adenosine triphosphate
AuNPs	gold nanoparticles
BLAST	basic local alignment search tool
bp	base pair
C	cytosine
Cas9	CRISPR-associated protein 9
CoA	coenzyme A
CRISPR	clustered regularly interspaced short palindromic repeats
dA ^{im} TP	8-histaminyl-deoxyadenosine
dC ^{aa} TP	5-aminoallyl-deoxycytidine
DFHBI	3,5-difluoro-4-hydroxybenzylidene imidazolinone
DMS	dimethyl sulfate
DMSO	dimethyl sulfoxide
DNA	deoxyribonucleic acid
DNAzyme	deoxyribozyme
dNTP	deoxynucleotide triphosphate
dPAGE	denaturing polyacrylamide gel electrophoresis

dsDNA	double-stranded DNA
DTT	dithiothreitol
dU ^{ga} TP	5-guanidinoallyl-deoxyuridine
EB	ethidium bromide
EDTA	ethylenediaminetetraacetic acid
EPR	electron paramagnetic resonance
ESI MS	electrospray ionization mass spectrometry
FA	formamide
FAM	6-carboxyfluorescein
FANA	2'-fluoroarabino nucleic acid
FBS	fetal bovine serum
FRET	fluorescence resonance energy transfer
G	guanine
GlcN6P	glucosamine-6-phosphate
GQ	G-quadruplex
HDV	hepatitis delta virus
HEPES	2-[4-(2-hydroxyethyl)piperazin-1-yl]ethanesulfonic acid
HHRz	hammerhead ribozyme
HIV	human immunodeficiency virus
I	hypoxanthine
K_d	apparent dissociation constant
k_{obs}	apparent rate constant
MCH	mercaptohexanol

MES	2-(<i>N</i> -morpholino)ethanesulfonic acid
mL	milliliter
mM	millimolar
MOPS	3-(<i>N</i> -morpholino)propanesulfonic acid
mRNA	messenger RNA
NAD	nicotinamide adenine dinucleotide
NMR	nuclear magnetic resonance
nt	nucleotide
NTP	nucleotide triphosphate
PCR	polymerase chain reaction
PIPES	2,2'-(piperazine-1,4-diyl)di(ethane-1-sulfonic acid)
PS	phosphorothioate
rA	ribo-adenosine
RNA	ribonucleic acid
rt-PCR	real-time polymerase chain reaction
SDS	sodium dodecyl sulfate
smFRET	single-molecular fluorescence resonance energy transfer
ssRNA	single-stranded RNA
T	thymine
TBE	Tris/Borate/EDTA
TEMED	tetramethylethylenediamine
T _m	melting temperature
TNA	α -L-threofuranosyl nucleic acid

Tris	tris(hydroxymethyl)aminomethane
U	uracil
UV-vis	ultraviolet-visible
VS	varkud satellite
XAS	X-ray absorption spectroscopy
XNA	xeno-nucleic acid
μL	microliter
μM	micromolar

Chapter 1. Introduction to Catalytic Nucleic Acids^a

Early discoveries on naturally occurring ribozymes (RNA molecules with catalytic activities) in the 1980s have broken the notion that all enzymes are proteins,^{1, 2} giving a strong evidence for the RNA world hypothesis.³ Since then, the catalytic functionality of RNA has been extensively explored revealing the diverse and crucial roles of ribozymes in living organisms.⁴ Meanwhile, *in vitro* selection has been used to discover artificial ribozymes catalyzing a variety of chemical reactions in laboratory. In 1994, the first catalytic DNA (or DNAzyme, deoxyribozyme) was discovered to accelerate an RNA cleavage reaction.⁵ To date, although DNAzymes have not yet been found in nature, they have been isolated via *in vitro* selection to achieve a diverse range of activities including RNA cleavage and ligation, DNA phosphorylation, Diels–Alder reaction, and nucleopeptide bond formation.^{6, 7} Over the past 20 years, DNAzyme-based applications have been thriving in different areas such as metal biosensing, gene silencing, pathogen detection, and nanotechnology.⁸⁻¹¹ Ribozymes and DNAzymes are collectively called catalytic nucleic acids. Compared to protein enzymes, catalytic nucleic acids are programmable in structure, easy to synthesize or modify, and more chemically stable especially for DNA. In particular, many RNA-cleaving DNAzymes display excellent activity and specificity toward metal ions, making them attractive for metal ion sensing. The search for novel DNAzymes and

^a Partial contents in this chapter are the basis for a published review manuscript: Ma, L.; Liu, J., Catalytic Nucleic Acids: Biochemistry, Chemical Biology, Biosensors, and Nanotechnology. *iScience* **2020**, 23 (1), 100815.

ribozymes is facilitated by developments in DNA sequencing and computational algorithms, further broadening our fundamental understanding of biochemical processes.

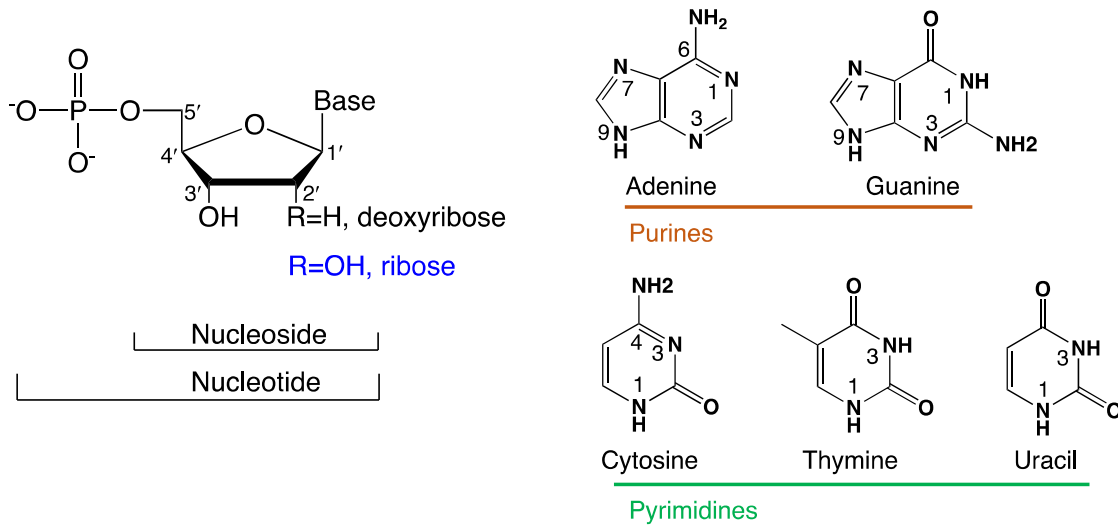


Figure 1.1 The chemical structure of nucleotides and five nucleobases including two purines (A, G) and three pyrimidines (C, T, U).

1.1 Chemical structure of nucleic acids

Along with carbohydrates, lipids, and proteins, nucleic acids are among the most important biological macromolecules in all forms of life. Within cells, nucleic acids, including deoxyribonucleic acid (DNA) and ribonucleic acid (RNA), function in preserving, transmitting, regulating, and expressing genetic information. Essentially, DNA and RNA are linear polymers with nucleotides as their repeating units. The three essential components of a nucleotide are: a) a pentose sugar; b) a heterocyclic nucleobase linked to the 1'-carbon on the sugar ring; and c) a phosphate group on the 5'-carbon (Figure 1.1). A nucleoside refers to a nucleotide without a phosphate group attached. The major difference between DNA and RNA lies in the pentose sugar:

the hydroxyl group on the 2'-carbon in an RNA ribose is missing in a DNA 2'-deoxyribose. The presence of 2'-OH in RNA provides more complexity in structure and more binding sites for metal ions. Meanwhile, it makes RNA more susceptible to hydrolysis compared to DNA.

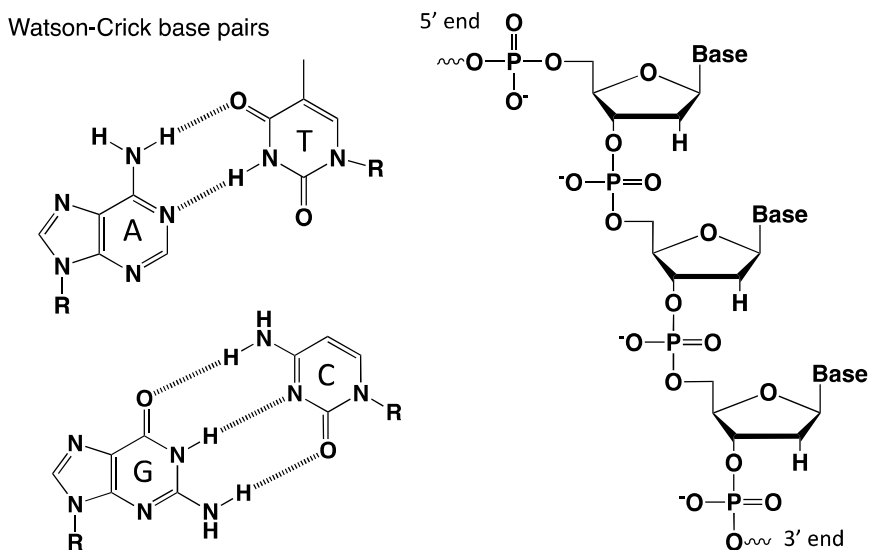


Figure 1.2 Watson-Crick base pairs (A•T and G•C) in DNA and a sugar–phosphate backbone with 5'-to-3' phosphodiester bonds.

The four natural occurring nucleobases in DNA are adenine (A), thymine (T), cytosine (C), and guanine (G). In RNA, uracil (U) is used to replace thymine (Figure 1.1). Nucleobases contain multiple hydrogen bond donor and acceptor sites allowing them to form inter-base H-bindings. The predominant type is Watson-Crick base pairing formed between A•T (or A•U) and C•G (Figure 1.2). Apart from Watson-Crick base pairs, a variety of other pairings such as Wobble (e.g., G•U) and Hoogsteen (e.g., A•T) base pairs are also important in stabilizing nucleic acid structures. In addition to hydrogen binding, π - π stacking is another type of base-base interaction happening between neighboring planar bases.

The neighbouring nucleotides can be connected through a phosphodiester linkage between the 3'-hydroxyl group of one nucleotide and 5'-phosphate group of the next, forming a long polymer (Figure 1.2). The alternating phosphate group and sugar residues construct the DNA backbone with 5'- and 3'-terminus. Resulting from the low pK_a value of the phosphate group ($pK_{a1} \sim 1.0$), the sugar-phosphate backbone is highly negatively charged at neutral pH. All the nucleobases carry no charge at physiological pH since their pK_a values are far from neutrality (Figure 1.3). For example, the N1 position of adenine can be protonated when the pH is lower than its pK_a of 3.5. Nevertheless, in catalytic nucleic acids, the pK_a value of certain nucleobases can be largely altered in a particular microenvironment such as interacting with nearby nucleotide residues or metal ions.¹² With its pK_a shifted toward neutrality, a nucleobase can become deprotonated or protonated more easily under physiological condition.

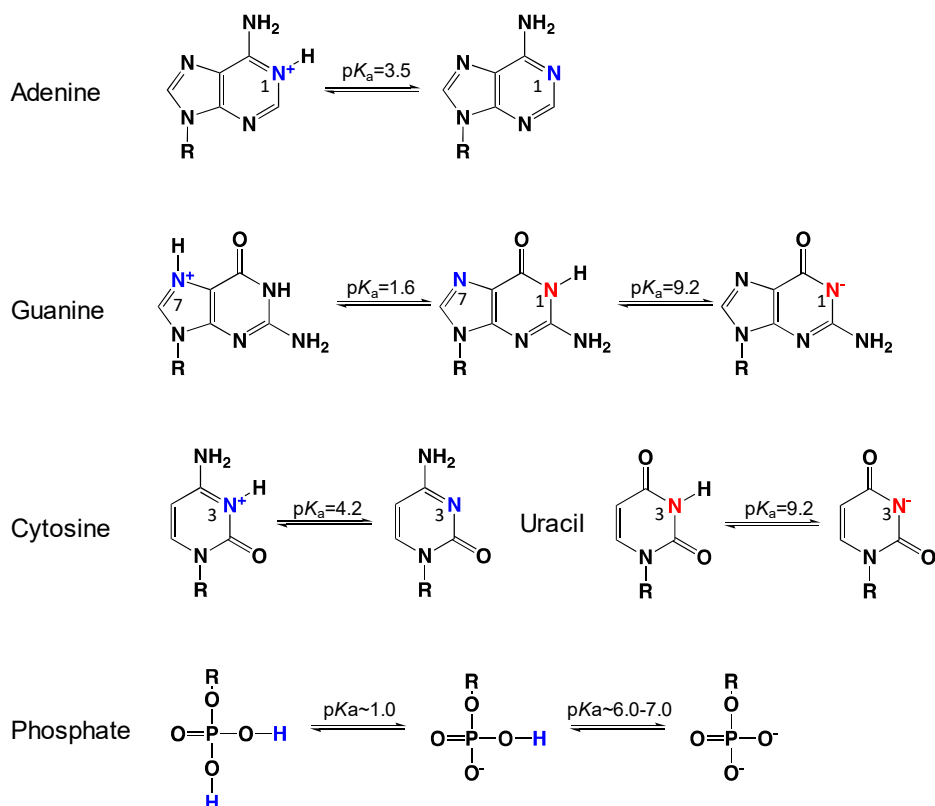


Figure 1.3 The unperturbed pK_a values of nucleobases and ionization sites.¹³

1.2 An overview on catalytic nucleic acids

The notion that all enzymes are proteins was changed with the discovery of ribozymes in the early 1980s. Since then, researchers have been motivated to search for new ribozymes in nature, in test tubes, and even *in silico*. Although not yet found in nature, the first DNAzyme was isolated using *in vitro* selection in 1994 by Breaker and Joyce. With nearly four decades of development, nucleic acid enzymes have impacted many fields ranging from biosensing, anti-virus, to materials science.¹⁴⁻¹⁷ For *in vivo* applications, RNA has advantage over DNA since RNA can be transcribed in cells, but single-stranded DNA often requires delivery. For applications outside cells, DNA is more attractive than RNA for stability and cost considerations. For example, the chemical stability of DNA against hydrolysis is around one-million-fold higher than that of RNA.¹⁸ Chemical synthesis also allows convenient DNA labeling with various functional moieties such as fluorophores, conjugation groups, and spacers.

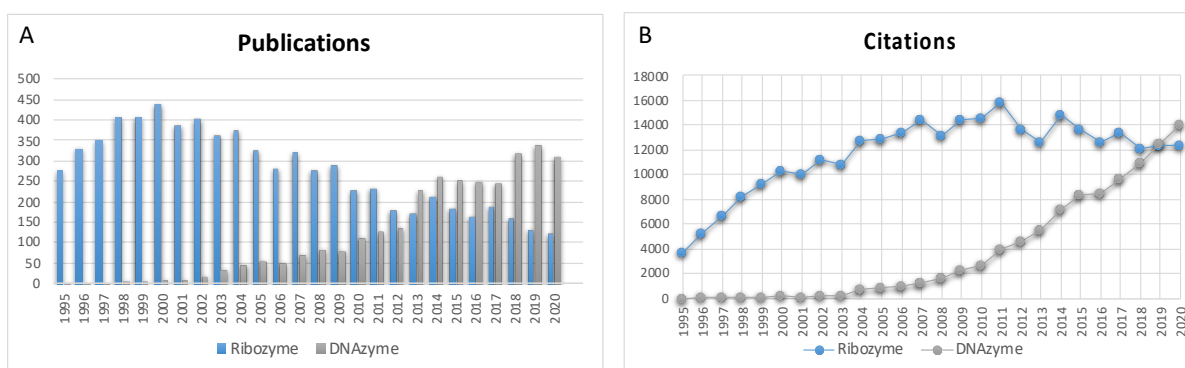


Figure 1.4 Comparisons on the number of publications (A) and citations (B) from 1995 to 2020 with “ribozyme” and “DNAzyme” or “deoxyribozyme” as keywords.

A brief survey on the Web of Science revealed interesting trends (Figure 1.4). Publications on ribozymes peaked in the early 2000s, when the DNAzyme field just started to take off. In recent years, both the publications and citations on DNAzymes (including G4 DNAzymes) have outnumbered that on ribozymes, which was largely driven by emerging applications on biosensors, intracellular RNA cleavage, and bionanotechnology.^{19,20}

1.3 Ribozymes in the early days

RNA for a long time was only known for mediating the production of proteins. In the early 1980s, the initial discovery of ribozymes was related to the RNA cleavage and self-splicing reactions, leading to the award of the Nobel Prize to Cech and Altman.^{1,2} Since then, ribozymes for many important biological reactions were discovered in nature, such as the ribosomal RNA catalyzing the formation of peptide bonds.²¹ The ribosome in cells is composed of both protein and RNA, while the peptidyl transferase activity was performed by the RNA component (Figure 1.5A).

Given that RNA possesses both genotype and enzymatic functions, the RNA world hypothesis was proposed, stating that RNA dominated the early life before DNA and protein.³ Many coenzymes or cofactors in protein enzymes, such as coenzyme A (CoA) and nicotinamide adenine dinucleotide (NAD), contain the basic structure of ribonucleotides, also supporting this hypothesis.²² In the meantime, *in vitro* evolution offers a powerful technique for exploring the capabilities of RNA in test tubes.²³ *In vitro* selection resembles the natural evolution, in which a large RNA library is subjected to a selection pressure and only those sequences with a particular activity can survive and be enriched. Benefiting from this accelerated process, ribozymes catalyzing a great variety of chemical reactions, such as RNA ligation, phosphorylation, self-

alkylation, and Diels-Alder reaction, have been obtained over the past decades.²⁴ Recently, interesting efforts were made for producing polymerizing ribozymes and self-replicating systems.^{25, 26} In 2021, a novel ribozyme was reported with abilities to recognize a promoter sequence and catalyze RNA polymerization using a clamp-like mechanism, providing more insights into the RNA-based self-evolving system.²⁷

Over the past 30 years, a variety of self-cleaving ribozymes catalyzing the cleavage of phosphodiester bonds have been discovered. The hammerhead ribozyme was first found in the tobacco ringspot virus satellite RNA.²⁸ Other ribozymes, including the hairpin, hepatitis delta virus (HDV), glucosamine-6-phosphate synthase (*glmS*), Varkud satellite (VS), twister, twister-sister, pistol, and hatchet ribozymes were subsequently identified in various organisms.²⁹ These enzymes catalyze the site-specific cleavage of 3', 5'-phosphodiester bonds with up to 10⁶-fold rate enhancement. Extensive structural and biochemical studies have been performed to provide mechanistic understanding of ribozyme catalysis.^{30, 31}

In general, the RNA cleavage reaction can be accelerated through four pathways (Figure 1.5C): arranging the in-line alignment between the 2'-O nucleophile, scissile phosphorus, and 5'-leaving oxygen (α factor); facilitating the deprotonation of 2'-OH in the nucleophilic attack (β factor); neutralizing the negative charge on the non-bridging phosphoryl oxygens in the transition state (γ factor); and stabilizing the negative charge on the 5'-leaving oxygen (δ factor).³² Nowadays, the general acid-base mechanism has been widely accepted for explaining ribozyme-catalyzed RNA cleavage reactions.

For a given ribozyme, critical nucleobases and metal ion cofactors can facilitate the cleavage reaction in the catalytic core. Experimental evidence has proved that conserved

nucleobases with shifted pK_a values are able to participate directly in the catalysis at the active site.¹³ Both biochemical and structural studies are required to provide insights into the catalytic mechanism. In the active site of the hammerhead ribozyme, a conserved guanine, G-12, can act as a general base by hydrogen bonding with the 2'-O nucleophile, while the 2'-OH of the other guanine G-8 can stabilize the leaving oxygen as a general acid (Figure 1.5B).³³ The HDV ribozyme utilizes a conserved cytosine (C75) as a general acid and a Mg^{2+} ion activating the 2'-OH at the cleavage site.³⁴ In the case of the *glmS* ribozyme, a metabolic molecule, glucosamine-6-phosphate (GlcN6P), is required as a cofactor for its catalysis instead of divalent metal ions.³⁵

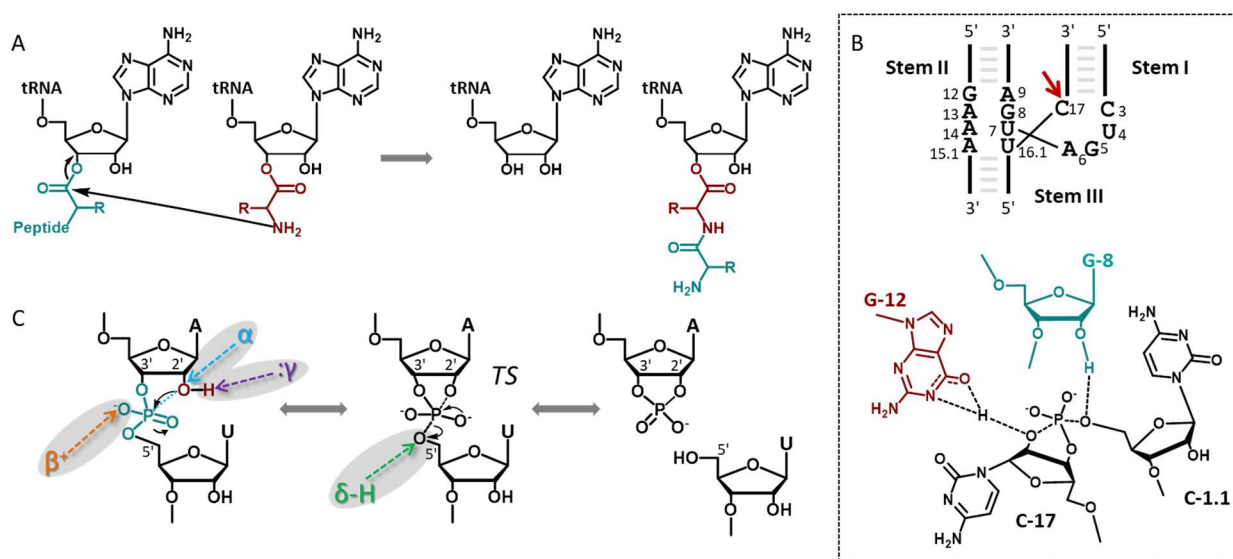


Figure 1.5 (A) The peptidyl transferase activity of the ribosomal RNA during a peptide bond formation. (B) The minimal secondary structure of the hammerhead ribozyme containing 13 conserved nucleotides (top). The active site in the transition state where G-12 functions as a general base and G-8 as a general acid (bottom). Redrawn from ref 33. (C) The cleavage of a 3', 5'-phosphodiester bond catalyzed by self-cleaving ribozymes. The nucleophilic attack of the 2'-OH to the nearest phosphate causes the leaving of the 5'-O, and produces a 2', 3'-cyclic phosphate and a 5'-OH. The α , β , γ , and δ represent four catalytic mechanisms for the reaction.

1.4 Ribozymes for therapeutic applications

After the discovery of self-cleaving ribozymes, their therapeutic potential in inhibiting gene expression was tested.³⁶ For this purpose, several self-cleaving ribozymes (e.g., the hammerhead and hairpin ribozymes) were engineered to catalyze RNA cleavage in the trans-cleaving manner (Figure 1.6A). By altering the binding sequence to be complementary to target mRNA, trans-cleaving ribozymes can selectively cleave essentially any mRNA target, such as HIV (human immunodeficiency virus) and cancer related genes.^{37,38} However, many challenges remain in applying ribozymes *in vivo*, such as the short lifetime of ribozymes *in vivo*, ineffective delivery of ribozymes to target cells, and poor enzymatic activity. To improve the intracellular activity of the hammerhead ribozyme, *in vivo* selection of trans-cleaving hammerhead mutants was recently performed in *E. coli* cells.³⁹ The selected variants showed an enhanced ability for intracellular gene-silencing toward various RNA targets. As a proof-of-concept, intracellularly expressed ribozymes were designed to cleave a reporter gene, spinach. The mutant suppressed fluorescence by disrupting the DFHBI (3,5-difluoro-4-hydroxybenzylidene imidazolinone) binding twice more efficiently than the original ribozyme (Figure 1.6B).

Apart from RNA cleavage, another major direction is to develop ribozymes for chemical biology applications such as biomolecular synthesis and modification.^{40, 41} In a recent example, self-alkylating ribozymes were selected to achieve covalent labeling of a fluorophore on RNA (Figure 1.6C).⁴² Another branch of application is to combine aptamers and ribozymes to achieve ligand-responsive gene regulation.

Riboswitches are natural RNA aptamers found in the untranslated regions of mRNA, which can regulate gene expression upon binding with target small molecules. The *glmS* ribozyme was identified in several Gram-positive bacteria to cleave certain messenger RNA using GlcN6P as a

cofactor.³⁵ Even before the discovery of riboswitches, aptazymes or allosteric ribozymes have been rationally designed by fusing existing aptamers and ribozymes, or by direct *in vitro* selection.⁴³ A rationally designed aptazyme is typically composed of an aptamer domain (e.g., for ATP, theophylline) and a ribozyme domain (e.g, hammerhead, hairpin).^{44, 45} Ligand binding induces a conformational change which subsequently influences the ribozyme activity and turns off or on the gene expression (Figure 1.6D). Recently, hammerhead-based aptazymes have been embedded in the guide RNAs of the CRISPR-Cas9 system to perform ligand-responsive genome editing.⁴⁶

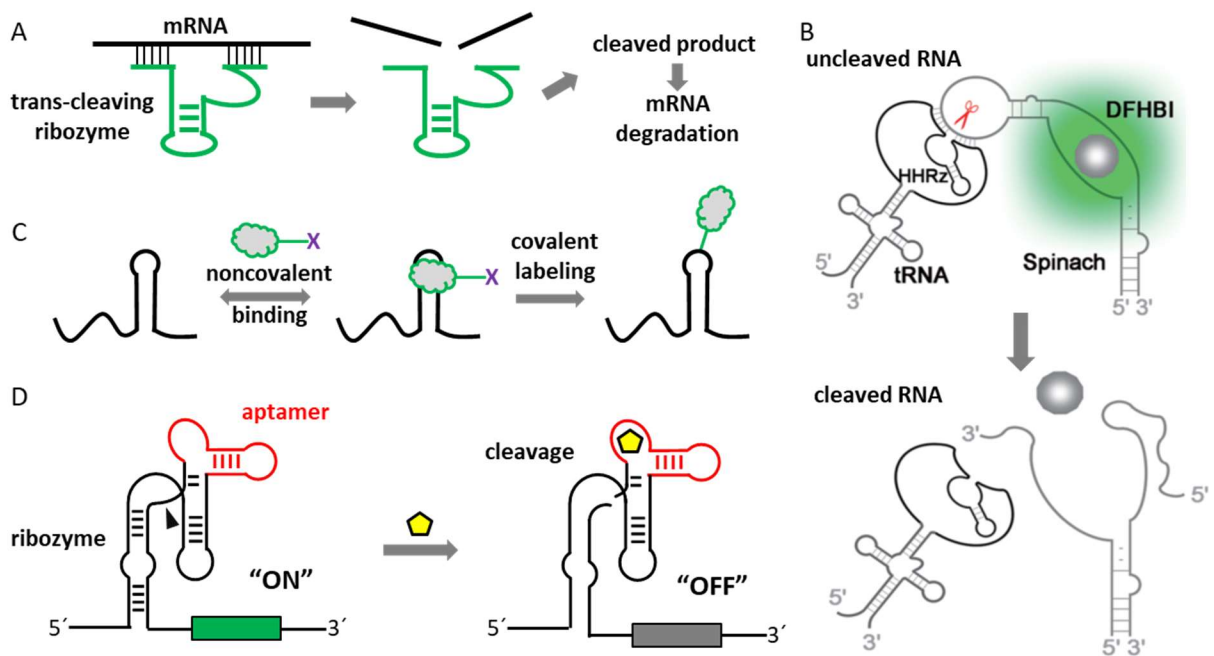


Figure 1.6 (A) Trans-cleaving ribozymes for gene-silencing. (B) Intracellularly selected hammerhead ribozymes with enhanced cleavage activity in living cells. Spinach is a report RNA that binds with a small molecule, DFHBI, and emits fluorescence. Reprinted with permission from ref 39. Copyright © 2019 Oxford University Press. (C) Covalent labeling of a fluorophore on RNA by a self-alkylating ribozyme. Redrawn from ref 42. (D) Rational design of an aptazyme for ligand-responsive gene expression.

1.5 RNA-cleaving DNazymes

Given the chemical similarity between DNA and RNA, a natural question is whether DNA can perform catalysis. Since most DNA molecules in nature are double-stranded, they are unlikely to be catalytically active. Single-stranded DNA, on the other hand, can form tertiary structures, allowing molecular recognition and catalysis. In the early 1990s, single-stranded DNAs with specific binding activity (aptamers) have been obtained through *in vitro* selection. Similar methods can also be used for the selection of DNazymes, and the first DNzyme was reported by Breaker and Joyce in 1994. This DNzyme, named GR5 (Figure 1.7A), was selected for RNA cleavage in the presence of Pb^{2+} .⁵ The initial choice of Pb^{2+} for the selection was probably motivated by Pb^{2+} catalyzed RNA cleavage as observed in the leadzyme.⁴⁷ GR5 is short with only 15 nucleotides in the catalytic loop, and its substrate contains a single RNA linkage serving as the cleavage site. In the original paper, the catalytic activity reached a turnover rate of 1 min^{-1} in the presence of 1 mM Pb^{2+} . Later, after optimization of the buffer condition, its activity easily reached $>10 \text{ min}^{-1}$ with $10 \text{ }\mu\text{M}$ Pb^{2+} .⁴⁸

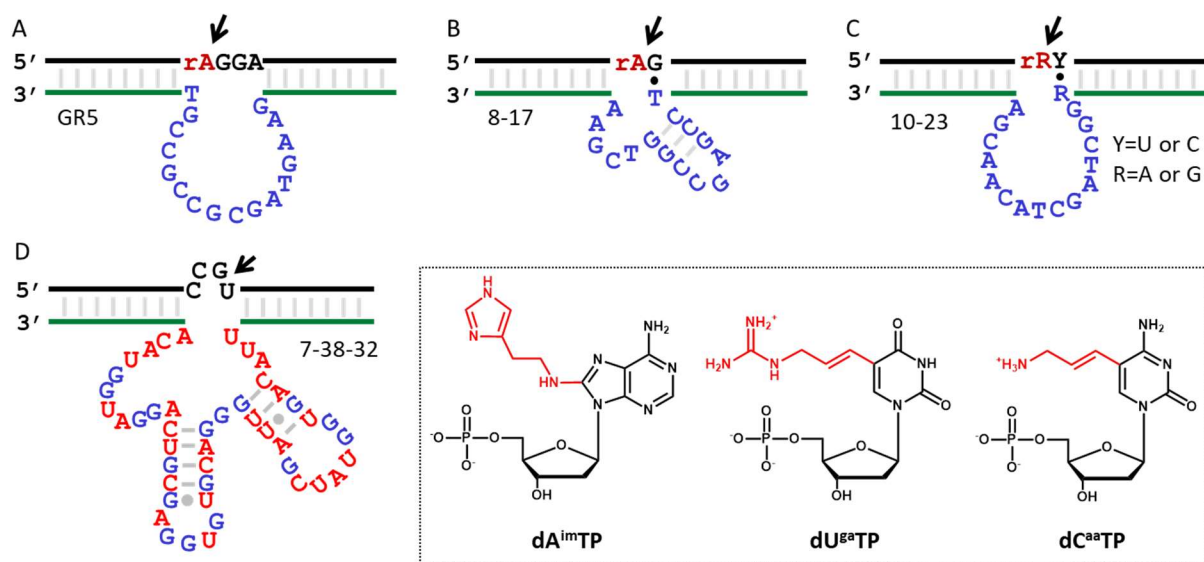


Figure 1.7 The secondary structures of the (A) GR5, (B) 8-17, and (C) 10-23 DNAzymes. (D) The 7-38-32 DNAzyme containing three modified nucleotides: 8-histaminyl-deoxyadenosine (dA^{im}TP), 5-guanidinoallyl-deoxyuridine (dU^{ga}TP), and 5-aminoallyl-deoxycytidine (dC^{aa}TP).

1.5.1 DNAzymes for gene-silencing in cells

One of the first motivations to develop RNA-cleaving DNAzymes was to cleave viral RNA. GR5 is apparent not appropriate for this purpose since it cannot cleave all-RNA substrates (it only cleaves the substrate with a single RNA linkage), and it requires toxic Pb²⁺ (no activity in the presence of Mg²⁺ alone). Subsequently, Santoro and Joyce reported two DNAzymes named 8-17 and 10-23 (Figure 1.7B and 1.7C), both of which can cleave full-RNA substrates with Mg²⁺ alone.⁴⁹ The catalytic rate reached a catalytic rate of $\sim 0.1 \text{ min}^{-1}$ with 2 mM Mg²⁺, and the catalytic efficiency (k_{cat}/K_m) reached $\sim 10^9 \text{ M}^{-1} \cdot \text{min}^{-1}$ for the 10-23 DNAzyme, which is comparable with the most efficient protein enzyme. The requirement of substrate sequence is very simple. Further studies revealed that all the 16 junctions can be cleaved at different efficiencies.⁵⁰ The specificity of cleavage is defined by the two substrate binding arms. With each arm containing 8 or more base pairs, these two DNAzymes can in principle be modified to target any specific RNA sequence.

This discovery has excited the field for pursuing anti-viral and later anti-cancer applications.^{51,52} However, to achieve a high cleavage activity, the required Mg²⁺ concentration is quite high and intracellular free Mg²⁺ can hardly meet the requirement. It has been argued that the observed intracellular inhibition of gene expression using DNAzymes could simply be due to the anti-sense effect.⁵³ To address this issue, using modified nucleotides to mimic the chemical functionalities of RNase A has been attempted and metal-free cleavage was achieved in some cases.

An example is the DNAzyme 7-38-32 (Figure 1.7D), which cleaves an RNA substrate with a catalytic rate of 1.06 min^{-1} in the presence of only 0.5 mM Mg^{2+} .⁵⁴

Apart from selection, chemical modifications have been used to engineer current DNAzymes to achieve improved activity and stability *in vivo*.⁵⁵⁻⁵⁷ In a recent study, xeno-nucleic acids (XNAs) such as 2'-fluoroarabino (FANA) and α -L-threofuranosyl (TNA) nucleic acids were used to modify the 10-23 DNAzyme.⁵⁸ XNA can provide an enhanced stability against nuclease degradation and support high binding affinity to RNA substrates. After optimization, the engineered 10-23 DNAzyme displayed enhanced biostability and multiple-turnover activity, which was successfully applied for knocking down mRNA sequences in living cells.⁵⁹

1.5.2 Representative metal-dependent DNAzymes

Compared to biomedical applications, the development of designing DNAzymes into biosensors has advanced more. Lu and coworkers selected the 17E DNAzyme in the presence of Zn^{2+} , which turned out to be very similar to the 8-17 DNAzyme.⁶⁰ These DNAzymes can be activated with various divalent metal ions (e.g., Zn^{2+} , Mg^{2+} , Mn^{2+}), but are most active with Pb^{2+} .⁶¹ Li and Lu first demonstrated designing the 17E DNAzyme into a fluorescent sensor for Pb^{2+} detection.⁶² Since then, the 17E DNAzyme has been used as a model system to develop different signaling mechanisms ranging from fluorescence, color, electrochemistry to Raman spectroscopy.¹⁹

Many subsequent selections have been intentionally carried out in the presence of target metal ions to achieve desired specificity. Several representative RNA-cleaving DNAzymes and their metal ion cofactors are summarized in Figure 1.8. The 39E DNAzyme was isolated in the presence of UO_2^{2+} and it has over 1-million-fold higher selectivity for UO_2^{2+} over other metal ions

(Figure 1.8A).⁶³ Several nucleotides in the budge loop were determined to contribute to the UO_2^{2+} -binding.⁶⁴ The EtNa DNAzyme is highly specific for Ca^{2+} in water, but becomes more active for Na^+ in ethanol (Figure 1.8D).⁶⁵ Biochemical studies revealed that EtNa requires a cooperative binding of two Ca^{2+} ions at the scissile phosphate, which may explain its excellent specificity.⁶⁶ For the Ce13d DNAzyme, all trivalent lanthanide ions exhibit similar activity by neutralizing the negative charge on the non-bridging oxygens (Figure 1.8G).⁶⁷ Furthermore, two more lanthanide-dependent DNAzymes were identified whose activities require the binding of multiple lanthanide ions (Figure 1.8E and 1.8F).^{68, 69} By introducing a phosphorothioate (PS) modification at the cleavage junction, Cd^{2+} (Figure 1.8B) and Cu^{2+} (Figure 1.8C) specific DNAzymes were selected.^{70, 71} The PS modification is critical for recognition of these softer metal ions, which in turn indicated that the binding of the scissile phosphate group is their main catalytic role.

In most cases, a well-defined metal binding pocket (e.g., an aptamer motif) cannot be identified in a metal-specific DNAzyme. Metal ions typically perform their catalytic functions by transiently associating with the cleavage site. Interestingly, a few new DNAzymes were reported with defined aptamer motifs. The NaA43 DNAzyme (Figure 1.8H) was selected in the presence of Na^+ and it can reach a rate of 0.1 min^{-1} with 400 mM Na^+ alone.⁷² It shares sequence similarity with the Ce13d DNAzyme and the common loop was later identified as a Na^+ aptamer.⁷³ The Ag^+ -specific DNAzyme, Ag10c, is another example in which two Ag^+ ions bind to the aptamer motif (Figure 1.8I).⁷⁴ The catalytic role of interacting with the scissile phosphate is fulfilled by the salt in buffer (e.g. Na^+ , Li^+ , K^+ , Mg^{2+}).⁷⁵

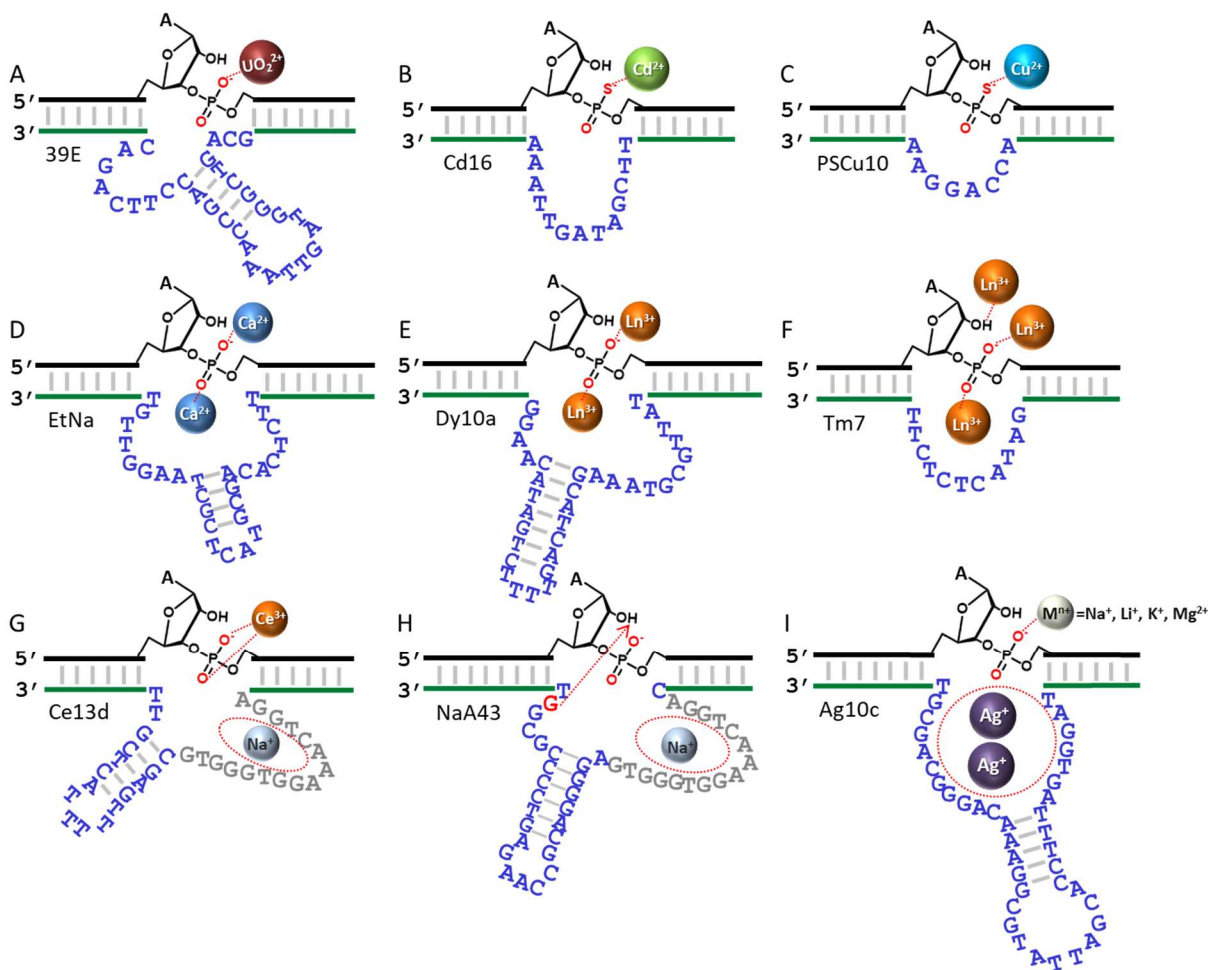


Figure 1.8 The secondary structures and metal binding sites of the (A) 39E, (B) Cd16, (C) PSCu10, (D) EtNa, (E) Dy10a, (F) Tm7, (G) Ce13d, (H) NaA43, and (I) Ag10c DNAzymes and their corresponding target meta ions. Some DNAzymes require multiple metal ions.

1.5.3 *In vitro* selection for DNAzymes

The method of *in vitro* selection has been widely used to discover DNA or RNA sequences with novel activities and target selectivity.²⁴ A general procedure of *in vitro* selection for RNA-cleaving DNAzymes is illustrated in Figure 1.9. For a typical selection experiment, a single-stranded DNA library containing a random region (e.g., N₅₀) is chemically synthesized. The library

is often designed to fold into a *cis*-cleaving secondary structure in which the cleavage site is close to the randomized region. Next, a selection pressure is applied to the DNA library aiming for inducing specific catalytic activity. Sequences with catalytic activities are isolated after the RNA cleavage. Commonly used separation methods are based on gel electrophoresis, streptavidin chromatography, and magnetic beads immobilization.^{76, 77} After PCR amplification, the library is enriched with active sequences and can be used for the next round of selection.

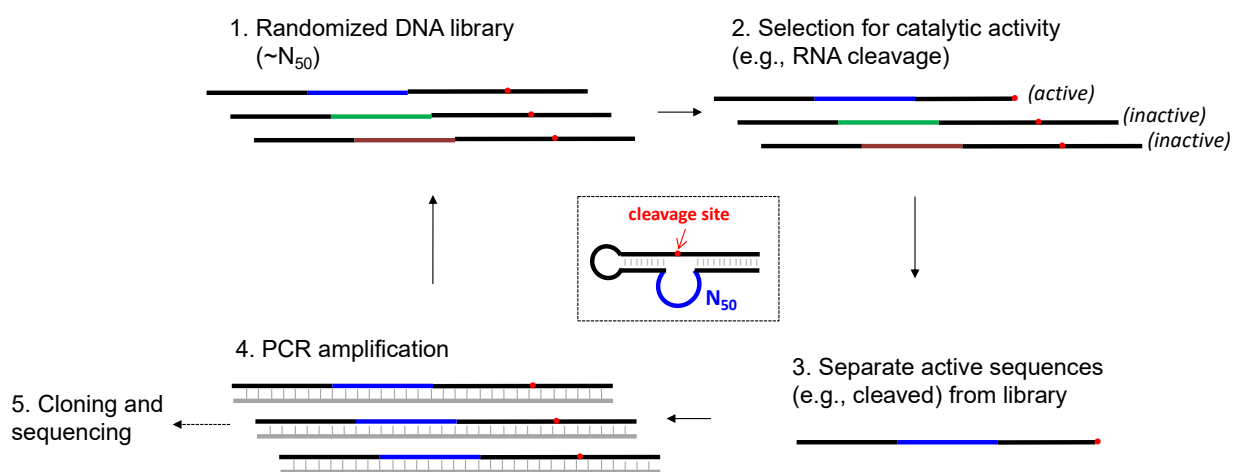


Figure 1.9 A scheme showing the key steps of *in vitro* selection for RNA-cleaving DNAzymes starting from a random DNA library. The boxed region shows the secondary structure of a typical random library with a single RNA linkage embedded (in red). After step 4, the PCR amplification, the resulting duplex product needs to be separated and only one of the strands is useful.

To enrich the DNA pool of catalytically active sequences, the above procedures are repeated for multiple rounds (e.g., 5-15 rounds) until the activity becomes saturated or sufficiently high. To improve the catalytic efficiency, a common way is to increase the selection pressure during the selection such as decreasing the target metal ion concentration. Meanwhile, negative

selections can be carried out to eliminate non-specific activity and improve selectivity.⁷⁸ At the end of the selection, individual sequences in the pool are cloned and sequenced. In general, *in vitro* selection for DNazymes is easier than the selection for ribozymes since no transcription/reverse transcription steps are needed.

1.5.4 DNazymes for metal sensing

Since the majority of RNA-cleaving DNazymes share a similar secondary structure, several universal strategies have been reported for converting DNazymes into biosensors.⁸ A fluorophore/quencher pair can be labeled on one end of the substrate strand and the corresponding end of the enzyme strand, resulting in an initially quenched state (Figure 1.10A). With the addition of metal ions, the reaction occurs and the cleaved fragment bearing the fluorophore is released giving an enhanced fluorescence signal. Such a fluorescent beacon design is commonly used as a proof-of-concept sensing application for DNazymes. To suppress the background signal, an additional quencher can be attached to the other end of the substrate. For example, the 39E DNzyme was converted into a catalytic beacon for UO_2^{2+} detection with a detection limit of 45 pM.⁶³ Alternatively, the fluorophore and quencher can be internally labeled near the cleavage site. Thus, a fluorescence increase can be detected instantly after the cleavage step with a low background signal.⁷⁹

Apart from fluorescent beacons, DNzyme-based colorimetric sensors have been constructed utilizing DNA-functionalized gold nanoparticles (AuNPs).¹⁹ A typical strategy is illustrated in Figure 1.10B, where DNazymes were used as linkers to assemble the AuNPs forming blue colored aggregates.⁸⁰ Upon cleavage, the AuNPs were disassembled resulting in a blue-to-red color change. Additionally, DNzyme-based sensing can also be achieved through

electrochemical signals. For example, the methylene blue-labeled enzyme strand (the 8-17 DNAzyme) can efficiently transfer electrons to the electrode surface upon the Pb^{2+} -induced cleavage (Figure 1.10C).⁸¹

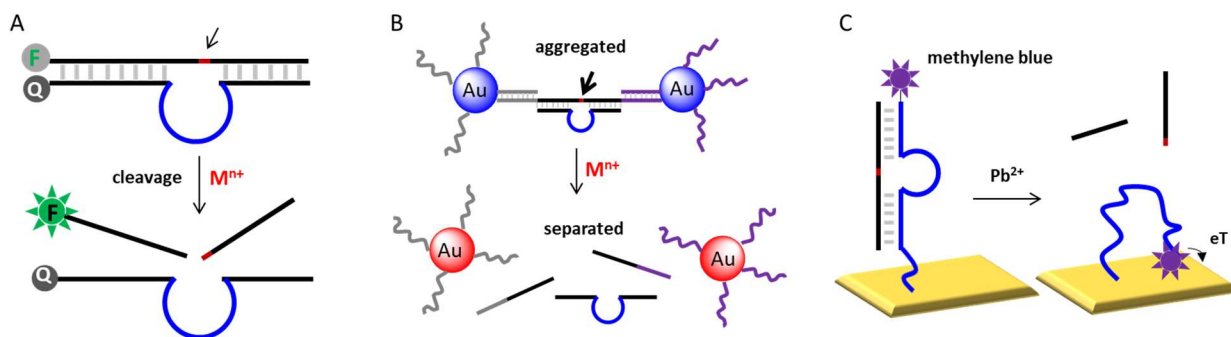


Figure 1.10 Three representative signaling strategies for RNA-cleaving DNAzymes. (A) Cleavage-induced fluorescent signal enhancement in a fluorescence beacon. (B) The disassembly of AuNPs after the cleavage reaction. (C) The conformational change of the 8-17 DNAzyme upon cleavage generates electrochemical signals for Pb^{2+} sensing.

1.6 Metal ions in DNA catalysis

To achieve catalytic activity, protein and nucleic acid enzymes often fold into ordered structures where functional groups are precisely positioned at the catalytic site. Unlike protein enzymes, nucleic acids inherently have limited functional groups (i.e., four nucleobases) available for catalysis in contrast to the variety of amino acids. Due to their pK_a values, nucleobases are generally unwilling to deprotonate or protonate at physiological pH serving as functional groups. Moreover, the heavy negative charge carried by a phosphate backbone hinders an RNA or DNA molecule from folding into a compact structure. Therefore, cations especially metal ions often play critical roles in RNA or DNA catalysis. This is especially evident in RNA-cleaving DNAzymes considering their remarkable sensitivity and selectivity toward a given metal ion cofactor.

1.6.1 Metal binding sites in nucleic acids

Metal ions can interact with various sites in nucleic acids including phosphate backbones, sugar rings, and nucleobases.^{82, 83} Metal ions can stabilize the secondary and tertiary structures by screening the charge repulsion between negatively charged phosphates. Group 1A and 2A metals, especially Na^+ , K^+ , and Mg^{2+} , have been extensively studied for this purpose since they are the abundant inorganic cations *in vivo*. For example, thermodynamic studies demonstrated that monovalent ions and Mg^{2+} can stabilize DNA duplex and tRNA tertiary structures (e.g., increased melting temperatures, T_m).^{84, 85}

The electrostatic interaction can be divided into three classes depending on the interaction strength.^{8, 86} Most of the time, cations interact with a phosphate backbone by a simple diffusion (Figure 1.11A). In aqueous solutions, hydrated metal ions distribute in the electronegative field near nucleic acids forming a diffuse ion atmosphere. This interaction is via a non-specific long-range attraction. For instance, the calculated electrostatic potential near a cross-section of an RNA hairpin was illustrated in Figure 1.11D.⁸⁶ The higher concentrations of monovalent ions also locate at higher electrostatic potential regions. In some cases, metal ions can bind to nucleic acids more tightly and even lose part of their hydration shells. In the outer-sphere interaction, a metal ion interacts with a ligand through its bridging waters (Figure 1.11B), while the inner-sphere interaction indicates a direct coordination without intervening waters (Figure 1.11C). For example, in the solved crystal structure of group I intron, a tri-hydrated Mg^{2+} directly coordinates with three phosphate oxygens in an A-rich bulge (Figure 1.11F).^{87, 88} Meanwhile, another Mg^{2+} in the major groove forms hydrogen bonds with three guanines through its water ligands (Figure 1.11E).

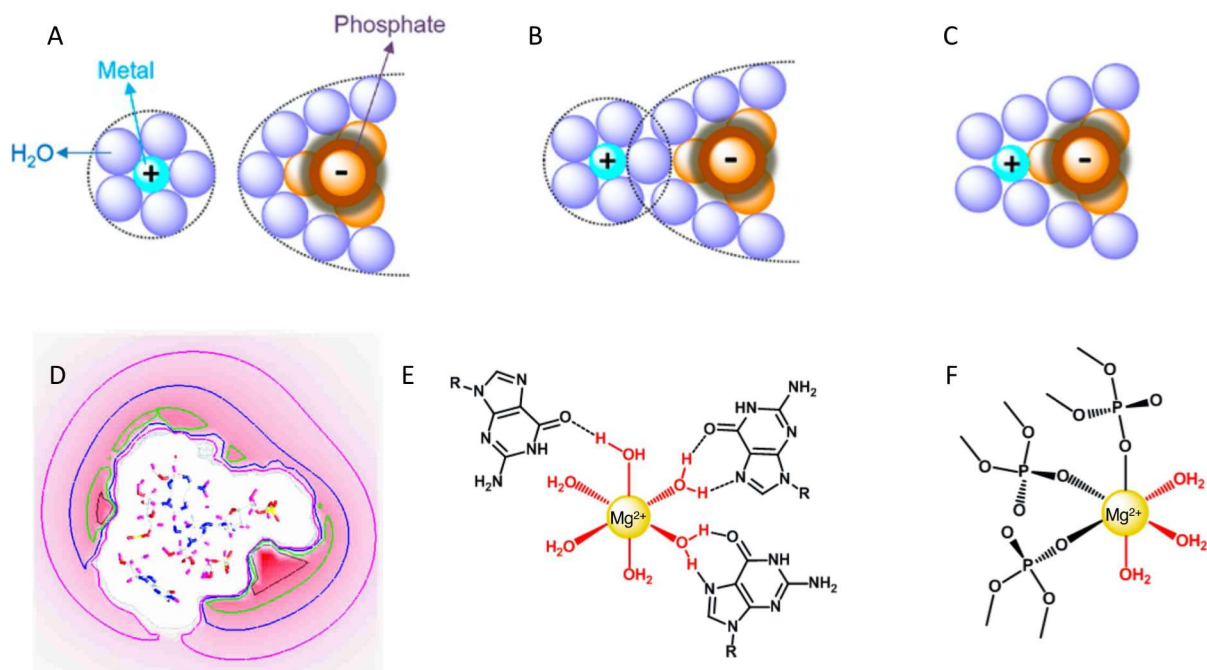


Figure 1.11 A hydrated metal ion interacts with a phosphate through (A) diffusion, (B) outer-sphere binding, and (C) inner-sphere binding. Adapted with permission from ref 8. (D) The ion atmosphere around a cross-section of an RNA hairpin. Reprinted with permission from ref 86. © Copyright 2004 by RNA Society. A Mg²⁺ ion binds with (E) three guanines through hydrogen bonds or (F) with phosphate groups through inner-sphere coordination. Adapted with permission from ref 8.

Metal ions can also coordinate with nucleobases. For instance, transition metal ions such as Zn²⁺, Mn²⁺, Cd²⁺, and Cu²⁺ were found to decrease the melting temperature of DNA duplex at relatively high concentrations.⁸⁹ These metal ions can interact with both phosphates and bases.⁹⁰ Thus, a moderate metal concentration contributes to the charge screening, while a high concentration interrupts the hydrogen binding between nucleobases. Trivalent lanthanide ions as hard Lewis acids can also coordinate with bases.⁹¹ Melting profiles measured by spectrophotometer showed that merely micromolar Tb³⁺ irreversibly denatured dsDNA.⁹² The

common binding sites in nucleobases for metal ions are summarized in Figure 1.12A. All the nucleobases carry no charge at physiological pH. Nevertheless, the endocyclic nitrogen atoms and the exocyclic carbonyl oxygen atoms are promising metal binding sites due to their lone pair electrons. Typical sites are N1, N3 and N7 in adenine; N3, N7 and O6 in guanine; N3 and O2 in cytosine; O2 and O4 in thymine. The exocyclic amino groups are not suitable for the task since their lone electron pairs are delocalized in the heterocyclic rings. The N3 atoms in purines are normally sterically hindered by the sugar, and rearrangement is required for metal binding.⁹³ In addition, the N1 position of thymine can also serve as a binding site when it becomes protonated ($pK_a=9.9$). A special case is the T-Hg²⁺-T base pair (Figure 1.12C) where the binding of Hg²⁺ removes the N1 proton at neutral even acidic pH. An NMR study demonstrated that the Hg²⁺ coordination can stabilize a DNA duplex containing T-T mismatches.⁹⁴ The site-specific binding between metal ions and nucleobases also exists in C-Ag⁺-C base pair (Figure 1.12B).

Within specific sequences, monovalent ions can stabilize nucleic acid structures through inner-sphere coordination. G-quadruplex (GQ) is a noncanonical nucleic acid structure formed within G-rich sequences. A GQ consists of two or more G-tetrads stacking together. Each G-tetrad (Figure 1.12D) contains four guanines assembled by Hoogsteen hydrogen bonding between N1/N2 (donor) and O6/N7 (acceptor). Monovalent metal ions play important roles in stabilizing a GQ structure. A K⁺ ion can lie between two G-tetrads and coordinate with eight O6 atoms, while a smaller Na⁺ can coordinate within a G-tetrad plane.⁹⁵ Overall, K⁺ is more efficient than Na⁺ in stabilizing a GQ structure which was correlated to the relatively lower energy cost of K⁺ dehydration.⁹⁶ GQ is also an important structural motif for DNAzymes, enabling porphyrin metalation and peroxidase-like activities.^{97, 98}

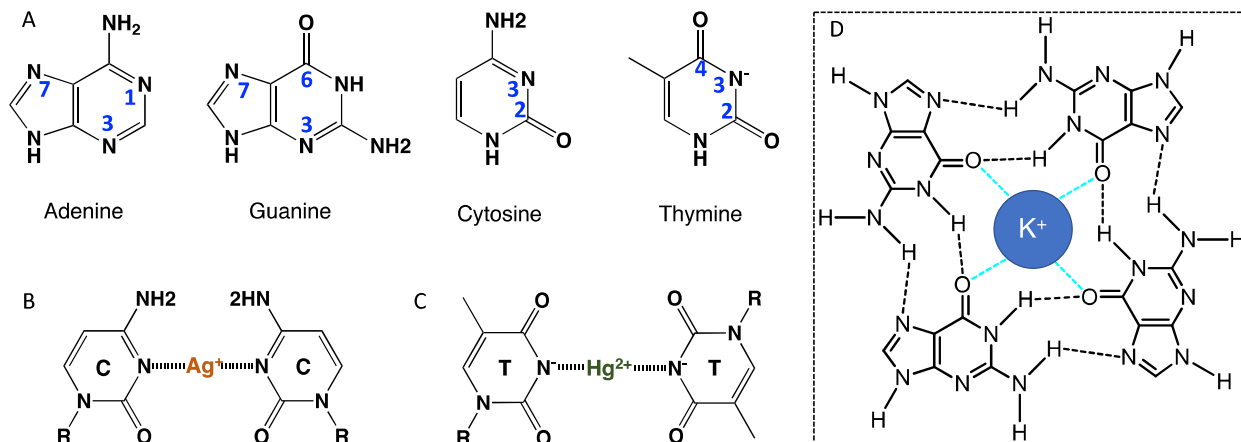


Figure 1.12 (A) Metal ion-binding sites in nucleobases. (B) The C-Ag⁺-C base pair. (C) The T-Hg²⁺-T base pair. (D) A G-tetrad stabilized by K⁺ coordination.

1.6.2 Metal ions in RNA cleavage reaction

In a nucleic acid enzyme, metal ions can facilitate the catalysis by playing a structural role or directly participating in the chemistry. From a structural perspective, metal ions can stabilize the tertiary structure or initiate the folding into a native structure. To date, the metal-dependent folding of the 8-17 DNAzyme has been extensively studied.⁹⁹⁻¹⁰¹ The 8-17 DNAzyme performs cleavage activity in the presence of various metal ions with the following descending order: Pb²⁺ > Zn²⁺ > Cd²⁺ > Mg²⁺ ~ Ca²⁺. Lu and others utilized FRET (fluorescence resonance energy transfer) at the single-molecular level (smFRET) to monitor the global folding of 8-17.¹⁰² The addition of Zn²⁺ and Mg²⁺ induced the folding of DNAzyme into a compact structure which supported the subsequent cleavage activity (Figure 1.13). On the contrary, no global folding was detected in the presence of Pb²⁺ which is the most effective cofactor for the cleavage. Since the cleavage happens without a precedent folding process, the Pb²⁺ ion may bind to a prearranged conformation and directly participate in the chemistry. These results also demonstrated the capability of DNAzymes

using multiple catalytic pathways which has been observed in some ribozymes.¹⁰³ A later study using the contact photo-crosslinking demonstrated that Pb^{2+} can induce a local folding near the active site instead of a global folding.¹⁰¹

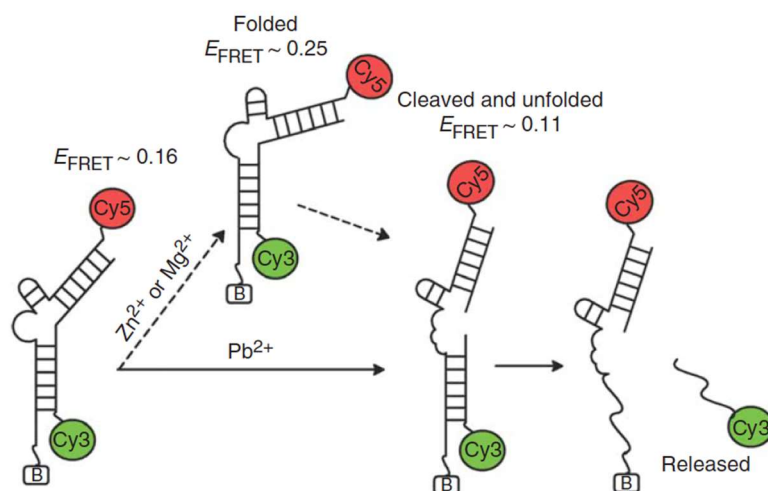


Figure 1.13 Divalent metal ion-induced folding of the 8-17 DNAzyme studied by FRET. Reprinted from ref 102. Copyright © 2007 Nature Publishing Group.

Apart from 8-17, the metal-induced folding was investigated in other DNAzymes. In the 39E DNAzyme, a FRET study showed that UO_2^{2+} -induced folding can only be detected under low ionic strength (30 mM Na^+).¹⁰⁴ Meanwhile, Zn^{2+} and Mg^{2+} also induced folding in 39E and inhibited the UO_2^{2+} -specific cleavage activity. In the Ag10c DNAzyme, 2-aminopurine (2AP) modifications were applied to observe the folding of the Ag^+ -binding aptamer identified in the enzyme strand.¹⁰⁵ By comparing with inactive mutants, they confirmed that the Ag^+ -induced folding is indeed crucial for its cleavage activity.

On the other hand, metal ions can directly participate in the RNA cleavage reaction. To date, the metal ion-assisted mechanism has been well-established benefitting from the extensive

biochemical and structural studies on self-cleaving ribozymes.¹⁰⁶ During a phosphoryl transfer reaction, metal ions can function in many possible ways (Figure 1.14). In aqueous solution, a metal-bound water molecule has a lower pK_a value than a free water molecule. The hydrated metal ion may release a proton and undergo hydrolysis depending on its pK_a value (Table 1). For example, the first pK_a of Mg^{2+} -bound water is lower than that of Pb^{2+} , suggesting that water molecules coordinated with Pb^{2+} is easier to deprotonate than Mg^{2+} .

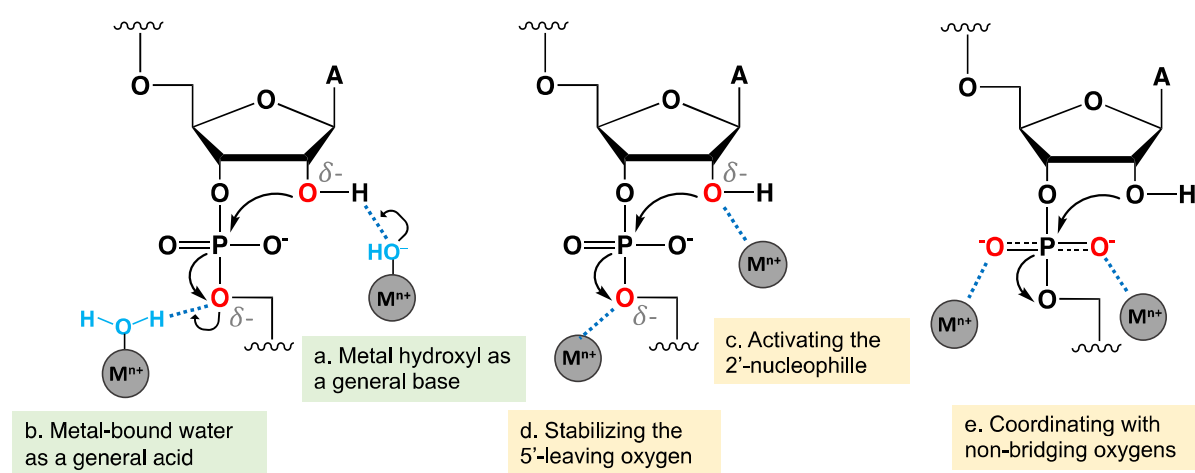


Figure 1.14 Possible catalytic roles of metal ions playing in an RNA cleavage reaction.

After deprotonation, the metal-bound hydroxyl group can serve as a general base, abstracting a proton from the internal nucleophile. The activated 2'-OH thus can better perform the nucleophilic attack on the neighboring phosphorus atom. Alternatively, inner-sphere coordination from a metal ion can also assist the deprotonation of 2'-OH. In addition, metal ions can stabilize the transition state by coordinating to the non-bridging oxygens. Another mechanism involves interacting with the leaving group. A metal-bound water (as a general base) or metal ion (as a Lewis acid) can stabilize the developing negative charge on the 5'-O.

Table 1. Chemical properties of several multivalent metal ions.^{106, 107}

Ion	Ionic radius (Å)	Coordination number	Typical geometry of inner-sphere complex	First p <i>K</i> _a of [M(H ₂ O) _x] ⁿ⁺
Mg ²⁺	0.57-0.89	6	Octahedral	11.4
Ca ²⁺	0.99	8	Square antiprism	12.6
Mn ²⁺	0.66-0.96	4,6,8	Octahedral	10.6
Zn ²⁺	0.60-0.90	4,6,8	Tetrahedral	8.2-9.8
Ni ²⁺	0.55-0.69	4,6	Octahedral	6.5-10.2
Fe ²⁺	0.63	4	Octahedral	6.0-6.7
Co ²⁺	0.72	6	Octahedral	7.6-9.9
Pb ²⁺	0.98-1.5	4,6,8,10,12	Octahedral	6.5-8.4
UO ₂ ²⁺	0.8 (U ⁶⁺)	6,8	Octahedral	5.7
Eu ³⁺	0.95	9	Variable	4.8-8.5

1.6.3 Methods to study metal binding sites

Due to limited availability of structural information, so far, mechanistic studies of DNAzymes were achieved mainly by biochemical methods. Since metal binding is often crucial for DNAzyme catalysis, extensive efforts have been made in identifying metal binding site in RNA-cleaving DNAzymes.¹⁰⁸ Phosphorothioate (PS) modification on the cleavage site has been widely used to probe metal binding on the scissile phosphate (Figure 1.15).^{109, 110} In a typical case, a non-thiophilic metal ion such as Mg²⁺ can directly interact with one of the non-bridging oxygens. A PS modification can significantly inhibit (often >100-fold) the cleavage activity compared to the original PO-substrate (a normal thio effect).^{111, 112} The activity loss normally will be rescued by the addition of more thiophilic metal ions (e.g., Mn²⁺ or Cd²⁺). Most of time, metal ions were determined to interact with the pro-*R*_p oxygen in the catalysis of ribozymes and DNAzymes. This observation however has exceptions. For example, in the Dy10a DNAzyme (Figure 1.8E), a

significant inhibition (>1000-fold) was observed for both the R_p and S_p isomers, indicating that both non-bridging oxygens are interacting with metal ions.⁶⁹

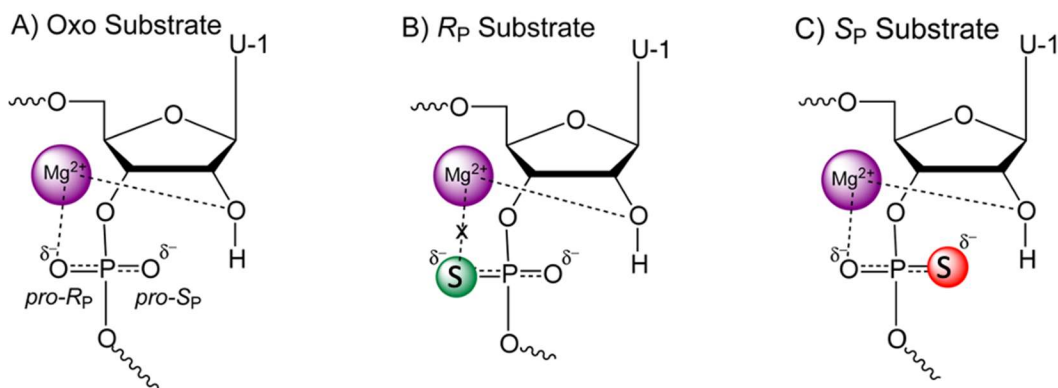


Figure 1.15 PS modification on the R_p substrate results in a thio effect by disturbing the interaction between a catalytic Mg^{2+} ion and the *pro-R_p* oxygen. Adapted with the permission from ref 112.

When nucleobases are involved in metal binding, DNA footprinting can provide valuable information. For example, dimethyl sulfate (DMS) footprinting has been applied to identify metal ion-binding aptamer in DNAzyme sequences. DMS can methylate the N7 position of a guanosine residue allowing it to be cleaved by piperidine. However, when the guanosine is protected in a folded structure, it can be prevented from methylation and thus from cleavage. By comparing DMS footprinting patterns, a silver-specific aptamer has been identified in the Ag10c DNAzyme.⁷⁵ Nevertheless, it needs to be noted that most DNAzymes and ribozymes do not have such well-defined metal binding aptamers. Metals only need to transiently bind to the active site to exert their catalytic functions.

Spectroscopic methods are also very useful in characterizing metal ion-nucleic acid interaction. Ultraviolet-visible (UV-vis), nuclear magnetic resonance (NMR), electron paramagnetic resonance (EPR), and X-ray absorption spectroscopy (XAS) are just a few examples

to obtain metal binding information.⁸³ The fluorescence spectroscopy is a popular tool due to its high sensitivity, rich molecular information, and simplicity in instrumentation. For example, the global or local folding of many RNA-cleaving DNazymes have been studied by fluorescence techniques such as Tb³⁺ luminescence, 2AP modification, and fluorescence resonance energy transfer (FRET).^{73, 102, 113}

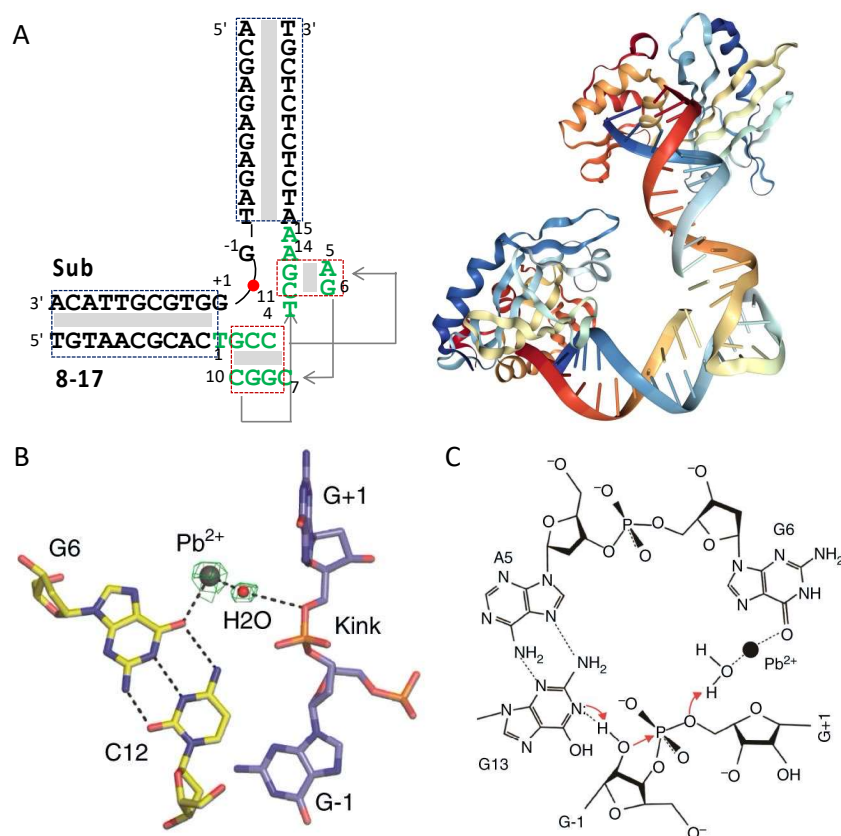


Figure 1.16 (A) The secondary (left) and crystal structure (right) of the RNA-cleaving DNzyme, 8-17, revealing a V-shaped overall folding (PDB: 5XM8). (B) A Pb²⁺-bound water captured in the catalytic core. (C) A hypothetical mechanism of 8-17 catalysis including a Pb²⁺-bound water molecule as a general acid and a conserved guanine (G13) as a general base. Adapted with the permission from Ref 114. Copyright © 2017 Springer Nature.

The most direct insights are often provided by structural biology data such as NMR and X-ray crystallography. Many RNA-cleavage ribozymes have crystal structures, which contributed significantly to their fundamental understanding.³¹ So far, only two DNazymes have crystal structures: one for RNA cleavage and the other for RNA ligation.^{114, 115} These structures were obtained after more than 20 years of the report of the first DNzyme. The challenges of crystallization suggest floppy and dynamic behavior of DNazymes and coexistence of multiple structures, which also posed challenges for NMR. The only crystal structure of an RNA-cleaving DNzyme (8-17) revealed a V-shaped folding containing two helical substrate-binding arms and a 15-nt pseudoknot catalytic core (Figure 1.16A).¹¹⁴ The 8-17 DNzyme catalyzes the RNA cleavage via the general acid-base mechanism. At the active site, a Pb^{2+} ion activates a water molecule and stabilizes the 5'-leaving oxygen as a general acid (Figure 1.16B), while a conserved guanine serves as a general base facilitating the deprotonation of 2'-OH group (Figure 1.16C). Biochemical studies on the pH-rate profiles also confirmed the general acid-base mechanism.^{116, 117} A recent dynamical simulation further revealed the supporting role of Na^+ during the catalysis.¹¹⁸ The crystal structure also revealed a similar conformation of the catalytic site between 8-17 and the hammerhead ribozyme.

1.7 Na^+ -dependent RNA-cleaving DNazymes

The study of nucleic acid enzymes has been mainly focusing on divalent and trivalent metal ions. With their ability to bind to DNA/RNA specifically, polyvalent metal ions are essential for folding and catalysis of nucleic acids.¹¹⁹ Monovalent ions such as Li^+ , Na^+ , K^+ only bind to nucleic acids non-specifically and distribute as a “ion atmosphere”. Surprisingly, studies demonstrated that the exchange inert cobalt hexammine [$\text{Co}(\text{NH}_3)_6^{3+}$] can fully replace Mg^{2+} in the hairpin

ribozyme catalysis.^{120, 121} These results suggested that its catalytic mechanism requires no inner-sphere coordination from metal cofactors. Instead, the rate enhancement could be explained by the structural role of divalent metal ions, or stabilization effect on the transition state through an outer-sphere coordination. Furthermore, molar concentrations of monovalent cations (e.g., Li^+ , Na^+ , K^+ , NH_4^+) were found to support cleavage without divalent metals in many self-cleaving ribozymes including the hairpin, hammerhead, VS, and HDV ribozymes.^{122, 123} These studies thus enabled us to reconsider the essential role of divalent ions in catalysis. Despite that metal ions are efficient cofactors, ribozymes are capable of performing catalysis using RNA functional groups. In addition, it is possible that ribozymes may adapt to multiple catalytic mechanisms depending on the experimental conditions.¹²⁴

1.7.1 The NaA43 DNAzyme

The searching for RNA-cleaving DNAzyme in the absence of divalent metal ions started from 1997. Geyer and Sen performed the *in vitro* selection of DNAzyme in the presence of Na^+ and EDTA.¹²⁵ The activity of the obtained DNAzyme was indeed independent on divalent metal ions with a rate enhancement of $\sim 10^8$ over the uncatalyzed reaction. However, the catalytic role of Na^+ can be replaced by other monovalent ions (e.g., NH_4^+ , K^+) suggesting a lack of metal selectivity. From the analytical perspective, functional nucleic acids with selectivity and sensitivity toward Na^+ are always attractive. As one of the most abundant cations in biology, Na^+ concentration is highly important in regulating cellular processes such as signal transduction and hormone action.¹²⁶ The detection of Na^+ with high selectivity over other monovalent ions remains challenging both *in vitro* and *in vivo*.

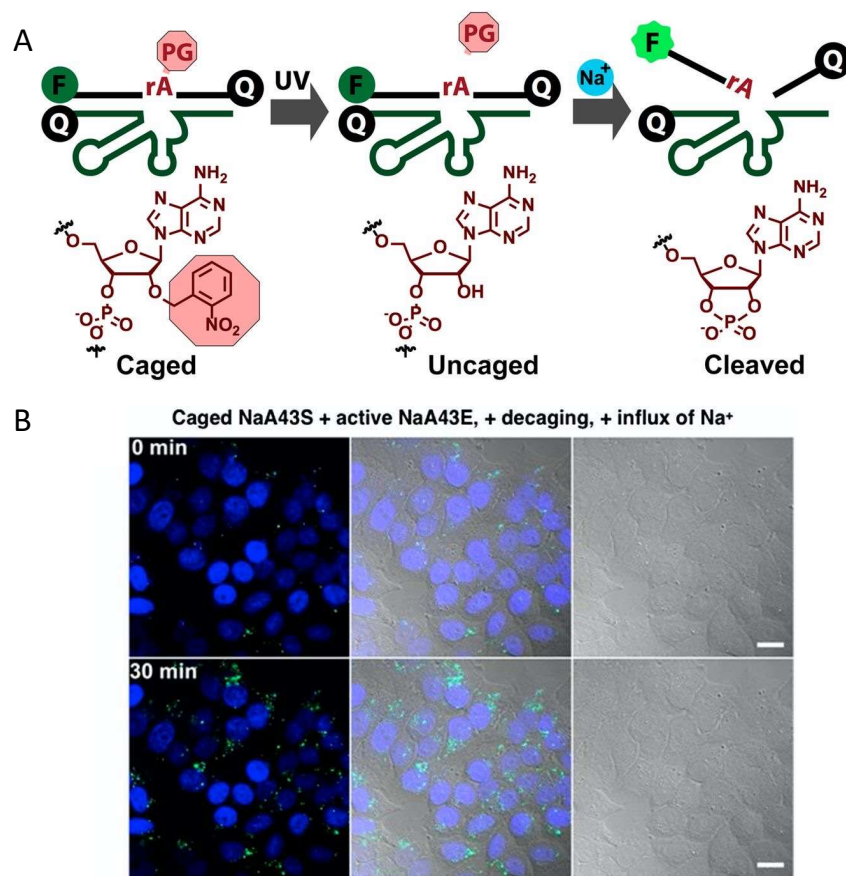


Figure 1.17 (A) The NaA43 DNAzyme-based intracellular sensing of Na⁺ based on the photocaging strategy. (B) Confocal microscopy images of HeLa cells transfected with caged NaA43 complex showing the Na⁺ influx upon irradiation. Reprinted with permission from ref 72. Copyright 2015 National Academy of Sciences.

In 2015, Lu and others reported the first Na⁺-selective DNAzyme obtained from *in vitro* selection.⁷² The NaA43 DNAzyme (Figure 1.8H) catalyzed the RNA cleavage with a rate constant of $0.11 \pm 0.01 \text{ min}^{-1}$ in 400 mM Na⁺. Most importantly, it displayed a remarkable selectivity (>10,000-fold) over other metal ions. They further designed a catalytic beacon by labeling fluorophore and quencher to the substrate and enzyme strands. By measuring the fluorescence signal, the cleavage rate of NaA43 increased with the addition of Na⁺, giving an apparent

dissociation constant of 39.1 ± 2.3 mM. The limit detection was determined to be $135 \mu\text{M}$ ($3\sigma/\text{slope}$). Furthermore, they applied the NaA43 sensor for intracellular Na^+ imaging. To prevent cleavage during the DNzyme delivery, they used a photolabile *o*-nitrobenzyl group to cage the 2'-OH at the cleavage site (Figure 1.17A). The G8 polypeptide was then used to deliver the DNzyme sensor into the cytoplasm of HeLa cells. Upon brief irradiation at 365 nm, the caging group was removed which in turn restored the cleavage activity. By monitoring the fluorescence, they imaged the influx of Na^+ from extracellular medium into the cell induced by ionophores (Figure 1.17B).

1.7.2 Identify the Na^+ -binding domain

Interestingly, a close examination of the NaA43 DNzyme revealed a 16-nt motif that is also present in the lanthanide-dependent DNzyme, Ce13d (Figure 1.8G). Thus, biochemical studies have been conducted to understand their activities. The Ce13d DNzyme was revealed to require not only lanthanide ions (e.g., Ce^{3+}) but also Na^+ for its cleavage activity.⁷³ By studying the PS-modified substrates, Ce^{3+} was determined to interact with the scissile phosphate. Their common 16-nt motif was revealed to be a Na^+ -binding aptamer by studying the Tb^{3+} luminescence and DMS footprinting. Mutation studies identified a conserved guanine in NaA43 which may play a catalytic role.

Furthermore, the Na^+ -induced folding was detected by using 2AP modifications. 2AP is a fluorescent adenine analog whose emission intensity is highly sensitive to local base stacking environment.¹²⁷ By introducing a 2AP modification in the substrate strand, a gradual increase in fluorescence was detected by titrating Na^+ indicating a relaxed base stacking near the 2AP probe (Figure 1.18). On the contrary, fluorescence quenching was observed after replacing a non-

conserved adenine in the enzyme strand with 2AP. This result suggested the enzyme loop folding into a more compact structure upon Na^+ binding. Since the signal was highly Na^+ -specific, they further designed a folding-based Na^+ sensor by introducing a double mutation which largely enhanced the signal. This aptamer was later found to bind to K^+ , which resulted in misfolding of DNase and an inhibited activity.¹²⁸

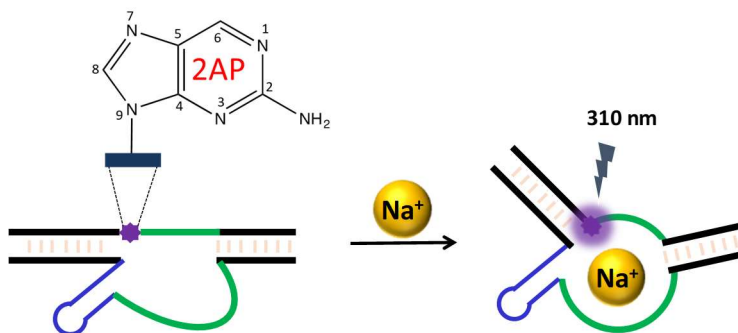


Figure 1.18 The folding-based sensing of Na^+ using 2AP-labeled Ce13d DNase and the chemical structure of 2-aminopurine.

1.7.3 The EtNa DNase

The EtNa DNase is another Na^+ -specific sequence selected by our lab.⁶⁵ The unexpected cleavage of EtNa was determined to occur during the isopropanol precipitation step. The biochemical characterization revealed the requirement of both alcoholic solvents and Na^+ . In 54% ethanol, the cleavage rate of EtNa measured in the presence of 120 mM Na^+ was 2.0 h^{-1} , whereas its activity in water was nearly undetectable. Interestingly, a later study found that freezing in water can enhance its Na^+ -mediated cleavage.¹²⁹ For example, the apparent K_d measured under frozen condition was over 20 times lower than room temperature. The mechanism behind this unique activity of EtNa was related to a higher local Na^+ concentration caused by both ethanol and freezing.

In water, the EtNa cleavage was more sensitive and selective toward Ca^{2+} .⁶⁶ For instance, the cleavage measured in 2 mM Ca^{2+} was ~90 time faster than in 2 mM Mg^{2+} . The double-log plots of rate versus metal concentration indicated two Ca^{2+} -binding sites in EtNa, but only one binding site for Mg^{2+} . This result thus explained its high selectivity for Ca^{2+} over Mg^{2+} . Strong thio effects were observed with both R_p and S_p isomers of PS-modified substrates, suggesting that Ca^{2+} bind to both non-bridging oxygens at the scissile phosphate.

1.8 Research focus

Compared to the development in DNAzyme applications, our fundamental understanding on the catalytic mechanism is still limited. Previous efforts have been mainly focusing on studying the role of metal ions, while the nucleotide-based catalysis has not been fully revealed in DNAzymes. In recent years, several Na^+ -dependent DNAzymes have been reported, indicating DNA catalysis without divalent or trivalent metal ions directly involved in the reaction. Therefore, my thesis research is focused on *in vitro* selection of monovalent-metal-dependent DNAzymes and ribozymes, and provide insights into their catalytic mechanism in the absence of divalent metal ions. In Chapter 2, a new Na^+ -dependent DNAzyme, NaH1, was selected under a relatively acidic condition, which turned out to be a variant of the previous NaA43 DNAzyme. Compared to other competing monovalent ions, NaH1 also displays an excellent selectivity for sodium. The NaA43 and NaH1 DNAzymes share the same 16-nt Na^+ -binding motif but differ in one or two nucleotides in a small catalytic loop. Nevertheless, they display an opposite pH-dependency, implicating distinct catalytic mechanisms. In Chapter 3, rational mutation studies demonstrated conserved nucleotide residues in these DNAzymes. The pH-rate profiles using pK_a -perturbed analogs further

revealed their distinct general acid-base mechanisms. Further biochemical experiments were conducted to provide more insights into the active site.

The sodium-dependent DNAzymes do not require multivalent metal ion for catalysis and can fold into well-defined structures. Thus, they provided an excellent platform for studying the metal ion effect at the cleavage site. In Chapter 4, I used them as models to explore the role of Pb^{2+} in RNA cleavage which has been frequently observed. By examining the Pb^{2+} effect, the capability of Pb^{2+} to bind specifically to the cleavage site has been demonstrated. Upon binding, the hydrated Pb^{2+} can serve as a poor general acid and facilitate the RNA cleavage. In a special case, Pb^{2+} can facilitate the binding of Ca^{2+} cofactor and significantly enhance the activity of a Ca^{2+} -dependent DNAzyme. The mechanism study on Pb^{2+} activity further revealed versatile roles of Pb^{2+} in RNA cleavage which is important for understanding DNAzyme catalysis.

Given the excellent Na^+ -binding selectivity of DNAzymes, a natural question is whether similar ribozymes exist. In the last chapter, I further performed *in vitro* selection to search for Na^+ -dependent self-cleaving ribozymes. Surprisingly, a novel ribozyme was obtained displaying a site-specific cleavage activity under denaturing conditions, such as high temperatures, denaturing solvents, and low salt concentrations.

Chapter 2. An *In Vitro* Selected DNAzyme Mutant Highly Specific for Na⁺ in Slightly Acidic Conditions^b

2.1 Introduction

Sodium is one of the most common and important metal ions in the environment and in biology. A high sodium level is a reflection of physiological disorders such as high blood pressure and water retention. Over the years, various methods have been developed to detect Na⁺ and most efforts were focused on crown ether-based fluorescent chelators.^{130, 131} Using DNA as a platform for developing metal sensors has been practiced for nearly two decades and many DNA sequences have been identified to bind to a wide range of metals.^{8, 19} These mainly include two classes of functional DNA molecules: aptamers and DNAzymes.^{11, 132} Aptamers perform a simple binding function, while DNAzymes are catalysts and they usually require a divalent metal ion for activity, such as Pb²⁺,⁵ Zn²⁺,¹³³ Cu²⁺,^{71, 134} UO₂²⁺,⁶³ Cd²⁺,⁷⁰ Ca²⁺,⁶⁶ and Hg²⁺.¹³⁵ Recently, trivalent lanthanides were also used in DNA-based catalysis.⁶⁸ Aside from Ag⁺,^{74, 136} binding monovalent cations (e.g. K⁺, and Tl⁺) mainly relied on G-quadruplex DNA.^{137, 138}

Using DNA for Na⁺ recognition has not caught much attention until 2015. Before that, Na⁺ was mainly used as a buffer salt to control ionic strength without considering its specific binding by DNA.¹²⁵ Recently, a few highly Na⁺-specific RNA-cleaving DNAzymes have been reported. The NaA43 DNAzyme was selected by Lu and coworkers, and it has a high sequence analogy to

^b This chapter is the basis for a published manuscript: Ma, L.; Liu, J., An In Vitro Selected DNAzyme Mutant Highly Specific for Na⁺ in Slightly Acidic Conditions. *ChemBioChem* **2019**, *20* (4), 537-542.

a lanthanide-dependent DNAzyme named Ce13d discovered in our lab.^{67, 72} Further assays indicated that Ce13d also requires Na^+ , suggesting a common Na^+ aptamer in these two DNAzymes.^{73, 139} Previous studies also discovered the EtNa DNAzyme that uses a different mechanism for specific Na^+ recognition.⁶⁵

So far, most of the work has been focused on the characterization of previously selected DNAzymes. Rational mutations were performed to understand individual nucleotides important for catalysis and metal binding,^{110, 140} while efforts on new selections were limited. New selections under different conditions can explore a larger sequence space and may offer new insights. In this chapter, I reported a mutant of NaA43, which was discovered from a selection effort using cobalt complexes as intended metal cofactors. The new DNAzyme sequence can be considered as a mutant since it is very similar to NaA43 in sequence, and it also catalyzes in the presence of Na^+ alone with an excellent Na^+ specificity. However, this mutant displayed a different pH optima indicating a distinct catalytic mechanism. This study further broadens our understanding of Na^+ -dependent DNAzymes and demonstrates the performance of a sodium sensor derived from this mutant.

2.2 Results and discussions

2.2.1 *In vitro* selection

The initial intention of *in vitro* selection was to obtain a RNA-cleaving DNAzyme using $\text{Co}(\text{NH}_3)_6^{3+}$ as metal cofactors. As an exchange-inert metal complex, $\text{Co}(\text{NH}_3)_6^{3+}$ cannot interact with nucleic acids through an inner-sphere coordination.¹⁴¹ With a similar size and geometry as $\text{Mg}(\text{H}_2\text{O})_6^{2+}$, $\text{Co}(\text{NH}_3)_6^{3+}$ was found to support the hairpin ribozyme cleavage with a comparable efficiency as Mg^{2+} .¹²¹ Thus, a $\text{Co}(\text{NH}_3)_6^{3+}$ -promoted DNAzyme can offer new insights into the

cleavage mechanism in terms of outer-sphere coordination. Our *in vitro* selection followed an established protocol in the lab with an initial library containing approximately 10^{14} random DNA sequences (Figure 2.1A).⁶⁷ Each DNA sequence contains a 50-nt random region flanked by two short binding arms in a *cis*-cleaving form (Figure 2.1B). This size is chosen as a balance of complexity, diversity, and sequence space coverage. The single RNA linkage (rA, ribo-adenine) represents the cleavage site.

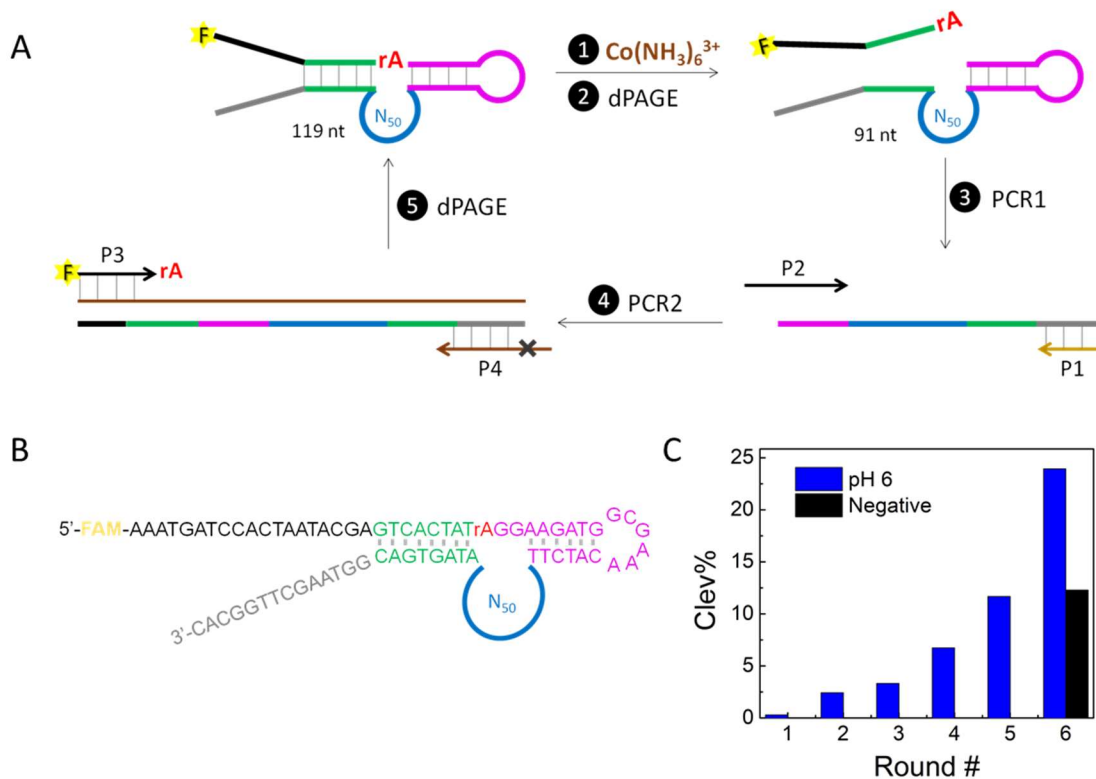


Figure 2.1 *In vitro* selection. (A) Our scheme for $\text{Co}(\text{NH}_3)_6^{3+}$ -dependent DNAzyme selection including five main steps. Two PCR steps were used to amplify the cleaved sequence and regenerate the full-length library. P3 primer had a FAM label and the rA, while P4 had a polymer spacer to stop PCR extension (denoted by a cross) beyond this point. Two denaturing polyacrylamide gel electrophoresis (dPAGE) steps were carried out to separate the cleavage product and to recover the positive strand from the duplex after PCR, respectively. (B) The sequence of the initial library containing an N_{50} randomized region with a FAM

labeled at the 5' end. (C) Progress of the *in vitro* selection at pH 6.0 showing the cleavage percentage of each round. Throughout the selection, the concentration of $\text{Co}(\text{NH}_3)_6\text{Cl}_3$ was 10 μM with 1 h incubation. The black bar is the cleavage yield at round 6 without the addition of $\text{Co}(\text{NH}_3)_6\text{Cl}_3$.

In each round, the library was incubated in the selection buffer (50 mM MES buffer, pH 6.0, 25 mM NaCl, 1 mM EDTA) with 10 μM $\text{Co}(\text{NH}_3)_6\text{Cl}_3$ added. After 1 h of incubation, the cleaved sequences were harvested using gel electrophoresis and then amplified by two PCR reactions to seed the next round of selection. With a FAM-label attached, the cleavage yield of each round was quantified by 10% dPAGE (Figure 2.1C). A gradual increase in the cleavage yield was observed (blue bars). At round 6, ~24% of the library was cleaved after the selection step. To conform the activity, one round of negative selection was performed using the selection buffer alone without $\text{Co}(\text{NH}_3)_6^{3+}$. However, ~12% cleavage was still observed (black bar), indicating that DNA sequences enriched in the library may not require $\text{Co}(\text{NH}_3)_6^{3+}$ for activity. At this point, I decided to stop the selection and send the final library for deep sequencing.

2.2.2 Sequence analysis

The deep sequencing yielded a total of 97,533 sequences. After sequence alignment, 21,919 reads were assembled into more than one thousand families. The most populated 200 families accounted for around 50% of the analyzed sequences. Table 2 lists the sequences from the 20 most abundant families. Among them, 19 families contain a 16-nt motif of AGGTCAAAGGTGGGTG (purple colored) in the N_{50} region which is highly conserved. This 16-nt motif was also found in the Ce13d and NaA43 DNAzymes.^{73, 139} Compared to the NaA43 sequence, the major difference lies in two nucleotides near the 3'-end of the N_{50} region. Statistically,

this position has roughly an equal chance of being T and A in our library, while NaA43 is a G at this position.

Table 2. The N₅₀ random region of representative families from the round 6 selection pool comparing with the NaA43 sequence. A homogeneous motif of 16 nucleotides (purple colored) was found in 19 out of the 20 listed families. The nucleotide varies most frequently was highlighted in red color. W represents either A or T.

Family #	Sequence (5'---N ₅₀ ---3')	# copy
1	-----GGAGCCATAGGTCAAAGGTGGGTGTGGTCGTATCATATCGACCA GC AWT-----	84
2	-----GGAGCCATAGGTCAAAGGTGGGTGTGGTCGTATCATATCGACCA GC AWT-----	81
3	-----GGAGCCATAGGTCAAAGGTGGGTGTGGTCGTATCATATCGACCA GC AAT-----	56
4	-----GGAGCCATAGGTCAAAGGTGGGTGTGGTCGTATCATATCGACCA GC AAT-----	49
5	-----GGAGCCATAGGTCAAAGGTGGGTGTGGTCGTATCATATCGACCA GC AAT-----	46
6	-----GGAGCCATAGGTCAAAGGTGGGTGTGGTCGTATCATATCGACCA GC AWT-----	44
7	-----GGAGCCATAGGTCAAAGGTGGGTGTGGTCGTATCATATCGACCA GC AWT-----	43
8	-----GGAGCCATAGGTCAAAGGTGGGTGTGGTCGTATCATATCGACCA GC AAT-----	41
9	-----GGAGCCATAGGTCAAAGGTGGGTGTGGTCGTATCATATCGACCA GC AAT-----	39
10	----GGAGCCATAGGTCAAAGGTGGGTGAGAGTCGTATCATAACGACT CG CAAT-----	38
11	-----GGAGCCATAGGTCAAAGGTGGGTGTGGTCGTATCATATCGACCA GC AWT-----	38
12	-----GGAGCCATAGGTCAAAGGTGGGTGTGGTCGTATCATATCGACCA GC AWT-----	38
13	----GGAGCCATAGGTCAAAGGTGGGTGAGAGTCGTATCATAACGACT CG CAAT-----	36
14	-----GGAGCCATAGGTCAAAGGTGGGTGTGGTCGTATCATATCGACCA GC AWT-----	35
15	-----GGAGCCATAGGTCAAAGGTGGGTGTGGTCGTATCATATCGACCA GC AAT-----	34
16	-----AGAGGCTTGCAATAAGCTGAGGGATTGAGCATGCGAGGAGTGGTAGTGGAT-----	32
17	-----GGAGCCATAGGTCAAAGGTGGGTGTGGTCGTATCATATCGACCA GC AAT-----	32
18	-----GGAGCCATAGGTCAAAGGTGGGTGTGGTCGTATAATATCGACCA GC AAT-----	30
19	-----GGAGCCATAGGTCAAAGGTGGGTGTGGTCGTATCATATCGACCA GC AAT-----	28
20	-----GGAGCCATAGGTCAAAGGTGGGTGTGGTCGTATCATATCGACCA GC AAT-----	28
NaA43	-----CCAGGTCAAAGGTGGGTGAGGGGACGCCAAGAGTCCCC GC GGT-----	

The main difference in these three DNazymes lies in the few nucleotides in blue. The Ce13d (Figure 2.3A) requires both Ce^{3+} and Na^+ for activity. The small motif of TG₂₃GCG in NaA43T was believed to replace the role of Ce^{3+} in the cleavage reaction. The guanine at the 23 position (G₂₃) cannot be mutated indicating its critical role for catalysis.⁷³ Interestingly, NaH1 has a TACG motif located at the corresponding position, and the critical guanine in NaA43T was removed. A closer examination of our selection library did not yield any sequence with the exact TGGCG motif and likely a mutant of NaA43 was obtained. On the other hand, in the original NaA43 selection paper,⁷² sequences containing a TACG motif were found in their Class A-I but with incomplete Na^+ -binding loops. Therefore, the NaH1 obtained from selection is indeed a new sequence that was not reported before either from *in vitro* selection or from rational mutations. Since this sequence appears to be interesting, I mainly focused on it in this work. Future efforts will be made with $Co(NH_3)_6^{3+}$ in a Na^+ -free buffer, which may eliminate such Na^+ -dependent sequences.

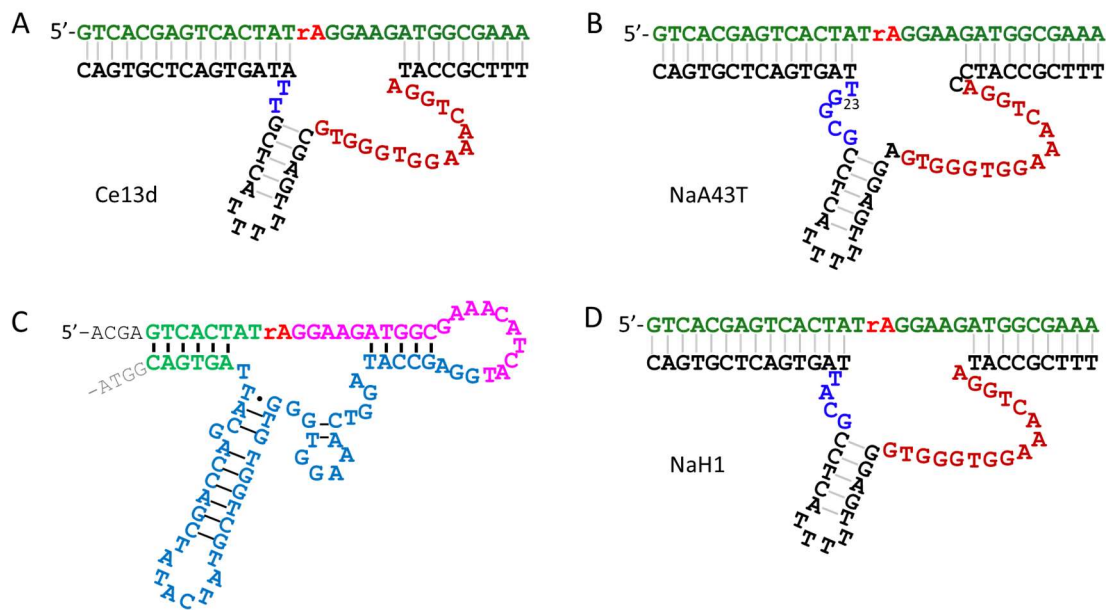


Figure 2.3 Secondary structures of (A) the Ce13d and (B) the NaA43T DNAszymes (NaA43 with a shortened hairpin). (C) The cis-cleaving version of the selected Na⁺-dependent DNAszyme. (D) The trans-cleaving form of the selected Na⁺-dependent DNAszyme with a shortened hairpin structure.

In vitro selection sometimes yielded similar sequences, and a representative example is the 17E DNAszyme.^{60, 143} The recurrence or tyranny of 17E has been a common problem in divalent metal-dependent selections. Li and coworkers attributed it to the small size, tolerance to mutation and high activity of the 17E motif.^{143, 144} The Ce13d DNAszyme was first reported to be lanthanide-dependent.⁶⁷ Interestingly, this sequence was demonstrated to be the most active family in a separate selection using Cr³⁺ as the intended target.¹⁴⁵ In the case of NaA43 and NaH1, the sequence requirement is more stringent since the 16-nt motif is highly conserved. When a typical divalent metal ions are absent and Na⁺ is present in selection buffers, this motif appears to be a good solution for achieving activity.

2.2.3 Biochemical characterization

Co(NH₃)₆³⁺ effect on activity. NaH1 activity was observed in the presence of 20 mM Na⁺ with ~49% cleavage yield after a 30 min incubation (Figure 2.4). Since Co(NH₃)₆³⁺ was used as the intended cofactor during the selection, its effect on NaH1 was first studied. The cleavage yield was measured with 10 μM Co(NH₃)₆³⁺ added but in the absence of Na⁺. In this case, no cleavage activity was observed. The addition of Co(NH₃)₆³⁺ in the presence of Na⁺ resulted in ~32% cleavage which is slightly lower than the activity measured in Na⁺ alone. Thus, Co(NH₃)₆³⁺ cannot support NaH1 activity but inhibits the Na⁺-induced activity. However, the insufficient inhibition caused by 10 μM Co(NH₃)₆³⁺ still allowed NaH1 to survive the selection process.

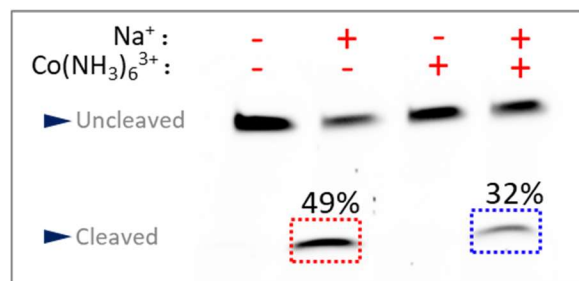


Figure 2.4 The inhibition effect of $\text{Co}(\text{NH}_3)_6^{3+}$ (10 μM) on the cleavage activity of NaH1 in the presence of 20 mM NaCl.

Cleavage kinetics. To characterize the activity of the NaH1 DNAzyme, its cleavage kinetics was measured in the presence of various concentrations of Na^+ at pH 6.0 (Figure 2.5A). The kinetic traces were fitted into a first-order equation, $\%P_{\text{cleavage},t} = \%P_{\text{max}}(1 - e^{-kt})$, where $\%P_{\text{max}}$ is the maximum cleavage yield at the end of the reaction and k is the cleavage rate constant. In the presence of 50 mM NaCl, NaH1 displayed a cleavage rate of $0.11 \pm 0.01 \text{ min}^{-1}$, which was around 3-fold faster compared to that of NaA43T at the same Na^+ concentration.⁷² The cleavage rate increased with a rising concentration of Na^+ and approached saturation beyond 50 mM Na^+ (Figure 2.5B). This data was then fitted into a one-site binding curve with an apparent dissociation constant (K_d) of $12.0 \pm 1.6 \text{ mM Na}^+$ at pH 6.0. The K_d of NaA43 using gel-based assays was estimated to be $\sim 70 \text{ mM Na}^+$ at pH 7.0.⁷² Therefore, the NaH1 mutant shows a tighter binding affinity to Na^+ than NaA43.

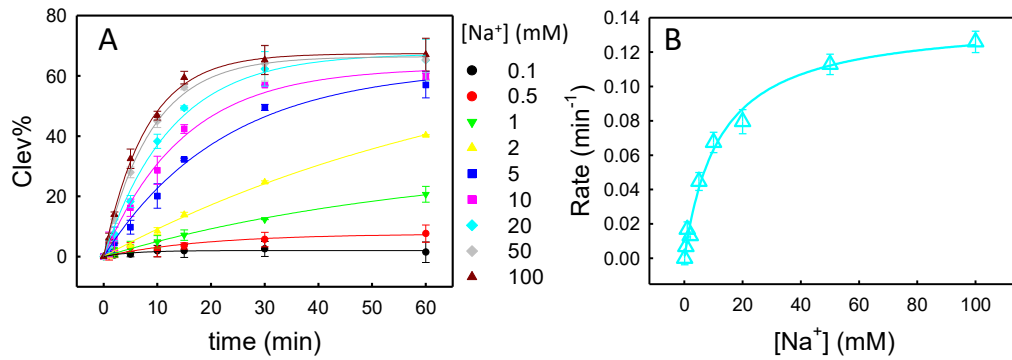


Figure 2.5 (A) Kinetic profile of the NaH1 DNAzyme with various concentrations of NaCl at pH 6.0. (B) The cleavage rate of NaH1 as a function of Na⁺ concentration.

To confirm the cleavage activity of NaH1 and NaA43T, assays were carried out in the presence of 10 mM Na⁺ for both DNAzymes side-by-side (Figure 2.6). The cleavage rate of NaA43T was ~0.02 min⁻¹ (pH 7.0), which agreed with the literature.⁷² With 10 mM Na⁺, NaH1 (pH 6.0) had a cleavage rate that was about 3-fold higher. NaH1 was tested in pH 6.0 buffer while NaA43T was in pH 7.0 buffer since these are their respective optimal pH for activity (*vide infra*).

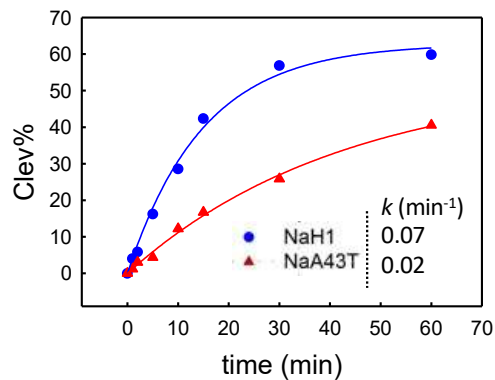


Figure 2.6 A comparison of the cleavage rates of the NaH1 and NaA43T DNAzymes with 10 mM NaCl. Note that NaH1 was tested in pH 6.0 MES buffer while NaA43T was in pH 7.0 HEPES buffer.

pH optima. NaH1 differs from NaA43T mainly on 2 nucleotides. Since NaH1 exhibited a higher cleavage rate at low Na^+ concentrations, a systematic comparison was made for a better understanding of these two Na^+ -dependent DNazymes. The reaction condition of NaA43 as reported was 50 mM Bis-Tris, pH 7.0, 90 mM LiCl, and it was also selected at this pH.⁷² The NaH1 DNzyme was selected using 50 mM MES buffer, pH 6.0. To have a full understanding on the pH effect, I compared the kinetics of NaH1 and NaA43T in the presence of 10 mM NaCl at both pH's. At pH 6.0, NaH1 displayed a higher cleavage rate than NaA43T (Figure 2.7A), while at pH 7.0, NaH1 became slower (Figure 2.7B).

After noticing this difference, their cleavage yields were measured with 10 mM Na^+ in various pH buffers (Figure 2.7C). The activity of NaH1 increased from pH 4.5 to 6.0 and then decreased at higher pH. The optimal reaction condition of NaH1 turned out to be pH 6.0, which is same as its selection condition. In contrast, the highest activity of NaA43 was observed at pH 7.0. Therefore, the fact that the NaH1 mutant was obtained instead of NaA43 might be related to the lower pH condition used during our selection experiment.

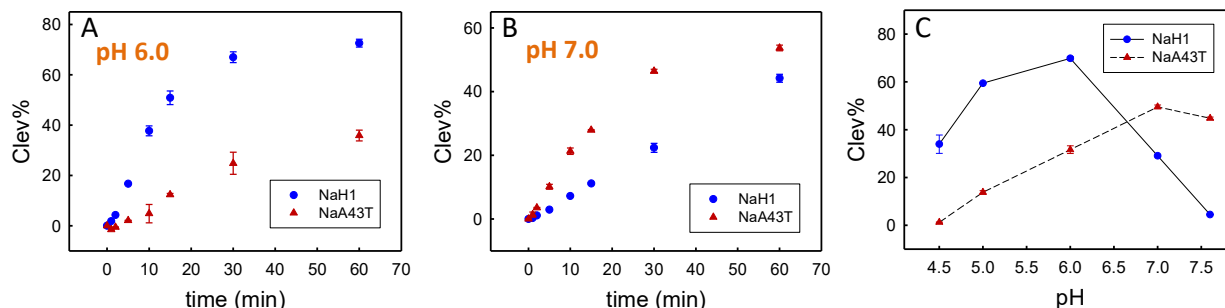


Figure 2.7 The kinetics studies of the NaA43T and NaH1 DNazymes with 10 mM NaCl at (A) pH 6.0 or (B) pH 7.0. (C) Cleavage yield of NaH1 and NaA43T with 10 mM NaCl at different pH's after 30 min incubation.

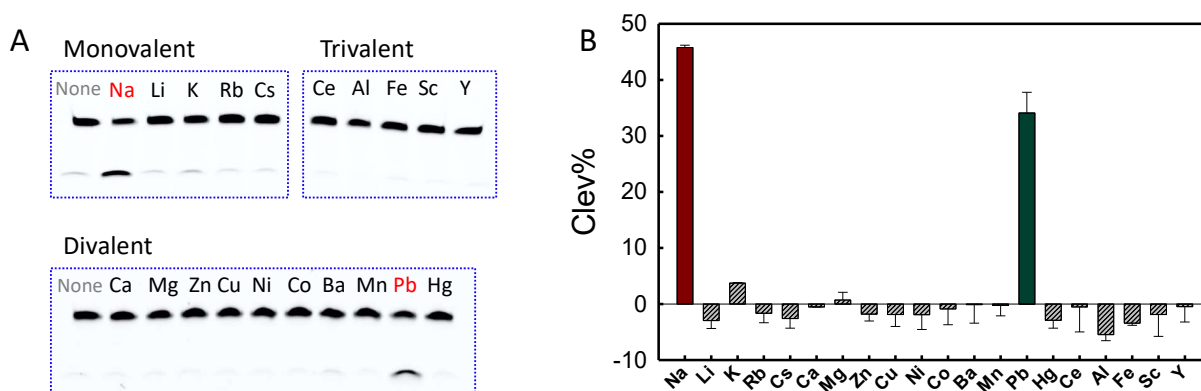


Figure 2.8 (A) Gel images showing the cleavage in the presence of monovalent (10 mM), divalent (1 mM) and trivalent (100 μ M) ions. (B) Quantification of the NaH1 cleavage yield with 20 different metal ions at pH 6.0 for 1 h. The background cleavage (without metal) was subtracted.

Metal selectivity. Furthermore, the cleavage activity of NaH1 was compared in the presence of various metal ions to confirm if the Na^+ specificity was retained. A total of 20 metal ions including monovalent, divalent, and trivalent ions were tested at pH 6.0 (Figure 2.8). NaH1 showed a significant cleavage only with Na^+ but not with other monovalent ions tested. The only exception was Pb^{2+} , which also showed $\sim 35\%$ cleavage. RNA cleavage by Pb^{2+} has been commonly observed in many DNAzymes.^{65, 67} Importantly, NaH1 displays an excellent Na^+ selectivity comparing to other monovalent and all physiologically relevant metal ions.

2.2.4 A Na^+ biosensor

Due to the superior activity of NaH1 under slightly acidic conditions (pH 5 to pH 6), a fluorescence-based biosensor was further designed for Na^+ detection (Figure 2.9A). A FAM label was placed on the 3'-end of the substrate strand, and a quencher was labeled at the 5'-end of the enzyme strand. Upon hybridization, the fluorescence was quenched in the duplex structure. In the

presence of Na^+ , the cleavage reaction can release the FAM-labeled fragment and induce a fluorescence signal. The 5'-end of the enzyme strand was shortened by two nucleotides to ensure a fast release of the fluorophore upon cleavage and thus a high fluorescence signal.

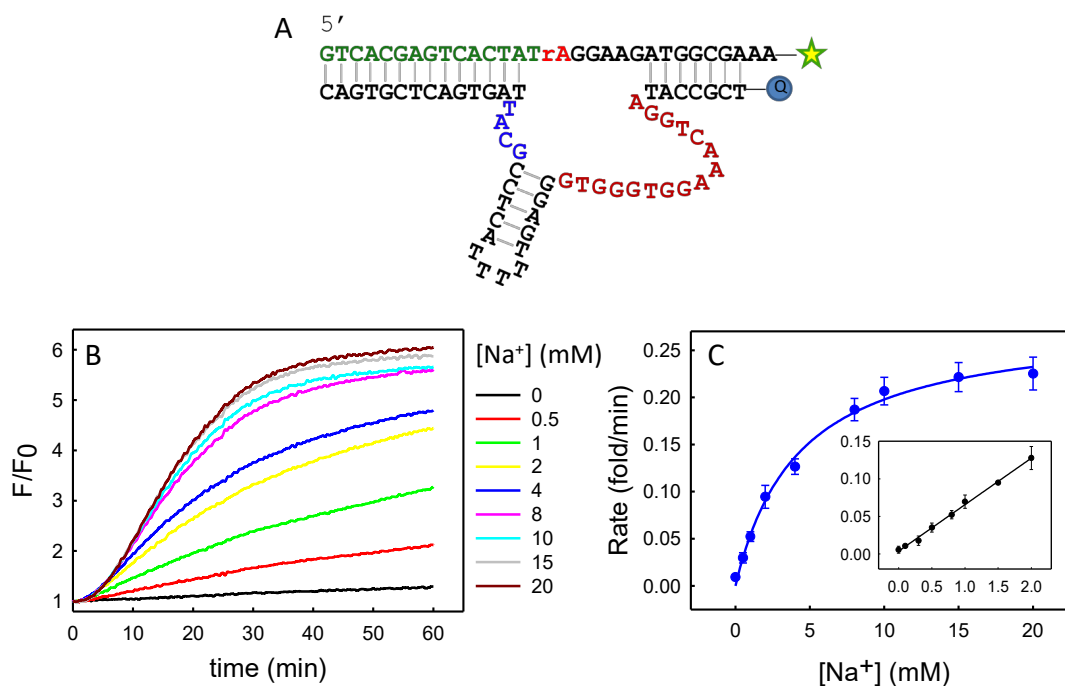


Figure 2.9 (A) Schematic description of the Na^+ DNzyme sensor design. (B) Sensor signaling kinetics measured with various concentrations of Na^+ . (C) Initial rates of fluorescence increase were quantified between 10 min to 15 min, and plotted as a function of Na^+ concentration. The one-site saturation binding equation used for fitting is $v = v_{max} \cdot [L^+]/(k_d + [L^+])$, where v is the reaction rate, $[L^+]$ is the Na^+ concentration, and k_d is the apparent dissociation constant. Inset: the linear response with $[\text{Na}^+]$ below 2 mM with an equation of $y = 0.0037 + 0.0619x$.

To test the sensor performance in buffer solution, the background signal containing 100 nM sensor complex was first monitored for 10 min. In the absence of Na^+ , the background fluorescence remained stable over 1 h of monitoring (Figure 2.9B). The addition of Na^+ induced a

rising fluorescence signal. A higher Na^+ concentration resulted in a faster fluorescence increase, and a 6-fold increase in fluorescence was detected with 20 mM Na^+ compared to the background. The initial rates of the fluorescence traces were quantified from 10 to 15 min after the Na^+ addition (Figure 2.9C). The fluorescence enhancement saturated at ~ 20 mM Na^+ . After fitting the curves with a one-site binding equation, an apparent K_d of 4.2 ± 0.5 mM was obtained. A linear calibration curve was obtained when Na^+ concentration was ≤ 2 mM. The detection limit was calculated to be $223 \mu\text{M Na}^+$ based on $3\sigma/\text{slope}$ (σ is the standard deviation of the background signal). The lower pH optima of this DNzyme might be useful for detection of Na^+ in acidic cellular environment such as the endosome and cancer cells.

Using NaA43 for detecting Na^+ in live cells has already been demonstrated.⁷² In this work, I further studied the fluorescent Na^+ biosensor in another biological sample matrix, fetal bovine serum (FBS). In the presence of 1% FBS (v/v), the background signal remained low (Figure 2.10A), indicating that the sensor complex was stable in the diluted serum solution. Fluorescence increases were observed when Na^+ was spiked in the solution. However, the fluorescence increase was lowered compared to the pure buffer which could be interfered by the component in serum. A linear response was obtained with Na^+ concentration below 20 mM and the detection limit determined was $676 \mu\text{M Na}^+$ (Figure 2.10B). To confirm the fluorescence increase is due to the cleavage, the reaction products after 30 min incubation were characterized using dPAGE (Figure 2.11). In the presence of 1% FBS (v/v), $\sim 66\%$ cleavage yield was detected with 10 mM NaCl. Meanwhile, the cleavage% increased with an increasing serum% which could be induced by Na^+ from the FBS sample. As a reference, the Na^+ concentration in FBS sample is approximately 142 mM.¹⁴⁶

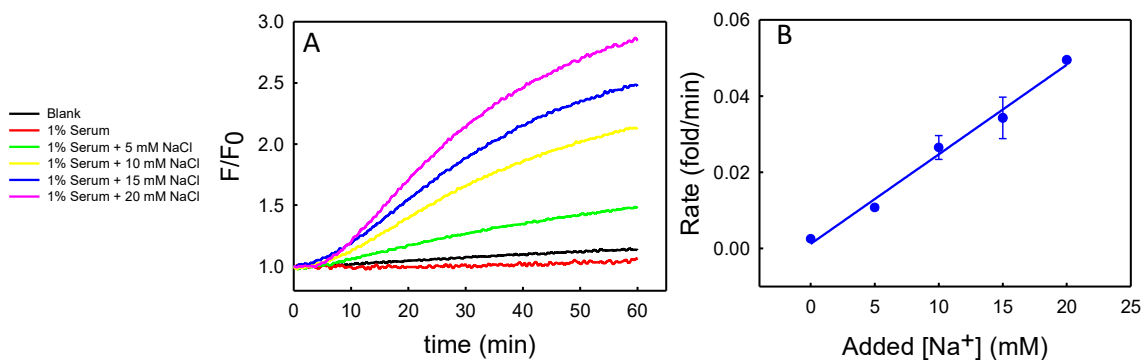


Figure 2.10 (A) Sensor response in the presence of 1% FBS monitored over 1 h. (B) A linear response between the fluorescence signal and [Na⁺] in 1% FBS.

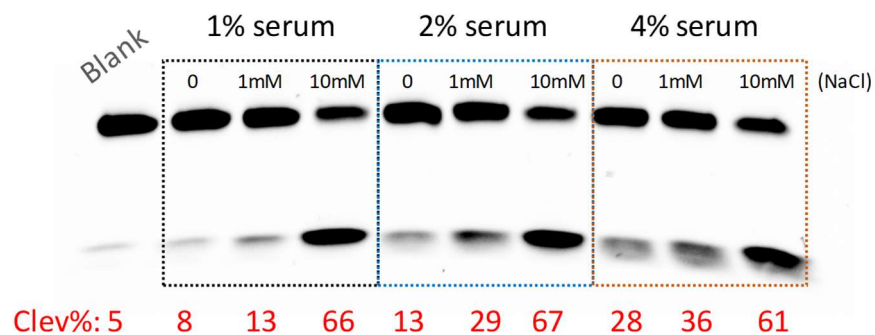


Figure 2.11 Gel image showing the cleavage of NaH1 in 1%, 2%, or 4% FBS samples (v/v) measured after 30 min incubation.

2.3 Summary

A new Na⁺-dependent DNAzyme mutant was discovered by a selection effort using a cobalt complex as the intended metal cofactor. The selected DNAzyme, named NaH1, possesses high selectivity for sodium over other monovalent ions and a fast catalytic rate of $0.11 \pm 0.01 \text{ min}^{-1}$ with 50 mM Na⁺ at pH 6. With a few nucleotides mutated in the small loop, NaH1 can catalyze the RNA cleavage reaction more efficiently than the previously reported NaA43 especially at low

Na⁺ concentrations. Additionally, they displayed distinct pH optima in which NaH1 preferred a relatively acidic condition (i.e., pH 5 to 6), while NaA43 was more active at neutral pH. A fluorescent Na⁺ sensor was also demonstrated with an apparent K_d value of 4.2 ± 0.5 mM and a limit of detection of 223 μ M Na⁺, which was further applied in a serum matrix.

2.4 Materials and methods

2.4.1 Oligonucleotides and chemicals

All the DNA samples used in the *in vitro* selection and sensing experiments were from Integrated DNA Technologies (Coralville, IA). The rest of the DNAs were from Eurofins Genomics (Louisville, KY). Hexamminecobalt (III) chloride and other metal salts including lithium chloride hydrate, potassium chloride, rubidium chloride, cerium chloride heptahydrate, scandium chloride hydrate, manganese chloride tetrahydrate, iron chloride hexahydrate, nickel chloride hexahydrate, cobalt chloride hexahydrate, copper chloride dehydrate, zinc chloride, mercury perchlorate, lead acetate, barium chloride dihydrate, aluminium chloride hydrate, yttrium chloride hexahydrate were purchased from Sigma-Aldrich. Sodium chloride, calcium chloride dihydrate, magnesium chloride hexahydrate, acetate acid, tris(hydroxymethyl)aminomethane (Tris), 2-(N-morpholino)ethanesulfonic acid (MES), 2-[4-(2-hydroxyethyl)piperazin-1-yl]ethanesulfonic acid (HEPES), ethylenediaminetetraacetic acid (EDTA) were from Mandel Scientific Inc. (Guelph, Ontario, Canada). Lithium hydroxide was from Alfa Aesar. Sso Fast EvaGreen supermix was from Bio-Rad. T4-DNA ligase, deoxynucleotide (dNTP) solution mix, Taq DNA polymerase with ThermoPol buffer, 10 \times gel loading dye, and low molecular weight DNA ladder were purchased from New England Biolabs. All solutions used in this chapter were prepared with Milli-Q water.

DNA name	Sequences and modifications
Lib-FAM-N50	5'-GGCGAAACATCTTN ₅₀ TAGTGACGGTAAGCTTGGCAC-FAM
Lib-rA	5'-AATACGAGTCACTATrAGGAAGAT
Splint	5'-AAGATGTTTCGCCATCTTCCTATAGTCCACCACCA
P1 primer	5'-GTGCCAAGCTTACCG
P2 primer	5'-CTGCAGAATTCTAATACGAGTCACTATAGGAAGATGGCGAAACA
P3 primer	5'-FAM-AAATGATCCACTAATACGACTCACTATrAGG
P4 primer	5'-AACAAACAACAAC-iSp18-GTGCCAAGCTTACCG
P701	5'-CAAGCAGAAGACGGCATAACGAGATTCGCCTTAGTGACTGGAGTTC AGACGTGTGCTCTTCCGATCTCTGCAGAATTCTAATACGAGTCAC
P501	5'-AATGATACGGCGACCACCGAGATCTACTAGATCGCACACTC TTCCCTACACGACGCTCTTCCGATCTGTGCCAAGCTTACCG

Table 3. List of all the DNA sequences and modifications used in the *in vitro* selection experiment. iSP18 is an internal 18-atom hexa-ethyleneglycol spacer.

2.4.2 *In vitro* selection

To prepare the DNA library, Lib-FAM DNA (200 pmol), Lib-rA DNA (300 pmol), and splint DNA (300 pmol) were first mixed in annealing buffer (10 mM Tris-HCl buffer, pH 7.5, 10 mM MgCl₂). The mixture was then annealed at 90 °C followed by slow cooling down to room temperature. The ligation reaction followed the T4 ligation protocol provided by New England Biolabs. As prepared DNA library was further purified and extracted from 10% dPAGE (650 V, 1 h). In this work, Bio-Rad ChemiDoc MP imaging system was used to take the gel images and quantify the fluorescence. A gel slice containing the DNA library was crushed and soaked in extraction buffer (1 mM EDTA, 10 mM Tris-HCl, pH 7.0). The further purification was achieved by using a Sep-Pak C18 column (Waters). The extracted DNA library was dried in an Eppendorf Vacufuge at 45 °C overnight.

For each round of selection, 10 μM of $\text{Co}(\text{NH}_3)_6\text{Cl}_3$ was introduced to the library in selection buffer (50 mM MES buffer, pH 6.0, 25 mM NaCl, 1 mM EDTA). After 1 h of incubation, 8 M urea was added to quench the reaction. The active sequences after cleavage (91-nt length) were then separated from inactive sequences using 10% dPAGE (denaturing polyacrylamide gel electrophoresis) and extracted from gel slices using the “crush and soak” method. Next, the active sequences were amplified by two rounds of polymerase chain reactions (PCR). The cycling protocol used is as follows: 94 °C for 5 min; 94°C for 30 s; 55 °C for 30 s; and 72°C for 30 s. In PCR1, the cleaved sequences were extended and amplified to generate full-length templates for PCR2. In PCR2, two modified primers were used to regenerate the library. The P3 primer contained a 6-carboxyfluorescein (FAM) fluorophore on its 5'-end terminus and a rA base on its 3'-end terminus. The P4 primer contained a polymer spacer that can stop the polymerase reaction. All the DNA sequences related to the selection are listed in Table 3.

2.4.3 Deep sequencing

To prepare the sample for deep sequencing, PCR1 was performed on the round 6 library. Then, PCR2 was performed to introduce specific index sequences into the library for the Illumina sequencing. Instead of P3 and P4, the forward primer (P701) and the reverse primer (P501) were used with their sequences listed in Table 3. The PCR product was then purified with 2% agarose gel (120 V, 50 min). A gel/PCR DNA fragment extraction kit (IBI Scientific) was used to extract the library from the gel. Finally, the purified DNA sample was eluted in 20 μL of Milli-Q water. The DNA concentration measured with a NanoDrop spectrophotometer was ~ 10 ng/ μL . The sample was shipped to McMaster University for sequencing.

2.4.4 Activity assays

For cleavage activity assays, the DNAzyme complex was prepared by annealing the FAM-labeled substrate and enzyme (ratio 1:1.5) in sodium-free buffer A (10 mM HEPES buffer, pH 7.6, 25 mM LiCl) to minimize background cleavage. Assays were performed with a final concentration of 0.3 μM of DNAzyme complex in buffer B (50 mM MES buffer, pH 6.0, 25 mM LiCl). A small volume (1 μL) of NaCl with various concentrations was added to initiate the cleavage reaction. After different incubation time periods, the reaction was quenched with 8 M urea. For pH-dependent assays, acetate buffer was used for pH 4.5 and pH 5.0, and HEPES buffer was used for pH 7.0 and pH 7.5. All the buffer pH was adjusted using 1 M LiOH to avoid Na^+ .

The FAM-labeled cleavage products were quantified by 15% dPAGE and analyzed by a Bio-Rad Chemi-Doc MP imaging system. The 15% dPAGE gel stock solution (500 mL) contains urea (240g), 40% acrylamide (29:1) (187.5 mL), and 10x TBE (50 mL). For each gel plate, 10% APS and TEMED are added to initiate the polymerization reaction. After a quick mix, the gel solution is transferred into a pre-assembled glass plate and set for over 30 min to allow solidification. After loading the reaction solution ($\sim 15 \mu\text{L}$) into one gel well, 200 V voltage is applied to the chamber and each gel runs for 1 h 20 min. The running buffer used for gel electrophoresis is 1x TBE.

2.4.5 Fluorescence-based Na^+ sensing

Sensor signaling kinetics were measured in 96-well plates using a microplate reader (Infinite F200Pro, Tecan). The excitation wavelength was 485 nm and the emission wavelength was 535 nm. The sensor complex was prepared by annealing the FAM-labeled substrate (5 μM) and the quencher-labeled enzyme (7.5 μM) in buffer B. Next, 2 μL of the sensor complex was diluted in 93 μL buffer (50 mM MES buffer, pH 6.0). The background signal was first monitored

for at least 5 min, followed by a quick addition of 5 μL of NaCl to induce the cleavage reaction. The fluorescence was continuously monitored for 1 h with 20 s intervals. For detection in serum, FBS sample was first filtered through a nitrocellulose membrane to remove aggregated proteins. The pre-treated FBS (1 μL) was then added to the sensor solution and the background fluorescence was monitored for at least 5 min. Afterwards, different concentrations of NaCl were added in the plate followed by monitoring fluorescence for 1 h.

Chapter 3. From General Base to General Acid Catalysis in a Sodium-Specific DNAzyme by a Guanine-to-Adenine Mutation^c

3.1 Introduction

DNAzymes are DNA sequences with catalytic activities.⁵ A variety of RNA-cleaving DNAzymes require various monovalent (e.g., Na⁺,^{65, 72} Ag⁺),⁷⁴ divalent (e.g., Pb²⁺,⁵ Zn²⁺,¹³³ Cu²⁺,¹³⁴ UO₂²⁺,⁶³ Hg²⁺,¹³⁵ Cd²⁺)⁷⁰, and trivalent (e.g., lanthanides)⁶⁸ metal ions for catalysis. DNAzymes are highly attractive for their excellent stability, programmability and cost-effectiveness, leading to interesting applications in biosensing and therapeutics. However, our understanding of DNAzyme catalysis is still limited compared to the substantial knowledge in ribozyme catalysis due to their rich structural biology data. Most self-cleaving ribozymes (e.g. the Rzb hammerhead,^{147, 148} *env25* pistol,^{149, 150} and twister ribozymes)¹⁵¹ utilize a general base mechanism, where a guanine helps activate the 2'-OH nucleophile. Adenines or cytosines can play the general acid role in the pistol,¹⁴⁹ twister,¹⁵¹ and hepatitis delta virus (HDV) ribozymes.¹⁵²

Compared to the development in DNAzyme applications, our fundamental understanding on the catalytic mechanism is still limited. Previous efforts have been mainly focusing on studying the role of metal ions, while the nucleotide-based catalysis has not been fully revealed in DNAzymes. The involvement of polyvalent metal ions may complicate data analysis. For mechanistic studies, monovalent-metal-dependent enzymes are more attractive. The first Na⁺-

^c This chapter is the basis for a published manuscript: Ma, L.; Kartik, S.; Liu, B.; Liu, J., From general base to general acid catalysis in a sodium-specific DNAzyme by a guanine-to-adenine mutation. *Nucleic Acids Research* **2019**, *47* (15), 8154-8162.

dependent DNAzyme, NaA43 was reported in 2015 by Lu and coworkers.⁷² Interestingly, its conserved sequence is quite similar to a lanthanide-dependent DNAzyme named Ce13d.⁶⁷ Their overlapping sequence was revealed to be part of a Na⁺-binding aptamer, which is responsible for their Na⁺ specificity.^{73, 139} Extensive studies have been performed on the aptamer part to understand specific Na⁺ binding.^{113, 153}

Recently, the NaH1 DNAzyme was reported, which differs from the NaA43T DNAzyme (a mutated shorter version of NaA43) by only two nucleotides in the enzyme loop.¹⁵⁴ An important guanine in NaA43 was replaced by an adenine in NaH1, and NaH1 also requires Na⁺ for activity. An interesting difference between them is their pH-dependency: the optimal pH being 7 for NaA43 and 6 for NaH1. Such DNAzymes are ideal for mechanistic studies since no polyvalent metals are involved, and catalysis is likely achieved via nucleobases. In this chapter, I performed careful biochemical and spectroscopic experiments, providing compelling evidence that on the same DNAzyme scaffold, a simple point mutation can switch the mechanism from being general base (for NaA43) to general acid (for NaH1) catalysis. The tolerance of different mechanisms may also explain the activity of this scaffold (e.g. Ce13d) with a diverse range of metal ions and even non-metals.

3.2 Results and discussions

3.2.1 The NaA43 and NaH1 DNAzymes

The secondary structures of the NaA43T and NaH1 DNAzymes are shown in Figure 3.1A and 3.1B, respectively. NaA43T is a truncated version of NaA43 with retained specificity for Na⁺.⁷³ These DNAzymes have the same substrate that contained a single RNA linkage (rA for ribo-adenine) serving as the cleavage site. NaA43T and NaH1 have the same 16-nt Na⁺-binding

motif. The catalytically important regions are drawn in red. Our previous study indicated that the G23 residue in NaA43 is highly conserved,⁷³ but no guanine is present in the corresponding region of NaH1. Therefore, these two DNAzymes might have distinct catalytic mechanisms.

The catalysis of many small self-cleaving ribozymes has been thoroughly studied.^{12, 30, 32} In general, the RNA cleavage reaction is initiated by a nucleophilic attack from the 2'-OH of the ribose to the scissile phosphate, resulting in the leaving of the 5'-oxygen of the next nucleotide (Figure 3.1C). In self-cleaving ribozymes, the cleavage reaction is often accelerated by a general base (e.g., a guanine or a metal bound water after deprotonation)^{149, 155} to help deprotonate the 2'-OH, or by a general acid (e.g., adenine or cytosine)^{152, 156} to neutralize the developing negative charge on the 5'-oxygen.³⁰ This study intends to compare these two Na⁺-specific DNAzymes for mechanistic insights taking advantage that no polyvalent metal ions are involved.

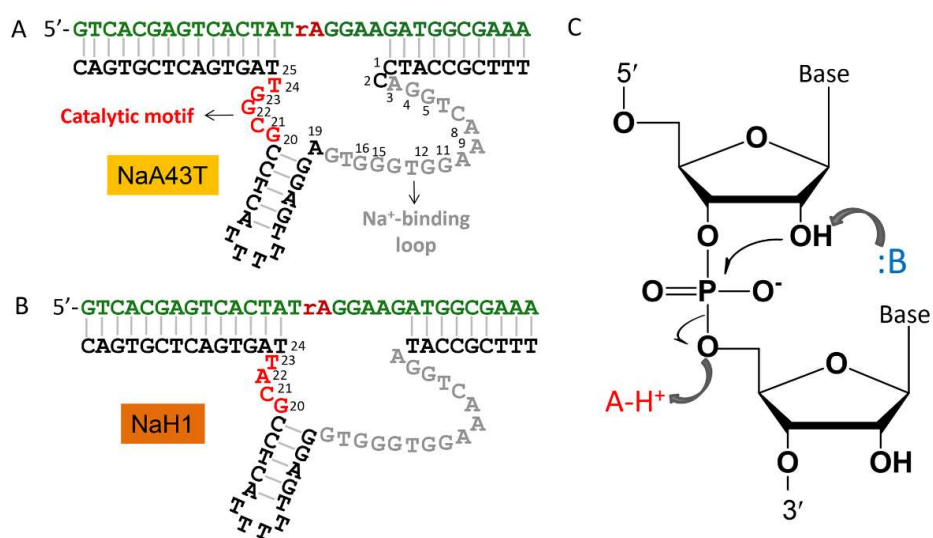


Figure 3.1 The secondary structures of two Na⁺-specific RNA-cleaving DNAzymes named (A) NaA43T and (B) NaH1. The key catalytic motifs are the small loops in red. (C) A general RNA cleavage reaction requires the nucleophilic attack from 2'-OH resulting in the leaving of the 5'-OH group, which can be accelerated by the general acid/base catalysis.

3.2.2 Rational evolution from NaA43T to NaH1

Since these two DNazymes are highly similar, I gradually mutated one DNzyme into the other to identify important residues. As shown in Figure 3.2A, the cleavage rate of NaA43T measured at pH 7 was ~3-fold faster than that at pH 6. Before modifying the catalytic motif, I first deleted the C1 and C2, and then A19 in NaA43T (Mut1 and Mut2 in Figure 3.2B). Mut1 and Mut2 showed gradually decreasing activity, but their activity became similar at both pH's. Based on Mut2, G22 (or G23) was further deleted in the small loop resulting in Mut3, which had almost no activity detected at either pH values. Based on our previous study, NaA43 was still active when G22 was mutated to A, T, or C.⁷³ However, deleting G22 inhibited the cleavage activity in this study. Therefore, G22 is likely to play a structural role (e.g. a spacer) to position the catalytically important G23 for catalysis.

Based on Mut3, I mutated G23 into an adenine and NaH1 was obtained (this adenine is A22 in NaH1). NaH1 exhibited a higher cleavage rate under pH 6, while its activity at pH 7 remained low. Additionally, a guanine was also added back to position 22 (Mut4), whose activity decreased at both pH's, but the pH 6 activity was still higher than that at pH 7. Therefore, the activity of Mut4 is more similar to NaH1 than to NaA43T. However, the additional G22 destabilizes the activity of NaH1 giving decreased rates.

Overall, the highest activity was at pH 7 when G23 was present and was at pH 6 when A22 was present. Based on this experiment, an enzyme can be defined to be from NaA43T if it has G23 and the activity at pH 7 is higher or comparable to that at pH 6. On the other hand, if the enzyme has A22 and its activity is higher at pH 6, it is NaH1. If these nucleotides are directly involved in catalysis, they likely have very different reaction mechanisms, since G and A can play different acid/base catalysis roles.^{12, 30}

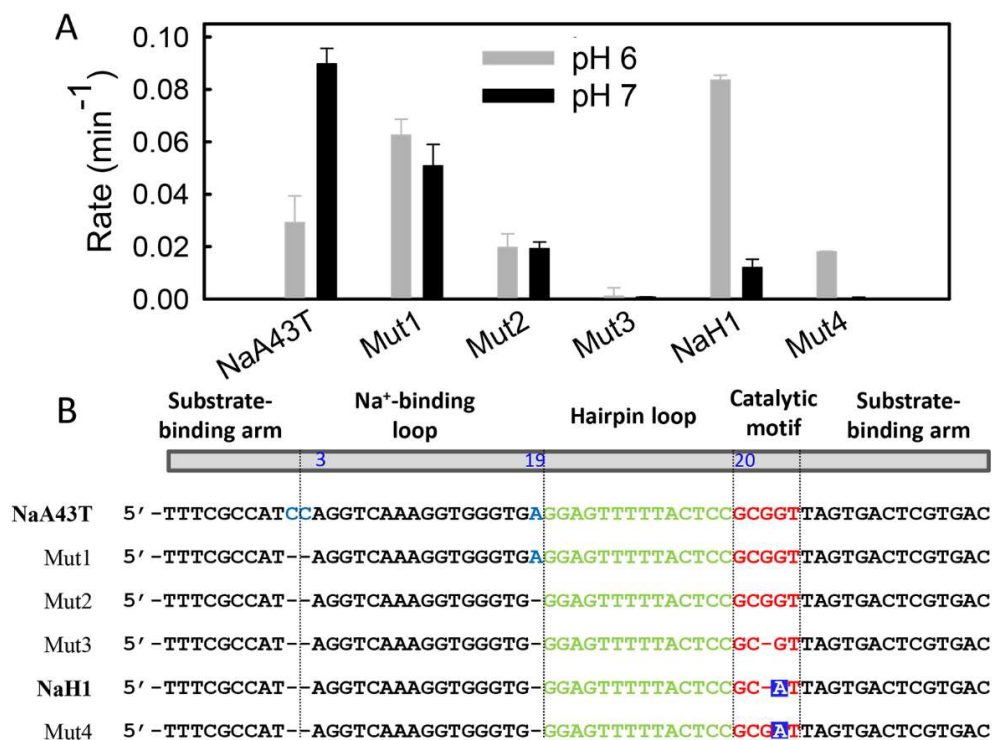


Figure 3.2 (A) The cleavage rate of each mutant in the presence of 10 mM NaCl at pH 6 (grey bars) and pH 7 (black bars). (B) List of the DNAzyme sequences used in this study. The A22 residue is highlighted with blue squares.

3.2.3 The A22 in NaH1 is highly conserved

To further locate important nucleotides in the catalytic loop of NaH1, point mutations were performed (Figure 3.3A). The cleavage rate of each mutant was measured at pH 6 (Figure 3.3B). Mutating T23 to A resulted in a ~1.6-fold reduction in rate, while mutating C21 to T or G decreased the rate by 2 to 3-fold. Besides, purine-to-purine replacement (G20A) was tolerated with ~50% rate remaining, which was also observed for the G20 site in NaA43T.⁷³ On the contrary, mutation of A22 to T, C or G led to a ~100 to 1000-fold decrease in rate. Therefore, A22 indeed plays a

crucial role in the cleavage reaction, which is in agreement with the above rational evolution experiments.

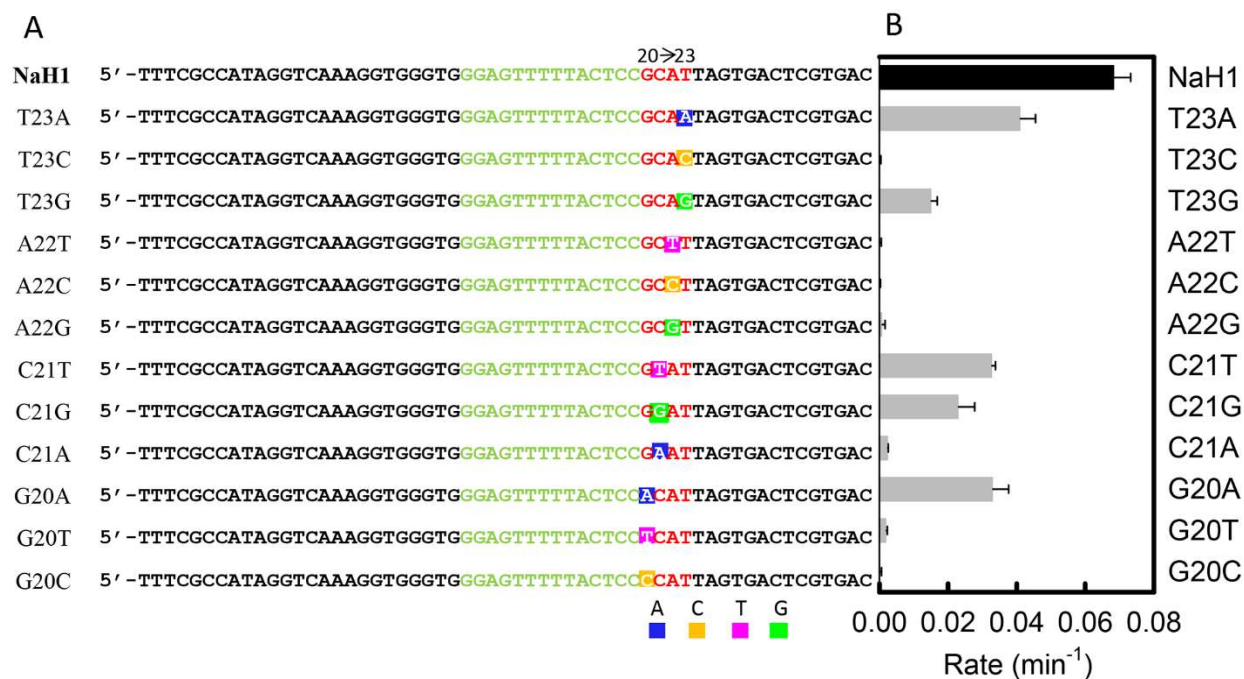


Figure 3.3 (A) The sequences used in this point mutation study based on NaH1 from G20 to T23. (B) The cleavage rate of each mutant measured with 10 mM NaCl in pH 6 buffer.

3.2.4 pH-rate profiles

Catalytically important guanines often play a general base role in ribozymes such as the Rzb hammerhead,^{147, 148} *env25* pistol,^{149, 150} and twister ribozymes.¹⁵¹ The pK_a of the N1 position of guanine is ~ 9.4 (Figure 1.3), which can be lowered toward neutrality by coordinating with nearby nucleobases or metal ions, allowing its general base role at neutral pH.^{157, 158} Adenine, on the other hand, is often known for its general acid role in stabilizing the leaving group (i.e. 5'-O).^{149, 156} To better understand the reaction mechanism, I carefully examined the pH-rate profiles. For NaA43T, a gradual increase in cleavage rate was observed with increasing pH, plateauing at

pH 7.5 (Figure 3.4A, circles). Such a pH-rate profile implies that a single general base functions during the cleavage reaction until it is fully deprotonated. In contrast, a declining trend was observed for NaH1 between pH 5.0 to 8.0 (Figure 3.4A, diamonds), indicating a general acid catalysis and its protonation was inhibited by raising pH.

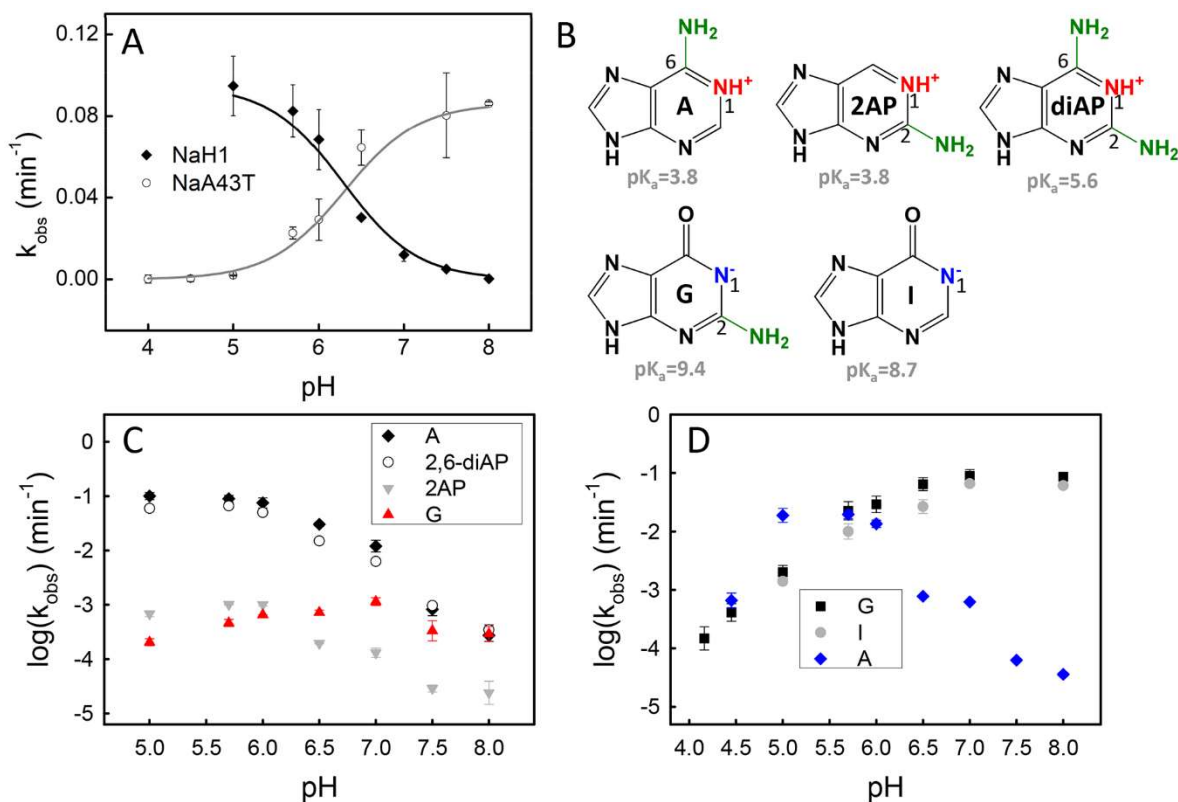


Figure 3.4 (A) pH-rate profiles of NaH1 and NaA43T in the presence of 10 mM Na^+ . The pK_a of the general acid catalyst in NaH1 was 6.3 ± 0.4 ($R^2=0.92$), while the pK_a of the general base in NaA43T was 6.6 ± 0.1 ($R^2=0.97$). (B) Chemical structures and pK_a values of adenine, 2-aminopurine (2AP), 2,6-diaminopurine (2,6-diAP), guanine, and hypoxanthine (I). (C) pH-rate profiles of the wild-type NaH1 and its 2,6-diAP-, 2AP- and G-substitutions in the presence of 10 mM NaCl. (D) pH-rate profiles of the wild-type NaA43T and its I- and A-substitutions in the presence of 10 mM NaCl.

In the mutation studies, G23 and A22 were determined to be crucial for the activity of NaA43 and NaH1, respectively. Taken together, I propose that G23 functions as a general base in NaA43T, while A22 as a general acid in NaH1 (see base analog studies below for further evidence). The pK_a of the general base in NaA43T shifts from ~ 9.4 (N1 position) to 6.6 ± 0.1 (Figure 3.4A, grey curve). For NaH1, a shifted pK_a of 6.3 ± 0.4 (Figure 3.4A, black curve) for the catalytic adenine was observed in the presence of 10 mM Na^+ .

It is very interesting that on the same DNAzyme scaffold, by just mutating one or two nucleotides, the catalytic mechanism is completely changed. Considering the very small size of these DNAzymes, the tolerance of different catalytic mechanisms by point mutations has not been seen previously. The closest example is a hammerhead ribozyme, where mutating an invariant guanine to adenine retained its general base role for the catalysis (instead of general acid).¹⁴⁷ Meanwhile, this mutant exhibited a 13 000-fold lower rate and required a high Mg^{2+} concentration.

This tolerating property and switchable general acid/base catalysis mechanism have reminded us of another related DNAzyme called Ce13d, which requires both Ce^{3+} (or another trivalent lanthanide) and Na^+ for activity. Ce13d has the same Na^+ binding motif, but the small catalytic loop is almost completely eliminated (Ce^{3+} to carry out the catalytic role). The Ce13d DNAzyme was extremely tolerant for various metal ions, including all the trivalent lanthanides, Y^{3+} ,¹¹⁰ a low activity with Cr^{3+} ,¹⁴⁵ and a moderate activity with Pb^{2+} .⁶⁷ After making a single phosphorothioate modification at the cleavage site, it became active with all thiophilic metals such as Hg^{2+} , Cd^{2+} , Pb^{2+} , Tl^{3+} and Au^{3+} .¹⁵⁹ It can even accelerate the cleavage of the PS substrate by I_2 , a non-metal.¹⁶⁰ The activity with various metal ions and even elimination of polyvalent metal ions indicates that the DNAzyme scaffold is highly tolerant for catalysis. Thus, the switching of general acid/base mechanism might also be quite reasonable.

3.2.5 Base analogs further probing catalytic mechanism

To confirm the general acid role of A22 in NaH1, I tested its mutants including using base analogs. A22 has three possible positions to donate protons to the 5'-O: N1, N3 and N7. In small ribozymes, the N1 and N3 positions were reported for general acid catalysis.^{149, 151} With a higher pK_a , N1 is more likely to donate protons.¹⁶¹ In this work, a series of pK_a -perturbed analogs (Figure 3.4B), such as 2-aminopurine (~3.8), 2,6-diaminopurine (~5.6), and guanine (~9.4) were tested (Figure 3.4C). The pH-rate profile of the 2,6-diaminopurine substitution (2,6-diAP, circles) overlapped with that of adenosine (diamonds). Mutating A to 2-aminopurine (2AP, grey triangles) decreased the activity by ~2 orders of magnitude, but its overall profile was parallel to that of the wild type NaH1. Therefore, the 6-amino group of A22 is important for catalytic rate, likely by forming hydrogen bonding to stabilize the transition state.¹² With their N1 positions still available for protonation, these analogs displayed a similar pH-dependent activity plateauing at pH <6. When substituting A with G (red triangles), a gradual rate decrease was observed below pH 7, with its maximum activity occurring at a higher pH. Therefore, the N1 position of A22 is indeed responsible for the general acid catalysis of NaH1.

In NaA43T, substitutions at G23 with hypoxanthine (I, pK_a ~8.7) and adenine (A, pK_a ~3.8) were tested to determine its catalytic role (Figure 3.4D). The G to I mutation did not affect its pH-rate dependence (Figure 3.4D, grey circles) and gave a comparable rate at pH 7.0 (Figure 3.5B). Thus, the 2-exocyclic amino group of G23 may not play an important role in catalysis. On the contrary, mutating G23 into adenine resulted in a bell-shaped pH-rate profile with the highest activity at pH~5.5, similar to that of NaH1 (blue diamonds). Therefore, the N1 position of G23 is likely to directly participate in the catalysis by serving as a general base.

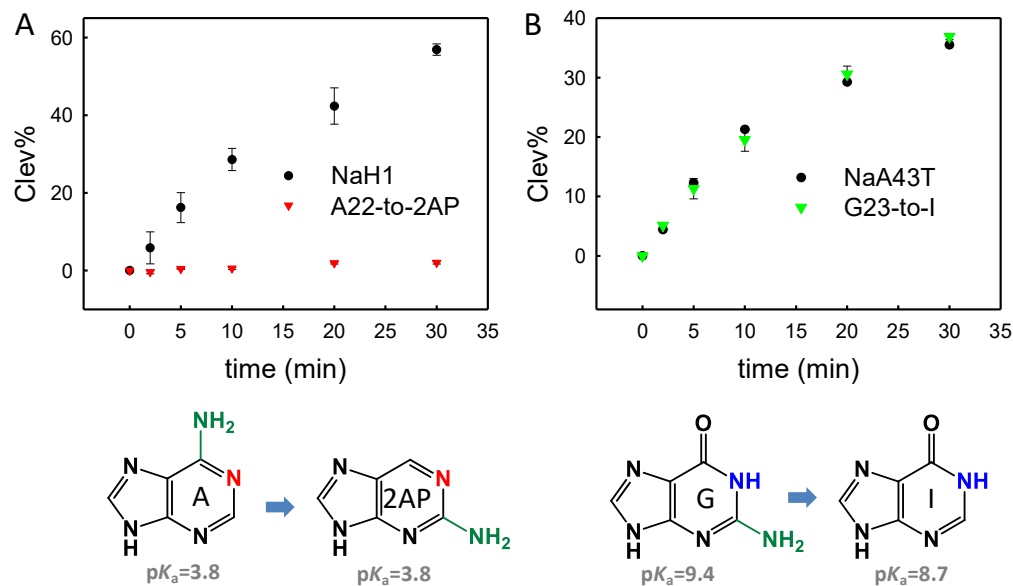


Figure 3.5 (A) Kinetics of NaH1 and the A22-to-2AP mutant measured in the presence of 10 mM Na⁺ at pH 6. (B) Kinetics of NaA43T and the G23-to-I mutant measured in the presence of 10 mM Na⁺ at pH 7.

The above mutation studies primarily focused on general acid/base catalysis. After mutation, the loss of activity could also be due to perturbed enzyme folding or Na⁺ binding. The fluorescence of 2AP is highly sensitive to its nearby base stacking environment.¹⁶² Thus, 2AP has been frequently used to probe local folding of DNazymes and ribozymes.^{127, 128, 163} I then substituted A22 by 2AP (Figure 3.6A). In activity assays, the enzyme bearing the A22-2AP mutation retained its cleavage activity with a ~100-fold lower rate compared to the wild type (Figure 3.5A). However, titrating NaCl induced a gradual increase in its fluorescence (Figure 3.6B). The fluorescence at 370 nm was further plotted as a function of Na⁺ concentration showing binding curve with a K_d of ~40 mM Na⁺ (Figure 3.6C).

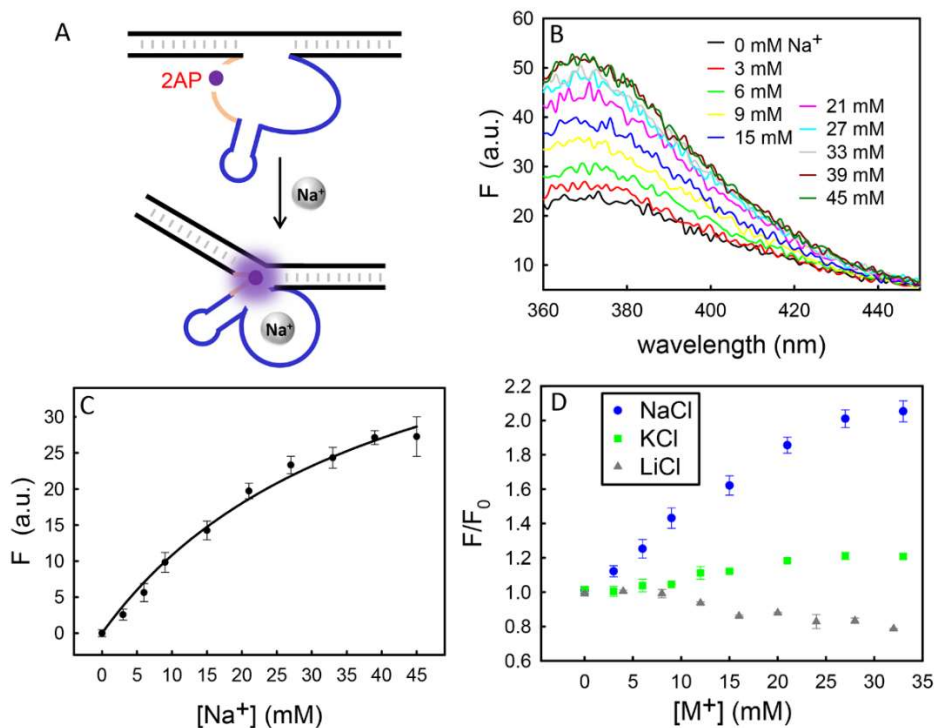


Figure 3.6 (A) Using 2AP to probe the local environment of the catalytic adenine due to Na^+ binding. (B) The fluorescence spectrum of the A22-to-2AP mutant after titrating NaCl. (C) The 2AP fluorescence at 370 nm versus the Na^+ concentration. (D) Fluorescence titration with Na^+ , K^+ or Li^+ .

To confirm the Na^+ specificity, Li^+ and K^+ were also titrated. The intensity barely changed (less than 20%) with up to ~ 30 mM KCl, while a slight fluorescence decrease was observed with LiCl (Figure 3.6D). Therefore, the 2AP-substitution does not affect the enzyme folding upon Na^+ binding. The activity drop of the A22-to-2AP mutant was likely caused by destabilizing the hydrogen bonding on the 6-amino of A22 instead of perturbed sodium binding. An enhanced fluorescence suggests a weakened base-base stacking near the catalytic residue,¹⁶² supporting the importance of A22 to the catalysis. A22 is likely to be released from stacking interactions from the neighbor bases due to Na^+ binding and exposed to the active site. As shown in Figure 3.4C, the pH-rate profile of NaH1 revealed a slope close to 1 in the high pH region, indicating one proton

transfer is the rate-limiting step. A similar relationship was also seen in the low pH region of NaA43T. This supports the idea that chemistry is the rate-limiting step instead of the folding.

3.2.6 Phosphorothioate substitution and metal rescue

In self-cleaving ribozymes, non-bridging oxygens at the scissile phosphate often play important roles in directly coordinating with catalytic metal ions or nucleobases. Phosphorothioate (PS) substitution has been widely applied in probing the importance of non-bridging oxygens.¹¹⁰
¹¹² Previous biochemical studies indicate that the Na^+ binding site in NaA43 is the 16-nt loop (Figure 3.1A), instead of the cleavage site.⁷³ To test metal binding at the cleavage site, the activity of NaH1 with the PS-substrates was examined in the presence of 10 mM Na^+ . First, a racemic mixture of the PS substrate was used, which contained an equal amount of the R_p and S_p diastereomers as shown in Figure 3.7A.

The cleavage rate with the PS-substrate was ~68-fold slower than the PO-substrate (Figure 3.7B), showing a normal thio effect at 10 mM Na^+ . A careful examination of the kinetic data can reveal that the cleavage did not have a fast phase and the yield was very low. Normally, for metal-based interactions, if the metal binds specifically to one of the non-bridging oxygens, one of the stereoisomers should remain active.¹¹¹ However, it is not the case here. In addition, adding thiophilic Cd^{2+} could not rescue the activity, also disapproving metal/phosphate interactions. For comparison, the lanthanide-dependent Ce13d DNAzyme has a normal thio effect which can be fully rescued by Cd^{2+} .¹¹⁰ Therefore, the role of Na^+ is to bind to the aptamer loop instead of directly interacting with the scissile phosphate.

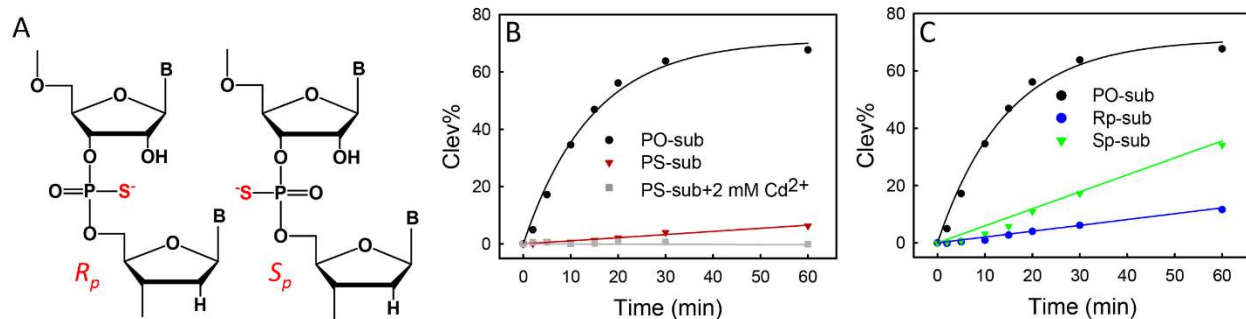


Figure 3.7 (A) The R_p and S_p phosphorothioate diastereomers at the cleavage junction. (B) The comparison between the normal PO-substrate and the PS-substrates of NaH1 in the presence of 10 mM NaCl with or without 2 mM Cd^{2+} . (C) Cleavage activity of NaH1 using PO-, R_p -, or S_p -substrates in the presence of 10 mM NaCl.

The loss of activity with PS-substrates could be due to a diminished hydrogen bonding between catalytic A22 and non-bridging oxygens caused by the sulfur substitution. The importance of the exocyclic amine of A22 has been addressed in the activity study of A22-to-2AP mutant. The activity of NaH1 was further measured with the two diastereomers R_p and S_p (Figure 3.7A). The cleavage rates of both R_p and S_p substrates were slower than the PO-substrate (Figure 3.7C). With a relatively lower activity, the *pro*- R_p oxygen seems to contribute more to interacting with the catalytic adenine at the cleavage site. Notably, the *pro*- R_p oxygen was reported to be more important in the catalysis of many RNA-cleaving ribozymes and DNAzymes including the hammerhead,¹⁶⁴ HDV ribozymes,^{111, 112} and the Ce13d DNAzyme.¹¹⁰ For example, in the HDV ribozyme, the *pro*- R_p oxygen directly interacts with a Mg^{2+} ion and is within hydrogen bonding distance of a catalytic C75 according to its crystal structure.^{34, 111}

In addition, the activity difference between the R_p - and S_p -substitutions was only ~3-fold, suggesting that both of the non-bridging oxygens are involved in interacting with the catalytic

adenine. A similar difference was also seen in a study of the activity of Ce13d (<10-fold) with the PS-substrates.¹¹⁰ As a comparison, the activity of the S_p was >100-fold faster than the R_p in the hammerhead ribozyme.^{164, 165} The importance of the 6-amino group in A22 has been addressed in the previous mutation study. Together, I propose that both of the non-bridging oxygens can form hydrogen bonding with the 6-amino of A22 in NaH1. The *pro-R_p* oxygen likely plays a slightly more important role than the *pro-S_p* oxygen. The involvement of both oxygens might also contribute to the tolerance to different catalytic mechanisms.

Finally, mass spectrometry has been applied to analyze the cleavage product of NaH1 (Figure 3.9). The 5'-fragment of the cleaved substrate terminated with a 2', 3'-cyclic phosphate (Figure 3.8). Therefore, a normal RNA cleavage mechanism was confirmed. Taken together, Figure 3.10 schematically illustrates the catalytic mechanism of the Na⁺-dependent RNA-cleaving DNazymes from this study. In NaH1, a N1-protonated adenine (A22) with a shifted pK_a of ~6.3 serves as a general acid, which could stabilize the negative charge on the 5'-leaving oxygen. Meanwhile, 2AP- and PS-substitution assays suggested that 6'-exocyclic amine directly participates in the cleavage by forming the hydrogen bonding with both of the non-bridging oxygens. In the wild-type NaA43, the N1 position of G23 functions as a general base with its pK_a shifted to ~6.6 during the reaction. Its deprotonated form facilitates the deprotonation of the 2'-OH, which then performs the nucleophilic attack on the scissile phosphate. Due to their high sequence similarity, the Na⁺-dependent DNzyme was proposed to fold into a defined structure upon Na⁺ binding with catalytic purine bases at the active site accelerating the RNA cleavage.

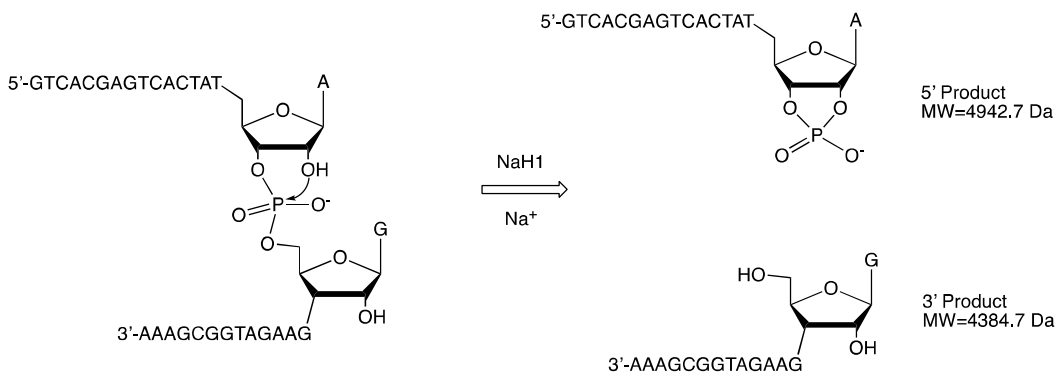


Figure 3.8 Scheme illustrating the cleavage products including a 2', 3'-cyclic phosphate and a 5'-hydroxyl.

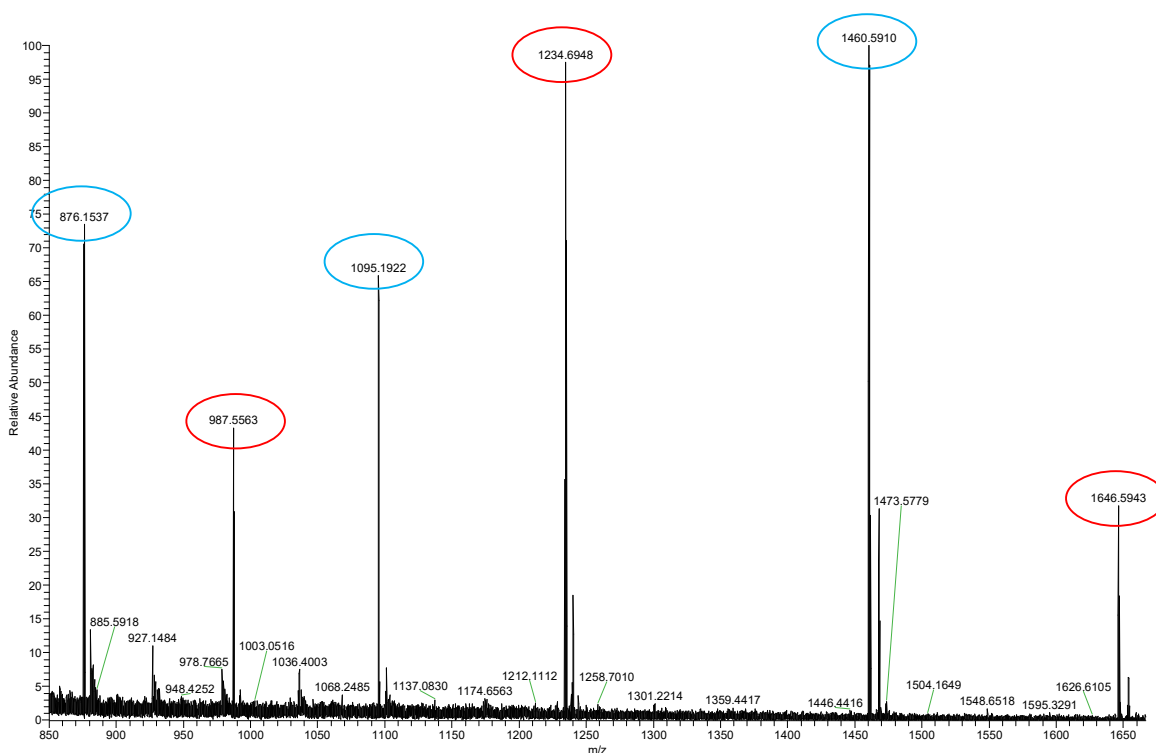


Figure 3.9 Mass spectrometry characterization of the NaH1 cleavage product. The red peaks represent the 5'-fragment of the cleaved-substrate containing a 2', 3'-cyclic phosphate group (MW=4942.7 Da, 3, 4 and 5 charges for three marked peaks). The blue peaks represent the 3'-fragment of the cleaved-substrate (MW=4384.7 Da, 3, 4 and 5 charges for the three marked peaks). The sample was prepared by reacting

non-labeled substrates (Table 4) with NaH1 DNAzymes (in 1:1.5 ratio) in 50 mM MES buffer (pH 6, 25 mM LiCl, 100 mM NaCl) for overnight. A Sep-Pak column was further used to desalt the sample. After dried, the sample was re-suspended in 20 μ L Milli-Q water with a final substrate concentration of \sim 50 μ M and analyzed with an ESI mass spectrometer.

3.3 Summary

The NaA43 and NaH1 DNAzymes were selected separately under different selection conditions. The pH optima of each DNAzyme matched the pH of their respective selection buffers. Despite their high sequence similarity, the minor differences near the cleavage site resulted in distinct pH preferences. In this work, rational evolution studies revealed a 4 to 5-nt catalytic motif in these DNAzymes. Furthermore, a series of mutation studies in NaH1 demonstrated that A22 is indispensable for its catalysis, and previous studies indicated that G23 plays an important role in NaA43. Combining with pH-rate profiles of their base analogs, the N1 position of A22 (pK_a shifted to \sim 6.3) functions as a general acid in NaH1, while N1 of G23 (pK_a shifted to \sim 6.6) serves as a general base in NaA43. Base analogs revealed the importance of 6-amine in A22 for the catalysis. To our knowledge, this is the first report of a shift between general acid and base catalysis mechanism by mutating only one or two nucleotides in a conserved DNAzyme scaffold. Notably, this scaffold is also active with a diverse range of polyvalent metal ions by removing the current catalytic motif. Such tolerance may explain the ability to use distinct reaction mechanisms on such a small structure. Future studies may include NMR spectroscopy to directly monitor the actual pK_a values of critical residues in the DNAzymes and study kinetic isotope effects for probing proton transfer.

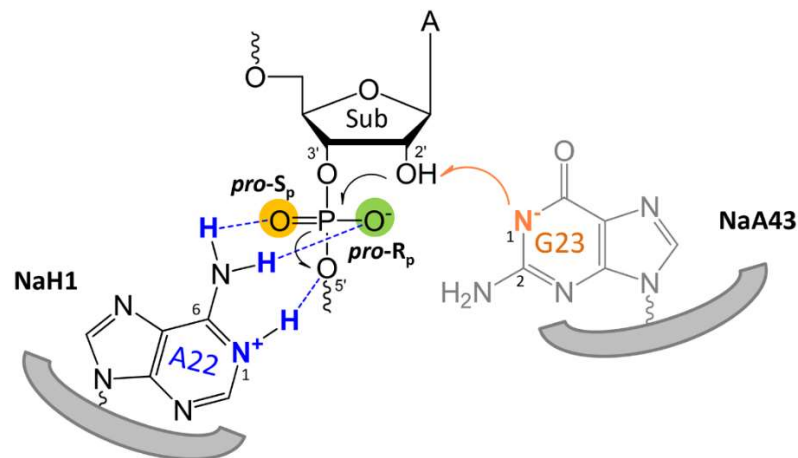


Figure 3.10 A model describing the general acid/base mechanism of the NaH1 and NaA43 DNAzymes in the RNA cleavage reaction.

3.4 Materials and methods

3.4.1 Oligonucleotides and chemicals

All the DNA samples used in this chapter were purchased from Integrated DNA Technologies (Coralville, IA). Sodium chloride, lithium chloride, potassium chloride, acetate acid, 2-(N-morpholino)ethanesulfonic acid (MES), 2-[4-(2-hydroxyethyl)piperazin-1-yl]ethanesulfonic acid (HEPES), and 3-(N-morpholino)propanesulfonic acid (MOPES) were from Mandel Scientific (Guelph, ON, Canada). Lithium hydroxide was purchased from Alfa Aesar. All solutions and buffers used in this work were prepared with Milli-Q water. All the DNA sequences used in this work are listed in Table 4.

Table 4. A list of DNA sequences (from 5' to 3') used in chapter 3.

DNA Names	Sequences and modifications
FAM-PO-Sub	GTCACGAGTCACTATrAGGAAGATGGCGAAA-FAM
NaH1	TTTCGCCATAGGTCAAAGGTGGGTGGGAGTTTTTACTCCGCATTAGTGA CTCGTGAC
NaA43T	TTTCGCCATCCAGGTCAAAGGTGGGTGAGGAGTTTTTACTCCGCGGTTA GTGACTCGTGAC
NaH1-G	TTTCGCCATAGGTCAAAGGTGGGTGGGAGTTTTTACTCCGCGTTAGTGA CTCGTGAC
NaH1-2AP	TTTCGCCATAGGTCAAAGGTGGGTGGGAGTTTTTACTCCGC/2AP/TTAGT GACTCGTGAC
NaH1-2,6diAP	TTTCGCCATAGGTCAAAGGTGGGTGGGAGTTTTTACTCCGC/2,6- diAP/TTAGTGACTCGTGAC
NaA43T-A	TTTCGCCATCCAGGTCAAAGGTGGGTGAGGAGTTTTTACTCCGCGATTA GTGACTCGTGAC
NaA43T-I	TTTCGCCATCCAGGTCAAAGGTGGGTGAGGAGTTTTTACTCCGCG/I/TTA GTGACTCGTGAC
Sub	GTCACGAGTCACTATrAGGAAGATGGCGAAA
Sub-dA	GTCACGAGTCACTATAGGAAGATGGCGAAA
FAM-PS-Sub	GTCACGAGTCACTATrA*GGAAGATGGCGAAA-FAM

3.4.2 Activity assays

The FAM-labeled substrate (2 μ M) was respectively hybridized with each enzyme or their mutants (3 μ M) in the reaction buffer to form the DNAzyme complexes. The mixtures were annealed by heating at 93 $^{\circ}$ C for 1 min and then gradually cooling down to 4 $^{\circ}$ C for over 30 min. The DNAzyme complexes were then diluted in reaction buffer (6 μ L) to 0.3 μ M. A small volume (1 μ L) of NaCl was then added to initiate the cleavage reaction with a final concentration of 10 mM Na⁺. At each time point, a 7 μ L reaction solution was quenched with 8 μ L of 8 M urea. The cleavage products were quantified by 15% denaturing polyacrylamide gel electrophoresis (dPAGE)

and analyzed by a Bio-Rad Chemi-Doc MP imaging system. Reaction buffer A (50 mM MES, pH 6.0, 25 mM LiCl) and buffer B (50 mM MOPES, pH 7.0, 25 mM LiCl) were used.

Kinetic data were fit with the first-order equation, $\%P_{cleavage,t} = \%P_{max}(1 - e^{-k_{obs}t})$, where $\%P_{max}$ is the maximum cleavage yield at the end of the reaction and k_{obs} is the cleavage rate constant. For pH-rate profiles, acetate buffer (50 mM) was used for pH 4.0 and 4.5; MES buffer (50 mM) for pH 5.5 to 6.5; and MOPES buffer (50 mM) for pH 7.0 to 8.0. All the buffer solutions were adjusted by 1 M LiOH to eliminate background Na^+ . The pH-rate profiles of NaH1 and NaA43 were fit with equations $k_{obs} = \frac{k_{max}}{1+10^{(pH-p_a)}}$ and $k_{obs} = \frac{k_{max}}{1+10^{(pK_a-pH)}}$ respectively, where k_{obs} is the observed rate constant, and k_{ma} is the maximal observed rate constant.

3.4.3 Phosphorothioate substitution

The FAM-labeled PS-modified substrates, R_p and S_p , were separated using HPLC as described previously.⁷⁰ The substrates were annealed with the DNazymes with a ratio of 1:1.5. Cleavage kinetics was measured in the presence of 10 mM NaCl for 1 h in reaction buffer A for NaH1 or buffer B for NaA43T. In the metal rescue assays, CdCl_2 was introduced in the reaction with a final concentration of 2 mM.

3.4.4 Fluorescence spectroscopy.

The DNzyme complex was prepared by annealing the 2-aminopurine (2AP)-modified enzyme and non-modified substrate with a ratio of 1:2 in buffer A (50 mM MES, 25 mM LiCl, pH 6.0). The mixture was heated to 93°C for 1 min followed by gradual cooling down to 4°C. With excitation at 310 nm, the emission was measured from 360 to 450 nm. Small volumes of chloride salts were gradually titrated into the sample to achieve a final concentration up to 45 mM. After a

quick mix, the fluorescence signal was immediately measured in a 1×1 cm quartz fluorescence cuvette using a Cary Eclipse fluorometer. The emission intensity enhancement at 370 nm was normalized by F/F_0 , where F_0 and F represent the fluorescence signal before and after the addition of Na^+ , respectively. The K_d value was obtained by fitting into the one-site binding equation: $F = F_0 + a \cdot [L^+]/(k_d + [L^+])$. $[L^+]$ is the metal concentration, and a is the fluorescence change when $[L^+] = \infty$.

3.4.5 Sample preparation for mass spectrometry

The sample was prepared by reacting non-labeled substrates (Table 4) with NaH1 DNazymes (in 1:1.5 ratio) in 50 mM MES buffer (pH 6, 25 mM LiCl, 100 mM NaCl) for overnight. A Sep-Pak C18 column (Waters) was further used to desalt the reacted sample. The Sep-Pak column was first prepared by washing with following solvents according to the order: 95% methanol (10 mL), acetonitrile: methanol: H_2O in 1:1:1 ratio (10 mL), Milli-Q water (20 mL), and 2M ammonium acetate (10 mL). The DNA sample (<1 mL) was then loaded on the column by slowing flowing through several times, followed by rinsing with 10 mL Milli-Q water. The DNA sample was then eluted out with acetonitrile: methanol: H_2O in 1:1:1 ratio. After dried, the sample was re-suspended in 20 μL Milli-Q water with a final substrate concentration of $\sim 50 \mu\text{M}$ and analyzed with an ESI mass spectrometer.

Chapter 4. Explore the Ubiquitous Activity of Lead (II) Ion in RNA-Cleaving DNazymes

4.1 Introduction

Lead (II) ions are known to promote RNA cleavage for a long time, and two types cleavage reactions have been extensively studied. In the 1990s, non-specific degradation of RNA with a high concentration of Pb^{2+} (mM level) at multiple sites was reported, which has been applied for probing RNA structure.¹⁶⁶ In the other type, much lower Pb^{2+} concentrations (nM to μM) can enable specific RNA cleavage in highly structured RNAs. A well-studied example is the Pb^{2+} -induced site-specific cleavage observed in the yeast tRNA^{Phe}.^{167, 168} Inspired by this, *in vitro* selection experiments were performed to obtain a small ribozyme that catalyzes site-specific RNA cleavage in the presence of Pb^{2+} , known as the leadzyme.^{47, 169} Biochemical and crystallographic data provided insights into its cleavage mechanism.¹⁷⁰⁻¹⁷² In the generally accepted mechanism, a Pb^{2+} -bound hydroxyl group (first pK_a of ~ 7.4) serves as a general base in promoting the deprotonation of 2'-hydroxyl group on the cleavage ribose.^{169, 171} The lead-induced cleavage rate was found to increase with an increasing pH up to pH 7.0-7.5, supporting the general base role played by Pb^{2+} hydroxides.¹⁷⁰ Further studies also showed that the addition of other metal ions (e.g., Mg^{2+} , Ba^{2+} , Nd^{3+} , Sm^{3+}) can enhance the Pb^{2+} -induced activity, indicating multiple metal binding sites in the leadzyme structure.^{173, 174}

The Pb^{2+} -induced RNA cleavage has inspired early *in vitro* selection works in finding catalytic DNA motifs. In 1994, the first RNA-cleaving DNzyme, GR5, was selected in the presence of Pb^{2+} by Breaker and Joyce.⁵ Its cleavage rate can easily reach $>10 \text{ min}^{-1}$ with only $10 \mu\text{M}$ Pb^{2+} .⁴⁸ In recent years, selection efforts have been made to search a Pb^{2+} -dependent DNzyme

with a smaller enzyme loop similar to a leadzyme.¹⁷⁵ These selections used Pb^{2+} and thus it is not surprising that the evolved DNAzymes were active with Pb^{2+} . Interestingly, Pb^{2+} -induced cleavage (even at μM and nM level) was frequently observed in many RNA-cleaving DNAzymes selected in the presence of other metal ions (Table 5).

The best-studied example is the 8-17 and 17E DNAzymes that were initially selected with Mg^{2+} and Zn^{2+} .^{49, 60} Nevertheless, the apparent K_d values are $13.5 \mu\text{M}$ Pb^{2+} and 0.97 mM Zn^{2+} (at pH 6.0), suggesting a higher binding affinity toward Pb^{2+} .^{61, 62} Therefore, the 17E DNAzyme has been widely designed into lead biosensors by coupling with various signaling methods.^{11, 19} The crystal structure of 17E was recently solved revealing a Pb^{2+} -bound water molecule as a general acid stabilizing the 5'-O on the leaving residue.¹¹⁴ Meanwhile, a conserved guanine near the cleavage site facilitates the deprotonation of 2'-OH as a general base. Biochemical studies on pH-rate profiles revealed the general base role of a guanine,^{61, 116} and the general acid role of Pb^{2+} was confirmed based on pH-rate profiles and phosphorothioate-modified DNAzymes.^{117, 176}

The commonly detected cleavage induced by Pb^{2+} can be considered as a potential interference when designing other DNAzymes into biosensors. For example, the presence of $10 \mu\text{M}$ Pb^{2+} can induce moderate fluorescence signal in DNAzyme-based molecular beacons for sensing metal ions such as lanthanide and calcium.^{66, 67} To overcome this issue, a thiol ligand such as mercaptohexanol (MCH) was introduced to mask the possible Pb^{2+} in the sensing environment.

Table 5. A literature summary of all the RNA-cleaving DNAzymes in which the Pb^{2+} -induced activity was detected in previous studies. Except for 17E, other Pb^{2+} -induced cleavage rates were approximately calculated based on the reported cleavage yields.

DNAzymes	Metal ion cofactor, k_{obs}	pH	Pb ²⁺ induced cleavage
17E ⁶¹	10 mM Zn ²⁺ , 1.35 min ⁻¹	6	100 μM, 5.75 min ⁻¹
EtNa ^{65, 66}	1 mM Ca ²⁺ , 2.5 h ⁻¹	6	20 μM, ~0.4 h ⁻¹
Ce13d ⁶⁷	10 μM Ce ³⁺ , 0.18 min ⁻¹	6	10 μM, ~0.01 min ⁻¹
Lu12 ¹⁷⁷	10 μM Nd ³⁺ , 0.12 min ⁻¹	6	100 μM, below 0.3 h ⁻¹
NaH1 ¹⁵⁴	50 mM Na ⁺ , 0.11 min ⁻¹	6	100 μM, below 0.1 h ⁻¹
Ag10c ⁷⁴	10 μM Ag ⁺ , 0.41 min ⁻¹	7.5	100 μM, below 0.1 h ⁻¹
39E ¹⁷⁸	10 μM UO ₂ ²⁺ , 1.23 min ⁻¹	5.5	1 mM, below 0.1 h ⁻¹

While the Pb²⁺ interference problem to biosensors can be solved by adding a masking agent, we know very little mechanistically why can Pb²⁺ induce cleavage in these DNAzymes that are evolved to be specific for other metal ions, and how does Pb²⁺ influence their intrinsic metal-specific activities? What makes Pb²⁺ more effective than other metal ions in catalyzing the RNA cleavage reaction? To answer these questions, I studied the effect of Pb²⁺ on two Na⁺-dependent DNAzymes. These DNAzymes share a common Na⁺-binding loop which forms a well-defined structure under a low Na⁺ concentration (e.g. ~10 mM). The activity of these DNAzymes depends solely on sodium ions which makes them an excellent model for studying this purpose since no divalent ion is present. Another DNAzyme that is active with both lanthanides and Pb²⁺ was studied. Finally, Pb²⁺ significantly enhanced the cleavage activity of a Ca²⁺-dependent DNAzyme. These studies point to the roles of Pb²⁺ as a general acid and a Lewis acid. The mechanistic versatility of Pb²⁺ may explain its ubiquitous promoting effect in DNAzymes.

4.2 Results

4.2.1 Distinct Pb^{2+} effects on sodium DNazymes

I first investigated the effect of Pb^{2+} on two Na^+ -dependent DNazymes, NaA43 and NaH1.^{72, 154} From their secondary structures, NaA43T (Figure 4.1A) and NaH1 (Figure 4.1B) both possess a Na^+ -binding aptamer loop (16-nt), which directs the global folding of DNazymes into active structures.^{73, 127} NaA43T is a truncated form of NaA43 with a similar activity and specificity for Na^+ .⁷³ Although these two DNazymes differ only by one or two bases, their opposite pH dependencies revealed distinct catalytic mechanisms.¹⁷⁹ Previous study demonstrated that NaA43T has a general base catalysis mechanism (G23 being the general base), while NaH1 has a general acid mechanism (A22 being the general acid).

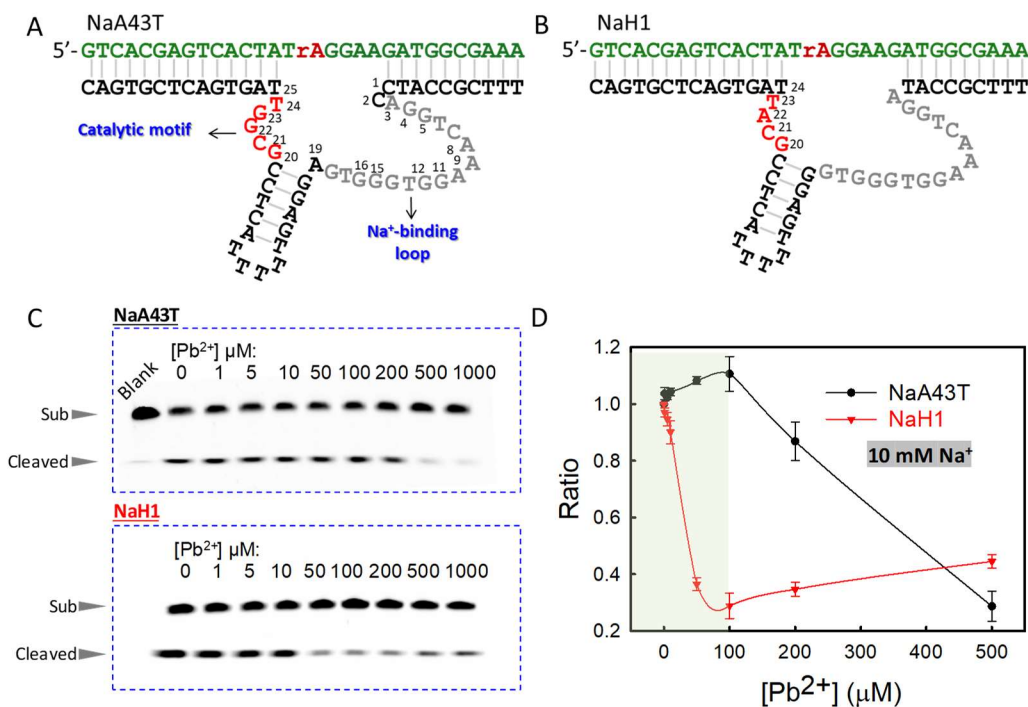


Figure 4.1 Secondary structures of two Na^+ -dependent DNazymes including (A) NaA43T and (B) NaH1. (C) Gel images of cleavage results after 1 h incubation in the presence of 10 mM Na^+ and various Pb^{2+}

concentrations. The cleavage reaction of NaA43T (top) and NaH1 (bottom) was measured at pH 7.0 and pH 6.0, respectively. (D) The cleavage ratio of NaA43T (black dots) and NaH1 (red triangles) in the presence of 10 mM Na⁺ and various Pb²⁺ concentrations. $Ratio = \frac{Cleavage\%}{Cleavage\%(without\ Pb^{2+})}$.

The activity of these two DNazymes depends solely on sodium ions, which makes them excellent models for studying the effect of Pb²⁺ since no additional divalent ions are required. I first tested the effect of Pb²⁺ on their activity in the presence of 10 mM Na⁺. Interestingly, distinct results for NaH1 and NaA43T were observed. For NaA43T, a low concentration of Pb²⁺ (below 100 μM) had almost no effect on its cleavage activity (Figure 4.1C, top). With over 100 μM Pb²⁺, the activity decreased with increasing Pb²⁺ concentration and thus Pb²⁺ acted as an inhibitor of the DNzyme (Figure 4.1D). On the contrary, a significant inhibition effect was observed in NaH1 with only 30% activity left in the presence of 100 μM Pb²⁺ (Figure 4.1C, bottom). Since a low Pb²⁺ concentration had no effect on NaA43T, such an inhibition in NaH1 was not due to nonspecific perturbation of the structure. After that, the activity only slightly increased upon adding more Pb²⁺. Based on the small amount of activity increase (thus a large apparent K_d for Pb²⁺ beyond 100 μM), it is likely due to Pb²⁺ acting as a poor cofactor to catalyze this reaction (Figure 4.1D). The following study mainly focused on Pb²⁺ concentrations below 100 μM.

Due to the distinct effects observed at low Pb²⁺ concentrations (below 100 μM), Pb²⁺ may play a specific role at the cleavage site of the Na⁺ DNazymes instead of non-specific structural effects. Especially for NaH1, based on previous studies, Na⁺ does not interact with the cleavage site.¹⁷⁹ Instead, Na⁺ indirectly assists the reaction by positioning A22 during the catalysis. This adenine is highly conserved and serves as a general acid by interacting with the 5'-O on the leaving residue. I suspected that the Pb²⁺-induced inhibition is likely through competing with a

catalytically important group at the cleavage site. To confirm the hypothesis, the cleavage rate of NaH1 was compared with or without 50 μM Pb^{2+} . As shown in Figure 4.2A, when the Na^+ concentration was sufficiently high (above 100 mM), the inhibition effect caused by Pb^{2+} was suppressed. On the contrary, the addition of 10 mM Na^+ and 90 mM Li^+ failed to resume the cleavage activity, ruling out the ionic strength effect of Na^+ (Figure 4.2B). Consequently, Pb^{2+} competitively inhibits the functional group in the cleavage reaction, which can be overcome by a high Na^+ concentration (above 100 mM). The apparent K_i was calculated to be 13.4 μM Pb^{2+} using the apparent K_d values measured with or without 50 μM Pb^{2+} (Figure 4.2A). A relatively high binding affinity further indicates a specific interaction of Pb^{2+} at the cleavage site which interrupting the catalysis mechanism.

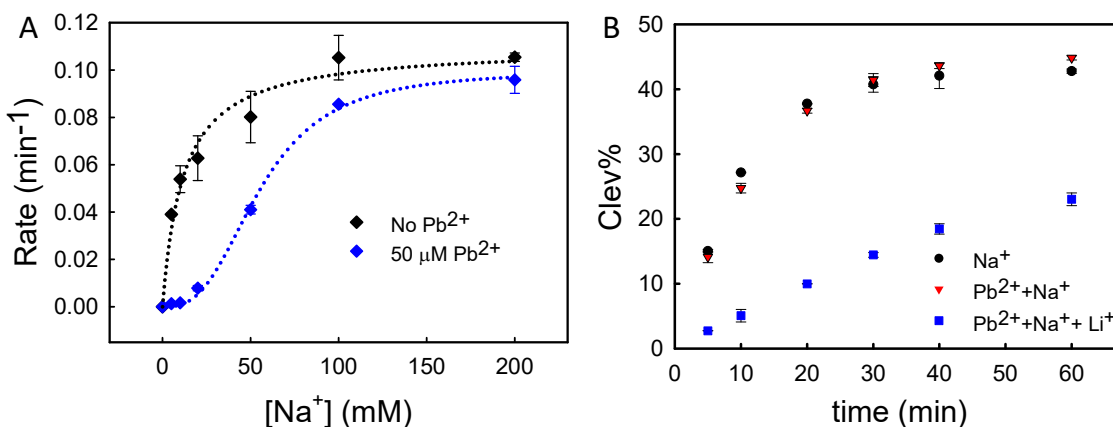


Figure 4.2 (A) A competitive inhibition of NaH1 induced by 50 μM Pb^{2+} . In the absence of Pb^{2+} , the binding curve is obtained by fitting data (black dots) into a single binding site equation: $V = \frac{V_{max} [S]}{K_d + [S]}$ (the apparent $K_d = 11.7 \pm 2.44$ mM Na^+). In the presence of 50 μM Pb^{2+} , the sigmodal curve is obtained by fitting (blue squares) into a Hill equation: $V = \frac{V_{max} [S]^n}{K_d^n + [S]^n}$ (the apparent $K_d = 55.5 \pm 2.03$ mM Na^+ , $n = 2.8$). Therefore,

the apparent K_i can be calculated from $\frac{K_d [Pb^{2+}]}{K_{d'} - K_d} = 13.4 \mu\text{M Pb}^{2+}$. (B) The inhibition of NaH1 activity by 50 $\mu\text{M Pb}^{2+}$ was rescued by 100 mM Na^+ but not by 10 mM Na^+ and 90 mM Li^+ .

It is notable that the shape of the two binding curves in Figure 4.2A was very different. Without Pb^{2+} , NaH1 displayed one Na^+ binding site with an apparent K_d of 11.7 mM Na^+ , which can be assigned to the 16-nt Na^+ aptamer. However, with 50 $\mu\text{M Pb}^{2+}$, a Hill coefficient of 2.8 was obtained indicating positive cooperativity of Na^+ binding. I reason that in addition to the aptamer pocket, Na^+ must also compete with Pb^{2+} at the active site to relief the inhibition effect (likely two Na^+ ions were needed for this purpose to account for an overall Hill coefficient of close to 3). With Pb^{2+} , the apparent K_d obtained was 55.5 mM Na^+ which suggested an overall lower binding affinity caused by the Pb^{2+} binding. In previous studies, the general acid role of Pb^{2+} has been revealed in the 17E and 8-17 DNazymes.^{117, 176} Combined with our results, Pb^{2+} was proposed serve as a non-productive general acid to compete with the original general acid (adenine) mechanism in NaH1. The hydrated Pb^{2+} may be less efficient than the conserved adenine as a general acid, resulting in an inhibition on NaH1 activity. On the contrary, Pb^{2+} failed to affect the cleavage of NaA43T in which a general base (guanine) dominating the catalysis.

4.2.2 Pb^{2+} -induced cleavage in the Ce13d DNzyme

To further probe the Pb^{2+} role in these DNazymes, the Pb^{2+} activity in another related DNzyme, Ce13d, was studied.⁶⁷ The secondary structure of the Ce13d DNzyme is shown in Figure 4.3A. Its enzyme strand also contains the same Na^+ aptamer representing an overall folding resembling NaH1 and NaA43T.^{73, 140} At its cleavage site, a lanthanide ion (e.g., Ce^{3+}) is required to perform the cleavage, while no catalytic nucleobases were identified. Phosphorothioate (PS)

substitution at the cleavage site revealed the direct coordination between Ce^{3+} and non-bridging oxygens.¹¹⁰ In previous study, Pb^{2+} also activated Ce13d, although at a lower catalytic rate (~20-fold) compared to Ce^{3+} .⁶⁷ Here, I carefully examined its enzyme activity with micromolar Pb^{2+} . In the absence of Na^+ , the DNAzyme could not fold properly, and 200 μM Pb^{2+} only induced a mild cleavage (~20%) (Figure 4.3B, grey triangles). The observed cleavage cannot be simply attributed to non-specific RNA degradation since no product was detected in the rA-substrates alone (Figure 4.3B, black squares). Interestingly, its original metal cofactor, Ce^{3+} , lacked the ability to cleave in the absence of Na^+ (Figure 4.4A). Meanwhile, the cleavage is not due to an increased ionic strength since 1 mM Mg^{2+} and Ca^{2+} failed to induce a comparable cleavage (Figure 4.4B).

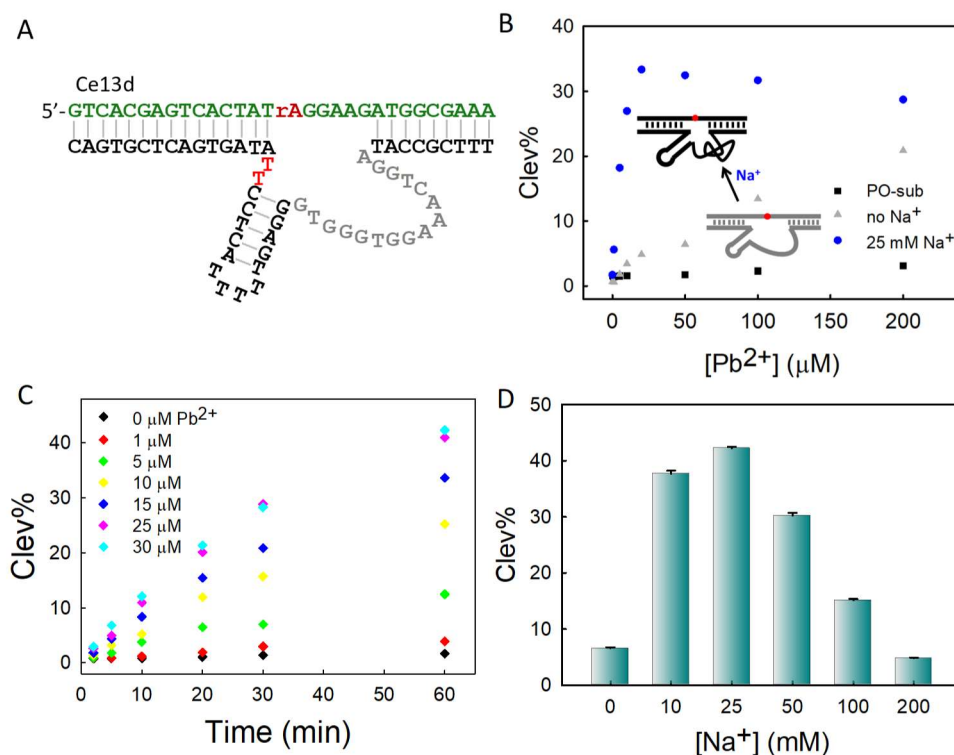


Figure 4.3 (A) Secondary structure of the Ce13d DNAzyme. (B) The Pb^{2+} -dependent activity of Ce13d measured with or without 25 mM Na^+ . Black circles represent the cleavages of PO-substrates alone as a

control. (C) Cleavage rates of Ce13d measured with various concentrations of Pb^{2+} and 25 mM Na^+ . (D) Effect of Na^+ concentration on the cleavage yields with 20 μM Pb^{2+} .

In the presence of 25 mM Na^+ (Figure 4.3B, blue circles), the activity of Ce13d became highly sensitive to low concentrations of Pb^{2+} (below 20 μM). The kinetics showed that the cleavage rates gradually increased with an increasing Pb^{2+} concentration up to 30 μM (Figure 4.3C). The Pb^{2+} -induced activity of Ce13d also depended on Na^+ concentration. The addition of 25 mM Na^+ can promote the global folding of the DNAzyme allowing Pb^{2+} cofactor to function in the reaction more efficiently (Figure 4.3D). However, further increasing the Na^+ concentration resulted in a lower cleavage yield. For example, almost no activity was detected in the presence of 200 mM Na^+ . This can be explained by an increased salt concentration which prevents Pb^{2+} from reaching the cleavage site in the DNAzyme structure. Together, in Ce13d, the global folding induced by Na^+ (~25 mM) allows Pb^{2+} to function in the cleavage reaction.

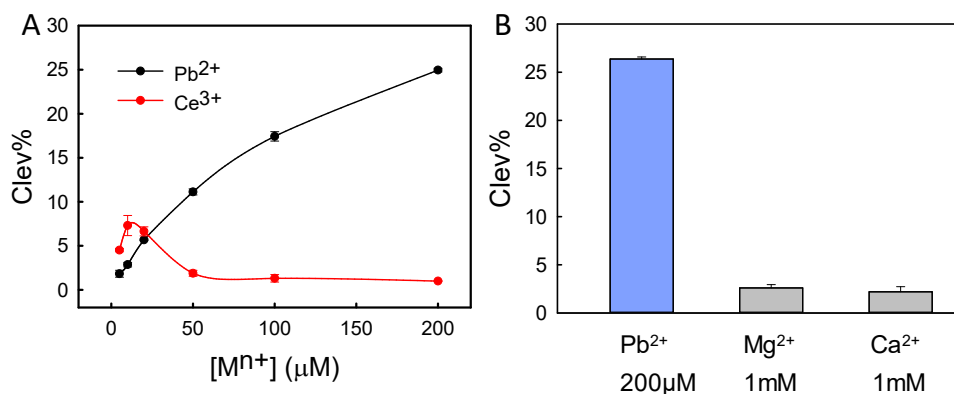


Figure 4.4 (A) Cleavage yields of Ce13d measured in various concentrations of Pb^{2+} or Ce^{3+} without Na^+ (1 h). (B) The comparison of cleavage% of Ce13d in the presence of 200 μM Pb^{2+} or 1 mM $\text{Mg}^{2+}/\text{Ca}^{2+}$ without Na^+ (1 h).

The pH dependency was then studied to gain insights into the participation of general acid or base groups during the catalysis. As shown in Figure 4.5A, the Pb^{2+} -induced activity gradually decreased when the pH increased from 6.4 to 7.3. The logarithm of rates linearly decreased in this pH range with a slope close to -1 (Figure 4.5B), indicating a single protonation step in the reaction. The first $\text{p}K_a$ of Pb^{2+} -bound water is within 6.5 to 8.4. Thus, Pb^{2+} may serve as a general acid group functioning in the rate-limiting step. Interestingly, the Ce^{3+} -induced activity in Ce13d remains between pH 6 to 7.¹¹⁰ Thus, Pb^{2+} can facilitate the Ce13d activity by acting as a general acid. This mechanism is different from that of Ce^{3+} (a Lewis acid interacting with the scissile phosphate) and the Pb^{2+} mechanism had a lower efficiency.¹¹⁰

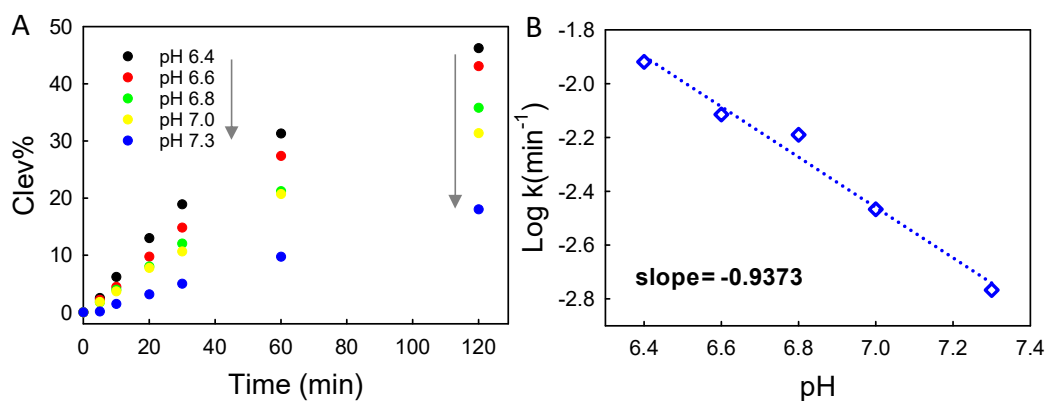


Figure 4.5 (A) Cleavage rates of 20 μM Pb^{2+} (25 mM Na^+) measured in different pH buffers from pH 6.4 to 7.3. The buffers used here are 20 mM PIPES buffer (40 mM LiCl). (B) The logarithm of rate against pH revealing a linear relationship with a slope of -0.9373.

4.2.3 Pb^{2+} -enhanced cleavage activity in the EtNa DNzyme

Apart from these Na^+ DNzyme scaffold, I further investigated the Pb^{2+} activity in an unrelated DNzyme, the EtNa DNzyme. The EtNa DNzyme (Figure 4.6A) was initially selected in the presence of Na^+ and isopropanol.⁶⁵ Further activity studies revealed its exceptional

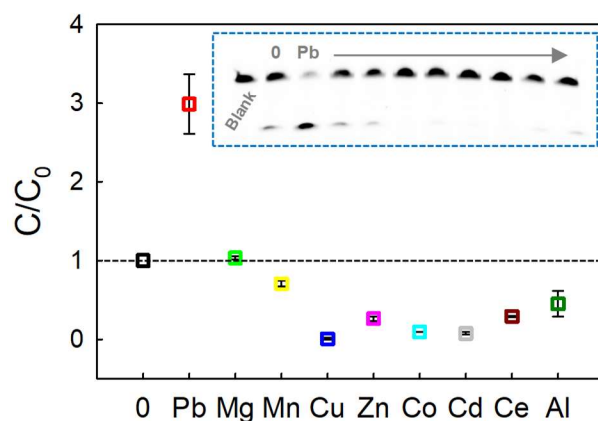


Figure 4.7 Metal ion effects on the EtNa activity in 100 μM Ca^{2+} . The reaction performed in 100 μM Ca^{2+} alone without additional metals was indicated as 0, which was the initial cleavage (C_0). All the cleavage yields were measured after 1 h incubation with the addition of 20 μM divalent (Pb^{2+} , Mg^{2+} , Mn^{2+} , Cu^{2+} , Zn^{2+} , Co^{2+} , Cd^{2+}) or trivalent (Ce^{3+} , Al^{3+}) metal ions. The y-axis was quantified by dividing the initial cleavage (C_0). Thus, the C/C_0 value >1 represents an enhancement, while $C/C_0 <1$ represents an inhibition.

When studying the effect of Pb^{2+} in EtNa, I found that Ca^{2+} -induced activity can be significantly enhanced by the addition of a low concentration of Pb^{2+} (Figure 4.6B). For instance, in the presence of 100 μM Ca^{2+} , a ~ 70 -fold increase in cleavage rate was detected after the addition of 20 μM Pb^{2+} (Figure 4.6B, green). The cleavage activity with 20 μM Pb^{2+} alone (Figure 4.6B, red) was also less efficient compared to the combination of Pb^{2+} and Ca^{2+} . Despite that Pb^{2+} can induce cleavage in many DNazymes, this is the only case where we found that Pb^{2+} enhances the original activity. The maximal cleavage rate detected is $\sim 0.4 \text{ min}^{-1}$ in the presence of 500 μM Ca^{2+} and 20 μM Pb^{2+} (Figure 4.6C). While the previously reported saturated cleavage rate of EtNa was $\sim 0.067 \text{ min}^{-1}$ in 2 mM Ca^{2+} .⁶⁶ Additionally, I compared the effect of other metal ions on the EtNa activity with 100 μM Ca^{2+} . As shown in Figure 4.7, Mg^{2+} had no effect on cleavage, while other

metal ions inhibited the Ca^{2+} -induced activity. Thus, the rate enhancement observed in Pb^{2+} is due to a specific function in the reaction.

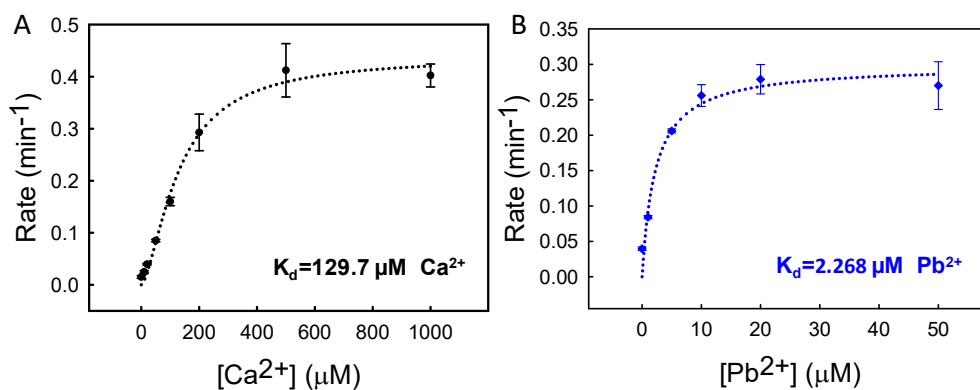


Figure 4.8 (A) Cleavage rates measured as a function of Ca^{2+} concentrations in the presence of $20 \mu\text{M Pb}^{2+}$.

The sigmoidal binding curve is fitted into a Hill equation, $V = \frac{V_{max} [L]^n}{K_d^n + [L]^n}$ ($[L]$ is the metal ion concentration),

where the apparent K_d is $129.7 \pm 17.03 \mu\text{M Ca}^{2+}$, $n=1.545$. (B) Cleavage rates increased with increasing Pb^{2+} concentrations in the presence of $500 \mu\text{M Ca}^{2+}$. The binding curve is fitted into a single binding site equation:

$$V = \frac{V_{max} [L]}{K_d + [L]} \text{ (the apparent } K_d = 2.268 \pm 0.747 \mu\text{M Pb}^{2+}\text{)}.$$

I then measured the cleavage rate of EtNa as a function of Ca^{2+} concentration. With $20 \mu\text{M Pb}^{2+}$ fixed, a sigmoidal binding curve was obtained with an apparent K_d of $129.7 \mu\text{M Ca}^{2+}$ (Figure 4.8A), which was approximately 8-fold smaller than that without Pb^{2+} .⁶⁶ A Hill coefficient (n) of 1.5 was obtained indicating more than one binding site for Ca^{2+} . This positive cooperativity is consistent with the binding curve reported in Ca^{2+} alone.⁶⁶ Therefore, the addition of Pb^{2+} did not disturb the Ca^{2+} binding at the cleavage site. In fact, EtNa displayed a stronger binding affinity toward Ca^{2+} promoted by Pb^{2+} . Thus, Pb^{2+} can be considered as an allosteric activator in protein enzymes, which binds to a different site than Ca^{2+} and stabilize the Ca^{2+} binding. To study the Pb^{2+}

binding, the Ca^{2+} concentration was then fixed and the Pb^{2+} -dependent cleavage rate was measured in EtNa. In the presence of $500\ \mu\text{M}\ \text{Ca}^{2+}$, an apparent K_d of $2.3\ \mu\text{M}\ \text{Pb}^{2+}$ was obtained from a single-site (hyperbolic) binding curve of EtNa (Figure 4.8B). Thus, one Pb^{2+} ion and at least one Ca^{2+} ion can bind to EtNa simultaneously.

To further explore the catalytic role of Pb^{2+} , I compared the pH dependency of EtNa in the presence of Ca^{2+} or Pb^{2+} , respectively. With $1\ \text{mM}\ \text{Ca}^{2+}$ (Figure 4.9B, red), the EtNa activity remained constant between pH 6.4 to 7.3, which was in an agreement with the previously reported data.⁶⁶ With $20\ \mu\text{M}\ \text{Pb}^{2+}$ alone (Figure 4.9B, blue), however, the activity decreased when pH increased from pH 6.4 to 7.3 (Figure 4.9A), which is consistent with the general acid role of Pb^{2+} . The linear decrease with a slope close to -1 supports the general acid role of Pb^{2+} . When both Ca^{2+} ($100\ \mu\text{M}$) and Pb^{2+} ($10\ \mu\text{M}$) are present (Figure 4.9B, green), the pH dependency was consistent with the Ca^{2+} -induced activity. This could be attributed to two possible scenarios. First, when the general acid (Pb^{2+}) decreases, the concentration of a general base group increases (e.g., an important guanine waiting to be identified), which results in an unaffected rate (k_{obs}). Alternatively, the combination effect of Ca^{2+} and Pb^{2+} may not be due to the general acid role of Pb^{2+} , but a stabilization to the Ca^{2+} -dominating catalysis (e.g. the rate-limiting step was related to Ca^{2+} instead of Pb^{2+}).

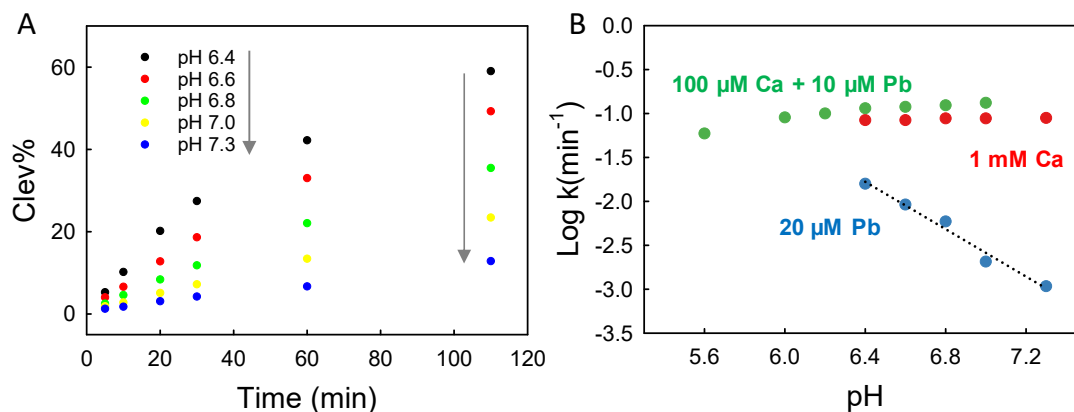


Figure 4.9 (A) Cleavage rates of EtNa measured in various pH buffers. The reaction was performed in 20 μM Pb^{2+} alone. (B) pH-rate profiles measured in 20 μM Pb^{2+} (blue), 1 mM Ca^{2+} (red), or 100 μM Ca^{2+} and 10 μM Pb^{2+} (green). The slope of 20 μM Pb^{2+} equals to -1.3498. The buffers used are: 20 mM MES buffer (40 mM LiCl) for pH 5.6 to 6.2; 20 mM PIPES buffer (40 mM LiCl) for pH 6.4 to 7.3.

4.3 Discussion

Lead-induced cleavage has been frequently reported when studying RNA-cleaving DNazymes. By studying the Pb^{2+} effect on the two Na^+ DNazymes, distinct results were observed. Low concentrations of Pb^{2+} (below 100 μM) significantly inhibited the NaH1 activity, while no inhibition effect was detected in NaA43T despite of their similarities. Considering that their major difference is the functional nucleobase in catalysis, Pb^{2+} may play a specific role at the cleavage site. In NaH1, a competitive inhibition was revealed with apparent K_i of 13.4 μM Pb^{2+} . Thus, the Pb^{2+} was proposed to specifically bind to the cleavage site and compete with the catalytic adenine (A22) in NaH1.

In Ce13d, micromolar Pb^{2+} (e.g., 200 μM) can induce a mild cleavage. In the presence of millimolar Na^+ , the DNzyme folds into a more compact structure which facilitates the binding

with even a lower concentration of Pb^{2+} (below 20 μM). The pH dependency revealed a general acid group functioning in the reaction. Since the first pK_a of Pb^{2+} -bound water is within 6.5 to 8.4, Pb^{2+} may fulfill this role by stabilizing the 5'-leaving oxygen. Thus, this provided another example for the same DNAzyme displaying alternative catalytic pathways.

Despite that Pb^{2+} can induce cleavage in many DNAzymes, EtNa is the only case where an enhancement was observed to its original activity. The EtNa activity can be supported by Ca^{2+} or Pb^{2+} individually. Nevertheless, the combination of Ca^{2+} and Pb^{2+} is much more efficient. Table 6 summarized cleavage rates of EtNa reported in different metal ions. Based on our results, Pb^{2+} ion performs a dual function in the catalysis (Figure 4.11D). First, Pb^{2+} can bind to EtNa specifically with an apparent $K_{d, \text{pb}}$ of 2.3 μM . The binding of Pb^{2+} in turn promotes the Ca^{2+} binding affinity in EtNa as indicated by a decreased $K_{d, \text{ca}}$ value. However, the reason for this stabilization induced by Pb^{2+} remains unknown. Meanwhile, Pb^{2+} can directly participate in the cleavage reaction possibly through a general acid mechanism. This is deduced from the increased activity detected under a lower pH condition which is different from Ca^{2+} alone. This general acid mechanism was not available in the absence of Pb^{2+} and thus Pb^{2+} assisted Ca^{2+} instead of competing with it.

Table 6. A summary of EtNa activity in various metal ions.

Metal ions	k_{obs}
2 mM Ca^{2+} ⁶⁶	0.067 min^{-1}
2 mM Mg^{2+} ⁶⁶	$8.3 \cdot 10^{-4} \text{ min}^{-1}$
20 μM Pb^{2+}	$9.8 \cdot 10^{-3} \text{ min}^{-1}$
500 μM Ca^{2+} , 20 μM Pb^{2+}	0.4 min^{-1}

Interestingly, a similar combined effect was also reported in the leadzyme, where rare earth ions (e.g., Nd^{3+} , Gd^{3+} , Tm^{3+} , and La^{3+}) enhanced its Pb^{2+} -induced cleavage.¹⁷⁴ Biochemical assays were carried out to study the combined effect of Nd^{3+} and Pb^{2+} .¹⁷³ The presence Nd^{3+} alone failed to induce cleavage and the enhancement highly depended on the concentration ratio of Nd^{3+} and Pb^{2+} . The optimal ratio was 1:1 while further increasing the Nd^{3+} concentration eliminated the enhancement. In the EtNa DNAzyme, I did not observe a rate decrease caused by increasing Pb^{2+} concentrations (up to 50 μM), but the Ca^{2+} concentration used was always higher than Pb^{2+} due to the relatively low binding affinity of Ca^{2+} to EtNa. In the leadzyme, a two-metal-ion mechanism was proposed in which Nd^{3+} -bound water serves as a general acid and the Pb^{2+} hydroxyl as a general base (Figure 4.11E).¹⁷³

Based on our observations, Pb^{2+} could affect catalysis of RNA-cleaving DNAzymes in multiple ways. In general, Pb^{2+} , as a soft Lewis acid, can bind to both phosphate groups and nucleobases in DNA or RNA. Most of time, Pb^{2+} was identified to directly interact with the cleavage site rather than direct the enzyme folding. For example, the 8-17 DNAzyme is most active in Pb^{2+} , and less active in Zn^{2+} and Mg^{2+} .⁶¹ However, a smFRET study demonstrated that both Zn^{2+} and Mg^{2+} induced the folding of DNAzyme into a compact structure which supported the subsequent cleavage activity, while no global folding was detected in Pb^{2+} , the most effective cofactor for the cleavage.¹⁰² Thus, Pb^{2+} does not necessarily require a global folding and can directly fit in the catalytic core of the 8-17 DNAzyme. In the uranyl-dependent DNAzyme (39E), FRET results suggested that Zn^{2+} and Mg^{2+} can induce global folding and thus inhibit its activity. No significant folding signal was observed with Pb^{2+} and UO_2^{2+} .¹⁰⁴ Therefore, Pb^{2+} tends to directly bind to the cleavage site without overly interfering the conformation. This can contribute to the ubiquitous activity of Pb^{2+} in RNA-cleaving DNAzymes.

With the pK_a of Pb^{2+} -bound water near neutral, Pb^{2+} is a natural candidate for general acid-base catalysis during the RNA hydrolysis. A Pb^{2+} -bound hydroxyl group was proposed to serve as a general base by deprotonating the 2'-OH which has been observed in tRNA^{Phe} and leadzyme.^{168, 169, 171} Alternatively, a Pb^{2+} -bound water can stabilize the 5'-O on the leaving ribose and therefore play a general acid role. So far, only the general acid role of Pb^{2+} has been proven in RNA-cleaving DNAzymes. The crystal structure of the 17E DNAzyme captured a Pb^{2+} in the catalytic core coordinating with both a nearby guanine and water molecules, suggesting a general acid role.¹¹⁴ However, biochemical studies on its pH-dependency revealed the protonation of a catalytic guanine being the rate-limiting step,^{61, 116} but the general acid role of Pb^{2+} was recently demonstrated as well.^{117, 176} In a recent study, by replacing the conserved guanine with 2-aminopurine, the general acid group was unmasked on the pH-rate profile with a pK_a value close to a hydrated Pb^{2+} (Figure 4.10).¹¹⁷ On the contrary, the Mg^{2+} -induced activity of the variant 17E was insensitive in the high pH region.

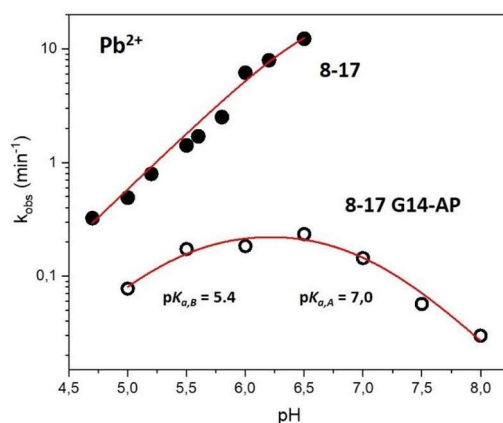


Figure 4.10 Comparison of pH dependency of the wild type 8-17 DNAzyme and the G14-AP variant in 200 and 100 μM Pb^{2+} , respectively. Reprinted with permission from ref 117. Copyright © Royal Society of Chemistry 2021.

In this current work, the Pb^{2+} -induced cleavage in Ce13d and EtNa both indicated a general acid functioning in the reaction that is rate-limiting. However, these results cannot exclude the possibility of Pb^{2+} serving as a general base at the meantime which might not be the rate-limiting role. In principle, Pb^{2+} can also stabilize the transition state by directly coordinating with the scissile phosphate as a Lewis acid. For example, the PS-modified Ce13d DNAzyme performed a high binding affinity to Pb^{2+} with an apparent K_d of 4.2 nM.¹⁵⁹ In this case, the PS modification at the cleavage site attracts the thiophilic Pb^{2+} ion to bind tightly (Figure 4.11A).

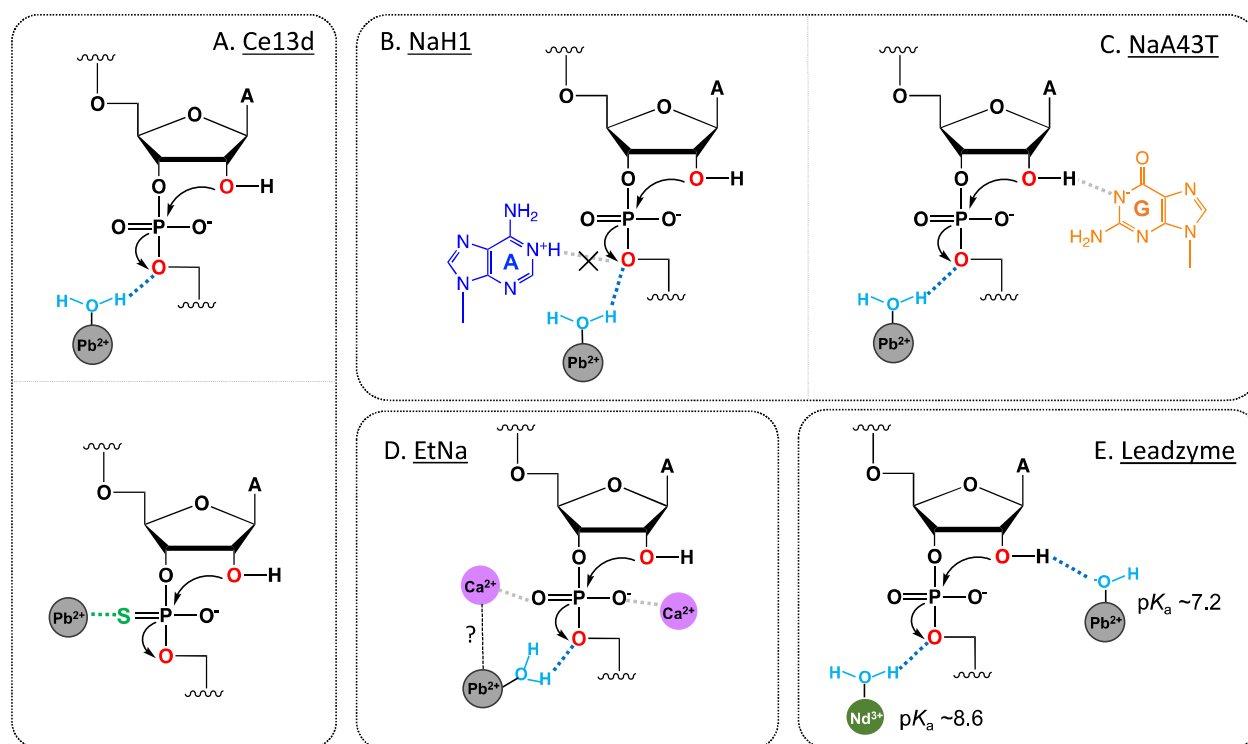


Figure 4.11 A schematic summary of various Pb^{2+} effects in the RNA cleavage reaction catalyzed by nucleic acid enzymes. (A) In Ce13d, a Pb^{2+} -bound water can function as a poor general acid. With a PS modification on the scissile phosphate, thiophilic Pb^{2+} ion can directly coordinate with the sulfur.¹⁵⁹ (B) In NaH1, a Pb^{2+} ion inhibits the activity by competing with the conserved adenine. (C) In NaA43T, no

inhibition effect of Pb^{2+} observed in the general base mechanism. (D) The combined effect of Ca^{2+} and Pb^{2+} in the EtNa DNAzyme. (E) The combined effect of Pb^{3+} and Nd^{3+} in the leadzyme. Redraw from ref¹⁷³.

4.4 Summary

In this chapter, I used several representative DNAzymes as examples to reveal the capability of Pb^{2+} binds specifically to the cleavage site (Figure 4.11). Upon binding, the hydrated Pb^{2+} can serve as a poor general acid and facilitate the RNA cleavage. In a special case, Pb^{2+} can cooperate with Ca^{2+} cofactor and enhance the activity of the EtNa DNAzyme. The mechanistic study of Pb^{2+} activity is important for understanding the DNAzyme catalysis. This could also provide insights in rational design of catalytic DNA or RNA with cleavage activity.

4.5 Materials and methods

4.5.1 Chemicals

The list of chemicals used in this chapter can be found in Chapter 2.4.1.

4.5.2 Activity assays

For cleavage activity assays, the DNAzyme complex was prepared by annealing the FAM-labeled substrate and enzyme (ratio 1:1.5) in 5 mM MES buffer (pH 6.0, 50 mM LiCl). The mixtures were annealed by heating at 93 °C for 2 min and then gradually cooling down to 4 °C for over 30 min. The DNAzyme complexes were then diluted to 0.2 μM in the reaction with a total volume of 7 μL . To initiate the cleavage, 0.5 or 1 μL metal ion solution was added. After incubation, a reaction solution (7 μL) was quenched with 8 μL of 8 M urea. The cleavage products were quantified by 15% denaturing polyacrylamide gel electrophoresis (dPAGE) and analyzed by a Bio-Rad Chemi-Doc MP imaging system. If not mentioned specifically, the reaction buffer used

was 50 mM MES buffer (pH 6, 25 mM LiCl). For pH-rate profiles, 20 mM MES buffers were used for pH 5.6 to 6.2, while 20 mM PIPES buffers were used for pH 6.4 to 7.3. All the buffers contain same LiCl concentration to eliminate the salt effect.

Chapter 5. *In Vitro* Selection of A Self-Cleaving Ribozyme Activated in Chemically and Thermally Denaturing Environment^d

5.1 Introduction

Many metal-specific DNAzymes have been isolated for biosensor development.^{8, 180, 181} Recently, a few related Na⁺-specific RNA-cleaving DNAzymes have been reported, including the NaA43,⁷² Ce13d,⁶⁷ and NaH1,¹⁸² all of which containing the same Na⁺ aptamer motif.⁷³ Ribozymes, on the other hand, were mainly selected in the presence of Mg²⁺,^{180, 183} since they were intended to work in cells. Some naturally occurring RNA motifs can recognize metal ions, with the best examples present in riboswitches, where riboswitches for Co²⁺/Ni²⁺,¹⁸⁴ W/Mo,¹⁸⁵ and even F⁻ have been reported.¹⁸⁶ Given the excellent Na⁺-binding property of these DNAzymes, I wondered whether similar ribozymes exist. Since Na⁺ is an important metal in biology, its ribozymes and aptamers might also be important in regulating its concentration. In this work, a selection experiment was performed in searching Na⁺-dependent ribozymes. Strikingly, the obtained ribozyme showed no metal dependency and was even inhibited by metal ions. However, it is highly active under all typical denaturing conditions for nucleic acids, including high temperature, denaturing solvents, and low metal concentrations.

Denaturants, such as formamide, urea, and DMSO, can disturb secondary and tertiary structures in nucleic acids resulting in a decreased melting temperature (T_m). An early interest in

^d This chapter is the basis for an accepted manuscript: Ma, L.; Huang, Z.; Liu, J., Selection of a self-cleaving ribozyme activated in chemically and thermally denaturing environment. *Chemical Communications* **2021**, 57 (62), 7641-7644.

using denaturants (1-5%) was to improve the specificity of primer annealing in PCR by minimizing unfavorable secondary structures.¹⁸⁷ In nucleic acid enzyme activity assays, denaturants (~7 to 10 M) along with EDTA were often added to destroy the active structures, thus quenching the reactions. A special example is the HDV ribozyme, where formamide (up to 20 M) or urea (up to 10 M) can enhance its Mg^{2+} -mediated cleavage activity.^{188, 189} Moreover, a vector sequence-containing HDV ribozyme was initially inactive, but started to show cleavage under partially denaturing conditions.¹⁹⁰

Divalent metal ions in millimolar concentrations are typically used for studying ribozyme activity *in vitro*. Metal ions (e.g., Mg^{2+} , Mn^{2+} , Ca^{2+}) can facilitate folding of active RNA structures and directly participate in catalytic reactions.^{119, 191} In the cleavage of a RNA phosphodiester bond, it is well established that hydrated metal ions can accelerate the reaction through a general acid-base mechanism. Alternatively, metal ions, as Lewis acids, can stabilize the negative charge developed on the nucleophile, the leaving group, or the non-bridging oxygens. Cleavage activity induced by high concentrations (~1 to 4 M) of monovalent ions (e.g., Na^+ , Li^+ , K^+ , NH_4^+) has been reported in a variety of ribozymes including hairpin, hammerhead, and hepatitis delta virus (HDV) ribozymes.^{122, 123, 192, 193} However, these activities are normally much slower (~10 to 100-fold) than the Mg^{2+} -dependent cleavage. In this work, the selection and characterization of an interesting ribozyme were described whose activity is promoted by denaturing conditions but without metal ion dependency.

5.2 Results and discussion

5.2.1 *In vitro* selection of self-cleaving ribozymes

The selection strategy is summarized in Figure 5.2. In each selection round, the RNA library (80-nt) was generated by *in vitro* transcription followed by dPAGE purification. The purified RNAs were incubated in the selection buffer (50 mM MES, pH 6, 100 mM NaCl, 2 mM EDTA•2Na⁺) at room temperature for 2 h. Afterwards, the downstream products with lengths between ~67 to 73-nt were purified by dPAGE and amplified by reverse transcription PCR.

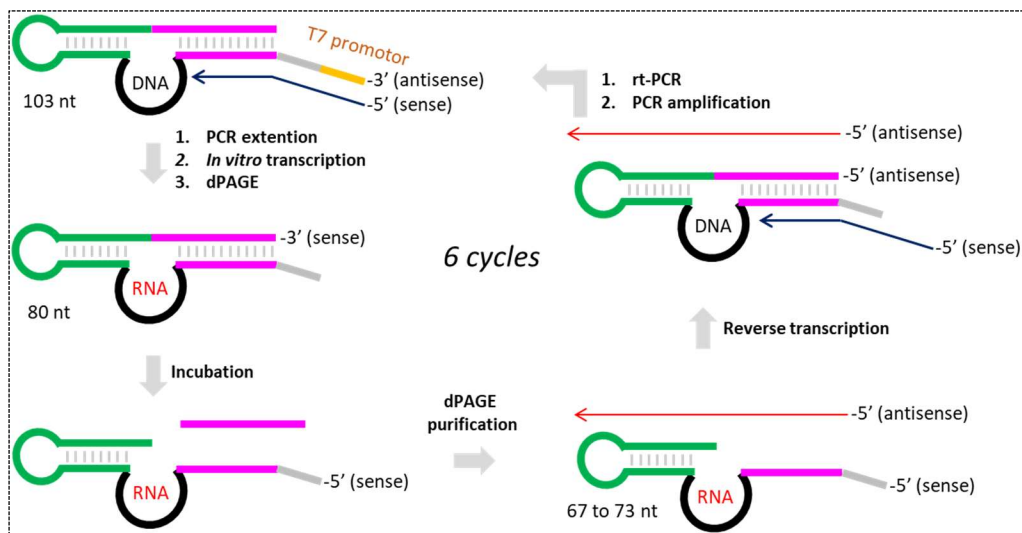


Figure 5.2 The *in vitro* selection procedure for self-cleaving ribozymes. In each selection round, the RNA library (80-nt) was generated by *in vitro* transcription followed by dPAGE purification. The purified RNAs were incubated in the selection buffer (50 mM MES, pH 6, 100 mM NaCl, 2 mM EDTA•2Na⁺) at room temperature for 2 h. Afterwards, the downstream products with lengths between ~67 to 73-nt were purified by dPAGE and amplified by reverse transcription PCR.

After six rounds of selection, ~20% self-cleavage activity was achieved in the final RNA library (Figure 5.3), which presented as one single band on the dPAGE gel. The selection progress was also monitored by real-time PCR (Figure 5.4), which indicated a gradually enriched library along with the selection progress. Thus, the DNA amplification products of round 6 were further

analyzed by deep sequencing. The sequenced library showed a high diversity with a total of 18,068 unique sequences. These sequences were further aligned into more than 1,000 families based on their sequence similarity. Some top families that contain the designed domains are listed in Table 7.

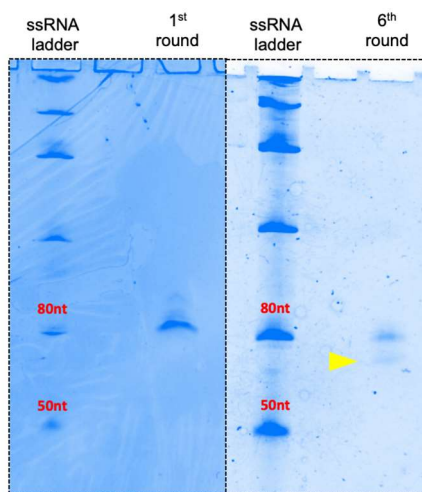


Figure 5.3 (A) Gel image showing the cleavage products of 1st and 6th round after selection step.

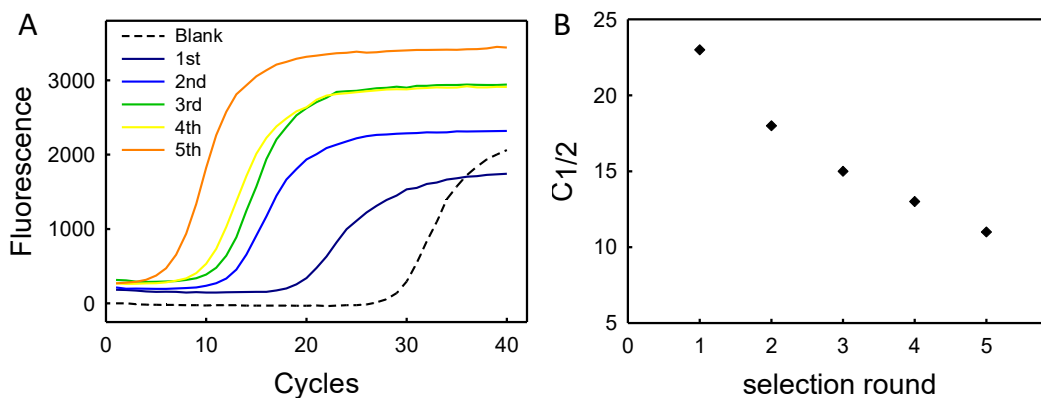


Figure 5.4 (A) Real-time PCR used to monitor the gradual increase in RNA population in library along with the selection progress. (B) The fractional cycles ($C_{1/2}$) at which reaction fluorescence reaches half of maximal (F_{max}).

Among them, the Rn2 family was the most abundant and its sequence was also found in several other minor families adding up to a total of 181 sequences in the final library. The sequences in the Rn2 family are highly conserved as summarized in Figure 5.5A. After evolution, the N₂₀ region possessed a high G+C content (75%). The secondary structure of the Rn2 sequence was predicted by Mfold (Figure 5.1D),¹⁴² showing a three-way junction structure. The short 3-bp hairpin structure appeared to shift positions compared to our original library design. Meanwhile, four nucleotides in N₇ region formed base pairs with the potential cleavage region, leaving two nucleotides (AA) sitting between binding arms serving as the putative cleavage sites (Figure 5.1C).

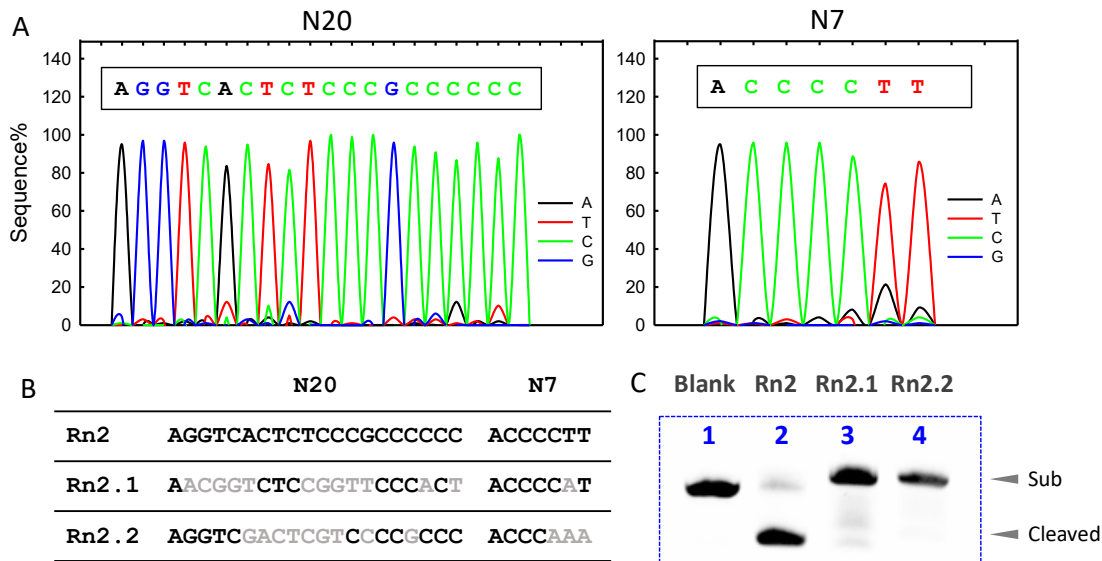


Figure 5.5 (A) Sequence analysis of Rn2 family by calculating the percentage of each nucleotide among a total of 98 sequences. (B) Comparison of two randomized domains in Rn2, Rn2.1, and Rn2.2 sequences. (C) Gel image showing the cleavage activity of Rn2, Rn2.1 and, Rn2.2. Lane 1 represents Rn2 without incubating. Lane 2-4 represents cleavage product of Rn2, Rn2.1 and, Rn2.2 in 50% formamide (25 mM Tris•HCl, pH 7.5, 1 mM EDTA•2Na⁺) after incubating at 65°C for 5 min. Top bands represent 80-nt complete ribozymes, and the bottom bands are cleaved products with shorter lengths.

Table 7. The eight most abundant families (from 5' to 3') after sequence alignment present in the final library. N₂₀ region is in red, and N₇ region is in blue.

2.	GGGAAGAGAGGCCATC	AGGTCACTCTCCGCCCCC	AGTGTGACT	ACCCCTT	TAGGCACAAGCCTATAGGAAGATGGCC (98 reads)
5.	GGGAAGAGAGGCCATC	CCTCGGTCTCCTAGCTTCCC	AGTGTGACT	ACTCCCC	TAGGCACAAGCCTATAGGAAGATGGCC (69 reads)
14.	GGGAAGAGAGGCCATC	CTATCATGGTCTCCGCTCCC	AGTGTGACT	CCACACG	TAGGCACAAGCCTATAGGAAGATGGCC (55 reads)
17.	GGGAAGAGAGGCCATC	ATGGTCTCCGATCCCATCCC	AGTGTGACT	CCTGACA	TAGGCACAAGCCTATAGGAAGATGGCC (52 reads)
19.	GGGAAGAGAGGCCATC	CCGGTCTCAGTTTCCCAG	AGTGTGACT	CTCCCC	TAGGCACAAGCCTATAGGAAGATGGCC (50 reads)
20.	GGGAAGAGAGGCCATC	CATCTGGTCTAACTTCCCGA	AGTGTGACT	CCCCCTC	TAGGCACAAGCCTATAGGAAGATGGCC (50 reads)
23.	GGGAAGAGAGGCCATC	CCGGTCTCAGTTTCCCAG	AGTGTGACT	CTCCCC	TAGGCACAAGCCTATAGGAAGATGGCC (48 reads)
24.	GGGAAGAGAGGCCATC	CGCGCACTCATTCCCAACCC	AGTGTGACT	CATCCT	TAGGCACAAGCCTATAGGAAGATGGCC (48 reads)

5.2.2 Formamide and high temperature enhance cleavage

To test whether Rn2 had the intended activity, the corresponding DNA template was purchased and transcribed it to Rn2. In activity tests, site-specific cleavage of Rn2 was observed showing as one concentrated band with a shortened length (Figure 5.5C). To identify the key factors that induced the cleavage, I found that the cleavage happened under a denaturing condition (50 vol% formamide, 25 mM Tris•HCl, pH 7.5, 1 mM EDTA•2Na⁺, 65°C for 5 min), which was used before gel electrophoresis in our selection and activity assays. Under the same condition, no self-cleavage activity was observed in two other sequences that contained multiple differences compared to Rn2 as shown in Figure 5.5B. Therefore, the conserved sequence of the Rn2 ribozyme is functionally important for its site-specific self-cleavage activity.

To understand the effect of formamide, I examined the cleavage yield of Rn2 by varying the volume fraction of formamide. As shown in Figure 5.6, when formamide was above 10% (v/v), the self-cleavage activity gradually enhanced. Especially, the highest cleavage yield was detected in the presence of 80% formamide (~20 M), which is typically a strong denaturing condition for

nucleic acids. Thus, high concentrations of formamide substantially stimulated the cleavage of Rn2 instead of terminating the reaction.

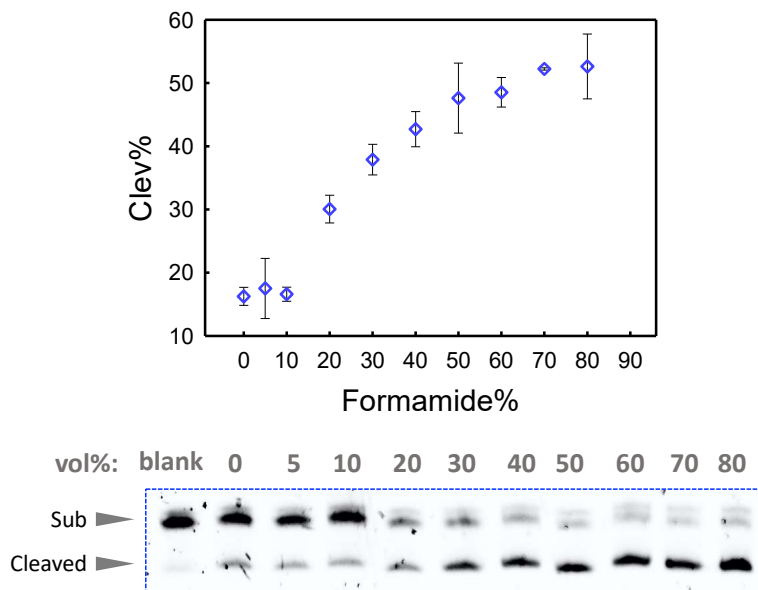


Figure 5.6 (A) The self-cleavage activity of Rn2 measured in various formamide vol% after incubating at 65°C for 5 min. The buffer solution used in the reaction is 50 mM Tris•HCl (pH 7.5). Meanwhile, a final concentration of 1 mM EDTA•2Na⁺ was added to all the reactions to eliminate divalent metal ions.

The formamide-enhanced activity was previously reported in the HDV ribozyme.^{188, 189} The cleavage rate of the genomic HDV ribozyme was increased by 50-fold in 10 M formamide with ~2 mM Mg²⁺.¹⁸⁹ However, >20 M formamide fully inhibited the cleavage likely by disturbing the structure. In the antigenomic HDV, a truncated version retained its activity even under 20 M formamide, but it was still more active at lower formamide concentrations.¹⁸⁸ A structural study confirmed that the HDV ribozyme can preserve its structure even in 24 M formamide by monitoring the fluorescence of the bound ethidium bromide (EB).¹⁹⁴ It was hypothesized that the HDV ribozyme was present in multiple conformations, and denaturants could lower the energy

barriers between them. Thus, an inactive folding can be destabilized and more easily converted to the active conformation. A similar mechanism can be applied here to understand the formamide-dependency observed in Rn2. However, it may present an even higher stability in formamide since no activity decrease was observed even under a very high concentration of 20 M.

I then examined the temperature effect on its cleavage activity. With 50 vol% (~12.5 M) formamide, the cleavage yields measured at -20°C, 4°C, and room temperature were fairly low after a 30 min incubation (Figure 5.7A). A high yield was observed when the samples were heated to above 50°C for 5 min, and the optimal temperature appeared to be between 65°C and 80°C. Note that even under such high temperatures, the cleavage was still specific and only a single major product band was observed (Figure 5.7A, gel image). This suggests a remarkable thermal stability of Rn2 ribozyme.

When studying the kinetics of the cleavage reaction at 65°C, the reaction was completed as soon as 65°C was reached (Figure 5.9A). Therefore, I measured the cleavage process by slowly heating the reaction at several temperatures (from 30°C to 90°C). As shown in Figure 5.7B, the cleavage yield started to rise when the temperature was above 45°C. The yield gradually increased with an increasing temperature between 45°C to 65°C, and saturated at above 70°C. This suggested that the Rn2 ribozyme in 50% formamide was “switched on” when the temperature was higher than 45°C. The activation temperature was lowered with a higher formamide% (Figure 5.8), suggesting that temperature may accelerate catalysis through a similar denaturing mechanism as formamide. Likely, both formamide and high temperature stimulated Rn2 cleavage by accessing the active structure, despite that they normally denature RNA/DNA.

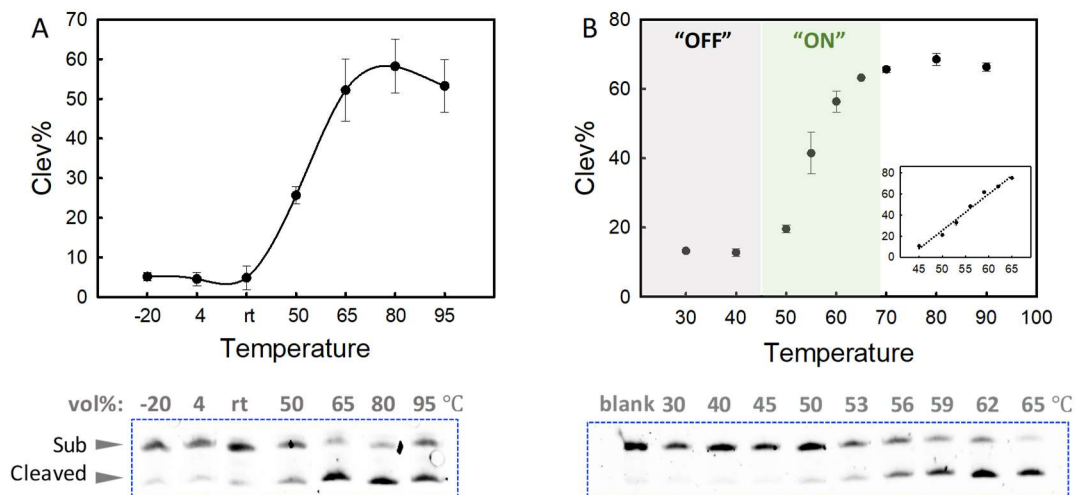


Figure 5.7 (A) The temperature effect on the self-cleavage activity of Rn2 in 50 vol% (~12.5 M) formamide. The reactions under -20°C , 4°C , and room temperature were incubated for 30 min, while the rest temperature points were measured after 5 min incubation. (B) The cleavage% of Rn2 measured during a slow heating process. The reaction was gradually heated from 30°C to 90°C . The reaction remained for 20 s at each temperature point. An accumulated cleavage% was measured after being quenched at each temperature point. The cleavage% of Rn2 linearly increased within 45 to 65°C (inset). Reactions were performed in 50 vol% formamide (25 mM Tris•HCl, pH 7.5, 1 mM EDTA• 2Na^{+}) and quenched by cooling at -20°C .

To study the kinetics of the cleavage reaction, the cleavage yield was measured at different time points at 53°C , which is a mild temperature condition for Rn2. As shown in Figure 5.9B, the cleavage in 50% formamide plateaued within 3 min with an apparent rate (K_{obs}) of $1.1 \pm 0.1 \text{ min}^{-1}$. Interestingly, the self-cleavage activity of Rn2 was greatly enhanced in the presence of 80% formamide, resulting in a cleavage rate of $2.1 \pm 0.3 \text{ min}^{-1}$ and a higher maximal cleavage yield. On the contrary, the cleavage in buffer without formamide remained low. These results further

confirmed the importance of formamide solvent in promoting the active conformation of Rn2, which allowed the cleavage reaction to occur.

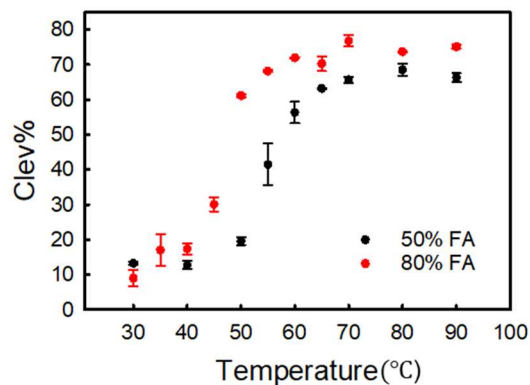


Figure 5.8 The cleavage% of Rn2 measured in 50% or 80% formamide during a slow heating process. The reaction was gradually heated from 30°C to 90°C. The reaction remained for 20 s at each temperature point. An accumulated cleavage% was measured after being quenched at each temperature point.

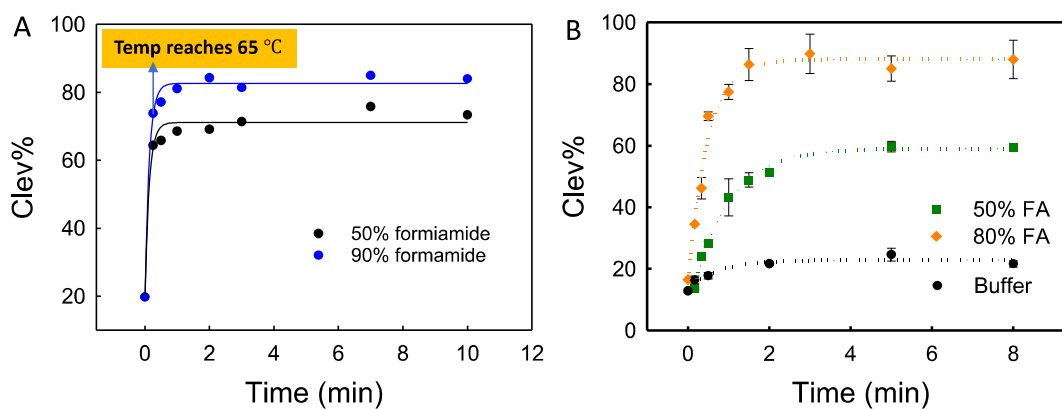


Figure 5.9 (A) The cleavage% measured at different time points in the presence of 50% and 90% formamide under 65°C. (B) Kinetics of Rn2 cleavage measured in buffer, 50%, or 80% formamide at 53°C.

5.2.3 Divalent metal ions inhibit cleavage

All reactions discussed earlier were performed without additional metal ions apart from 1 mM EDTA•2Na⁺, where only 2 mM Na⁺ was present. Since divalent metal ions are often added to promote RNA cleavage reaction, I tested the effect of Mg²⁺ and Ca²⁺ on the activity of Rn2. Surprisingly, Mg²⁺ and Ca²⁺ (up to 2 mM, 50% formamide, 53°C) significantly inhibited the cleavage activity (Figure 5.10A). On the contrary, the Rn2 showed a better tolerance for monovalent ions, where the cleavage started to decrease only when the concentration of Na⁺ or K⁺ was higher than 10 mM (Figure 5.10B). To fully inhibit the activity, more than 100 mM Na⁺ or K⁺ was required. In fact, a slight increase in the cleavage activity (~20 to 30%) was detected in the presence of relatively low concentrations of Na⁺ or K⁺ (below 1 mM). Metal ions can screen charge repulsion of nucleic acids. With an extremely low ionic strength, nucleic acids also tend to denature in aqueous solutions.

The tolerance of Rn2 to monovalent metal ions is reasonable considering the selection was carried out in the presence of Na⁺ and divalent metal ions were strictly avoided. The inhibition observed under high concentrations of monovalent ions is likely due to an increased ionic strength which induced misfolding of the ribozyme thus disfavoring the active conformation. Divalent metal ions may interact with the ribozyme more strongly resulting in a more significant decrease in cleavage. This result also sets Rn2 apart from HDV since Mg²⁺ (~2 to 10 mM) was always required for the formamide-enhanced activity in the HDV ribozyme, and EDTA inhibited HDV cleavage.^{188, 189} Furthermore, monovalent metal ions could play a role in the chemical reaction since a cleavage increase was observed in low concentrations (below 1 mM) of Na⁺ and K⁺. This improvement in chemistry may be defeated by the structural disruption under higher salt concentrations. Since the cleavage is supported by denaturants or temperature rather than metal ions, the Rn2 catalysis may be rate-limited by the conformational change instead of the chemistry.

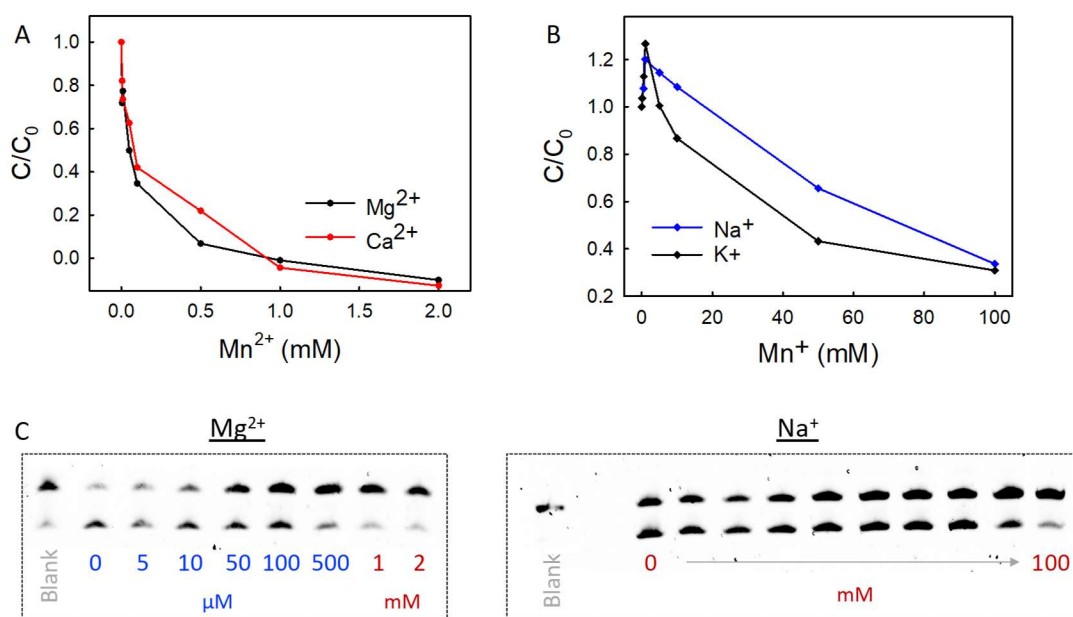


Figure 5.10 The cleavage activity of Rn2 measured in various concentration of (A) divalent and (B) monovalent metal ions. Reactions were performed in 50% formamide at 53°C (for 2 min). The y-axis was quantified by dividing the cleavage% measured in the absence of metal ions. (C) Gel images of Rn2 cleavage in various concentrations of Mg^{2+} or Na^+ .

5.2.4 Effect of other solvents

Formamide is an effective denaturant for nucleic acids by weakening hydrogen bonds. Since formamide can promote Rn2 cleavage, I also studied the activity in other organic solvents and denaturing reagents at 65°C (Figure 5.11). Indeed, urea and DMSO also efficiently promoted the cleavage with similar cleavage yields as formamide. In pure buffer solution, the cleavage was nearly 50% less than that of formamide, while fairly low activities were observed in 50 vol% ethanol or methanol solutions.

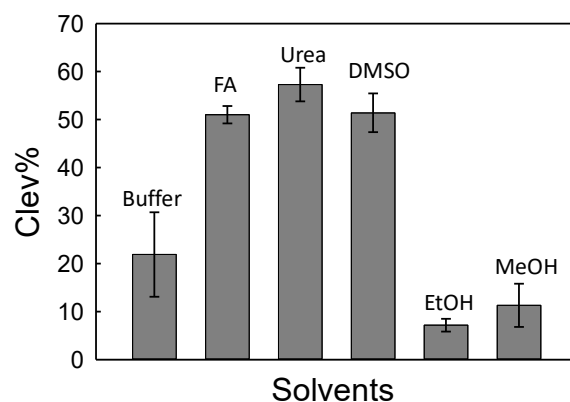


Figure 5.11 Solvent effect on the self-cleavage activity of Rn2 (65°C, 5 min). The cleavage% was measured in 50 vol% of formamide, DMSO, ethanol, or methanol, while 10 M urea was used. Buffer used was 50 mM Tris•HCl (pH 7.5), and 1 mM EDTA•2Na⁺ was added in all reactions.

Cosolvents can affect the stability and catalytic activity of RNA and DNA via complicated mechanisms. Noticeable differences between these solvents are dielectric constant (ϵ_r) and water activity (a_w). Formamide, urea, water, and DMSO have medium to high dielectric constants, while ethanol and methanol have lower dielectric constants. Based on the previous study of self-cleaving ribozymes, a low dielectric constant environment is generally more favorable for the cleavage activity.²⁴ For example, the cleavage rate of hammerhead ribozyme mediated by 1.5 M NaCl was reported to be increased in ethanol and methanol (20 wt%). However, 20 wt% of urea and formamide decreased the rate by 100-fold.¹⁹⁵ This was explained by a low dielectric constant medium promoting the electrostatic interaction between cations and ribozymes. In another study, the binding affinity of Mg²⁺ in the hammerhead ribozyme was also enhanced by over 10-fold in mixed solutions containing 20% ethanol or 1,2-dimethoxyethane.¹⁹⁶ The fact that the Rn2 activity being promoted by high dielectric constant solvents suggested a distinct role of the solvent in

catalysis (e.g., acting on the ribozyme instead of mediating metal ion interactions). On the other hand, the water activity of organic solvents can also affect DNA/RNA structural stability. A reduced water activity was often correlated with a destabilized duplex structure.^{195, 197, 198} In Rn2, 50% ethanol or methanol lowered the water activity but failed to support the cleavage. Thus, we can conclude that Rn2 cleavage requires a stronger destabilization effect provided by denaturants.

5.2.5 Searching ribozyme sequence in nature

Ribozymes are known to play critical roles in regulating gene expression in cells. Started from late 1980s, a great number of naturally occurring small self-cleaving ribozymes have been discovered, providing a powerful support for the RNA world hypothesis. In recent years, efforts have been made to combine experimental and bioinformatic approaches to identify ribozymes in genomes.¹⁹⁹ A well-studied example is the hammerhead ribozyme (HHRz) that was initially found in plant virus such as viroids and viral satellites.^{28, 200} Bioinformatic approaches were later applied in searching HHRz motifs in genome databases, finding its ubiquitous and widespread existence in almost all life kingdoms.²⁰¹⁻²⁰³ Typically, searching is based on the consensus motifs of a ribozyme identified in biochemical and structural studies. In HHRz, a minimized catalytic core containing ~11 to 15 conserved nucleotides was widely used.²⁰²

Apart from known ribozymes, artificial RNAs with novel activities can be discovered by *in vitro* selection experiments, and bioinformatic methods can be used to look for their natural analogs. Our Rn2 ribozyme displays a unique denaturant-dependent and thermophilic activity. To search whether this novel catalytic RNA motif appears in nature, the BLASTN program was applied for searching the Rn2 motif among microbes.²⁰⁴ The entire N₂₀ region in Rn2 sequence was used as the input since it's a highly conserved sequence as shown in Figure 5.5B. The sequence

hits with highest query coverages were aligned in Figure 5.12. Interestingly, this motif was widely found in plasmid DNA of a thermophilic bacterium, *Thermus thermophilus*. It locates at the S8 family serine peptidase genome, which is noted as incomplete with N-terminals missing. This motif is also present in the plasmid of another organism called *Deinococcus wulumuqiensis*, which also belongs to the *Deinococcus* family. Additionally, Rn2 motif was mapped in the chromosome of *Deinococcus radiodurans*, which is highly radiation-resistant. The presence of Rn2 motif in these extremophilic bacteria could be correlated with its unique activity under denaturing conditions. The phylogenetic tree based on the genomic alignments showed the close genetic distance between sequence hits (Figure 5.13). The biologically functional relevance of such hits will be a topic of future studies.

A. Complete plasmids database

NCBI Multiple Sequence Alignment Viewer, Version 1.20.0

Sequence ID	Start	Alignment	End	Organism
Query_11475	(+) 1	A G G T C A C T C T C C C G C C C C C C	20	
NZ_CP053288.1	(-) 228,396G.....	228,379	<i>Thermus thermophilus</i>
NZ_CP031163.1	(-) 234,704G.....	234,688	<i>Deinococcus wulumuqiensis</i>
NC_017590.1	(-) 52,489G.....	52,472	<i>Thermus thermophilus</i> JL-18
NC_005838.1	(-) 190,846G.....	190,829	<i>Thermus thermophilus</i> HB27
NZ_LR027519.1	(+) 15,750G.....	15,737	<i>Thermus thermophilus</i>
NC_017273.1	(+) 403,444G.....	403,461	<i>Thermus thermophilus</i> SG0.5JP17...
NZ_AP024272.1	(-) 155,297G.....	155,280	<i>Thermus thermophilus</i>
NZ_CP041241.1	(+) 443,659G.....	443,675	<i>Ensifer mexicanus</i>
NZ_CP020572.1	(-) 46,027G.....	46,010	<i>Thermus aquaticus</i>
NZ_CM007204.1	(-) 63,239A.....	63,222	<i>Streptomyces subtrilus</i>
NZ_CP032054.1	(+) 94,623A.....	94,639	<i>Streptomyces clavuligerus</i>
NZ_CP030263.1	(-) 62,235A.....	62,219	<i>Ensifer adhaerens</i>
NZ_CP015881.1	(+) 365,221A.....	365,237	<i>Ensifer adhaerens</i>

B. Complete genomes database

NCBI Multiple Sequence Alignment Viewer, Version 1.20.0

Sequence ID	Start	Alignment	End	Organism
Query_24537	(+) 1	A G G T C A C T C T C C C G C C C C C C	20	
NZ_CP011273.1	(+) 4,501...C.....	4,501...	<i>Planctomyces</i> sp. SH-PL62
NZ_CP044543.1	(-) 5,745...C.....	5,745...	<i>Bradyrhizobium betae</i>
NZ_CP027231.1	(+) 1,292...C.....	1,292...	<i>Bacteroides zoogloeiformans</i>
NZ_CP043959.1	(+) 1,732...C.....	1,732...	<i>Streptomyces tendae</i>
NZ_CP032402.1	(-) 219,217C.....	219,201	<i>Thermomonospora amylo...</i>
NZ_CP009754.1	(+) 802,726A.....	802,742	<i>Streptomyces</i> sp. CCM...
NZ_CP029788.1	(-) 1,409...G.....	1,409...	<i>Streptomyces actuosus</i>
NZ_CP050120.1	(-) 2,248...G.....	2,248...	<i>Deinococcus radiodurans</i>
NZ_CP015219.1	(-) 3,089...G.....	3,089...	<i>Rhodococcus</i> sp. PBTS 1
CP042594.1	(+) 5,376...G.....	5,376...	<i>Streptomyces albobrigesolus</i>
NZ_CP030263.1	(-) 62,235G.....	62,219	<i>Ensifer adhaerens</i>

Figure 5.12 Nucleotide NCBI-BLAST results showing the alignments of Rn2 motif in complete plasmids (A) or genomes (B) databases of microbes. The N₂₀ region of Rn2 ribozyme was used as the input sequence.

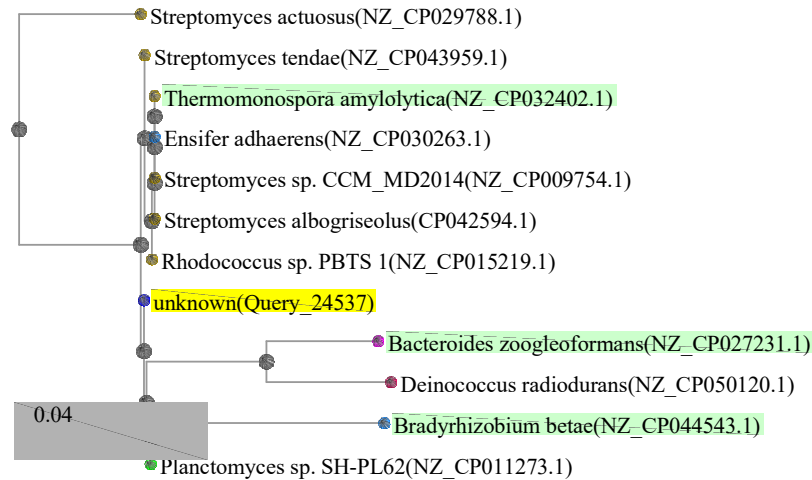


Figure 5.13 The phylogenetic tree generated by BLAST in complete genomes database.

5.3 Summary

In this chapter, the self-cleaving Rn2 ribozyme was *in vitro* selected with unexpected activity under chemically and thermally denaturing conditions. Its cleavage activity prefers a high formamide concentration (~20 M) and a high temperature (between 65 to 80°C). Most importantly, no additional metal ion is required for its activity which makes it unique among other self-cleaving ribozymes. In fact, low concentrations of Mg²⁺ and Ca²⁺ significantly inhibited its activity. Its rate-limiting step might be a conformational change that can be promoted under various denaturing conditions. Finally, the bioinformatic method was tentatively applied to search the Rn2 motif in genomes. Several sequence hits were found in extremophilic bacteria genomes, indicating the promising presence of Rn2 analogs in nature. If a Rn2 resembling ribozyme functions *in vivo*, certain regulatory factors or unwinding process could mimic the denaturing condition. This work further broadened the horizon of catalytic RNAs functioning under extreme conditions, and thus provided another strong support for the RNA world hypothesis.

5.4 Materials and methods

5.4.1 Oligonucleotides and chemicals

All the oligonucleotide sequences involved in the selection experiment were purchased from Eurofins Genomics LLC (Table 8). Chemical reagents including T7 RNA polymerase, 10X RNAPol reaction buffer, NTPs mixture, ProtoScript® II reverse transcriptase, 5X ProtoScript II buffer, dNTPs mixture, 0.1 M DTT, low range ssRNA ladder, 2X RNA loading dye, and *Taq* DNA polymerase with standard *Tag* buffer were purchased from New England BioLabs. SYBR gold dye (10,000X) was purchased from Thermo Fisher Scientific. Water used in *in vitro* selection experiments was pre-treated with RNAsecure™ reagent (Thermo Fisher Scientific).

Table 8. Oligonucleotide sequences used in the *in vitro* selection experiment.

Antisense DNA template (103-nt)	5' GGCCATC TTCCCTAT AGGCTTGTGCCTAN ₇ AGTCAACACTN ₂₀ GATGGCC TCTCTTCCCT <u>ATAGTGAGTCGTATTA</u> GAATTC
Sense DNA template (103-nt)	5' GAATTC TAATACGACTCACTATA GGGAAGAGAG GGCCATC N ₂₀ AGTGTTGACTN ₇ TAGGC ACAAGCCTATAGGAAG GATGGCC
Primer 1 (39 nt)	5' <u>GAATTC</u> TAATACGACTCACTATA GGGAAGAGAG GGCCATC
Primer 2 (21 nt)	5' GGCCATC TTCCCTAT AGGCTTG
Primer 3 (27 nt)	5' GGCCATC TTCCCTAT AGGCTTGTGCCTA
S505 primer	5' AATGATACGGCGACCACCGAGATCTACAC- GTAAGGAG - ACACTCTTTCCTACACGACGCTCTTCCGATCT-NNNN-GGGAAGAGAG GGCCATC
N702 primer	5' CAAGCAGAAGACGGCATAACGAGAT- CTAGTACG - GTGACTGGAGTTCAGACGTGTGCTCTTCCGATCT- GGCCATC TTCCCTAT AGGCTTG
Rn2 DNA template	5' GGGAAGAGAGGGCCATC AGGTCAC TCTCCCGCCCCAGTGTTGACT ACCCCTT TAGGC ACAAGCCTATAGGAAGATGGCC
Rn2.1 DNA template	5' GGGAAGAGAGGGCCATC AACGGTCTCCGGTCCCACT AGTGTTGACT ACCCCAT TAGGC ACAAGCCTATAGGAAGATGGCC
Rn2.2 DNA template	5' GGGAAGAGAGGGCCATC AGGTCGACTCGTCCCGCCC AGTGTTGACT ACCCAAA TAGGC ACAAGCCTATAGGAAGATGGCC

Note: **Red coloured domain** represents the T7 promotor sequence; Underlined domain is to ensure T7 promotor in duplex; Grey coloured domain is for primer binding.

5.4.2 *In vitro* selection

The initial RNA library was *in vitro* transcribed from a double-stranded DNA template using T7 RNA polymerase. To generate the dsDNA template, one cycle of PCR extension (95°C for 2 min, 95°C for 20 s, 59°C for 20 s, and 72°C for 30 s) was performed using single-stranded antisense DNA template (200 pmol) and primer 1 (200 pmol). The dsDNA template contains 103 base pairs as confirmed on a 2% agarose gel (Figure 5.14A). The extended DNA template was then purified with a PCR clean-up kit (IBI Scientific) and resuspended in water. The *in vitro* transcription was conducted in a 20 μ L reaction (~100 pmol dsDNA template, 2 mM NTPs, 5 U/ μ L T7 RNA polymerase) by incubating at 37°C for 2 h. The transcription product was precipitated by incubating with 5M ammonium acetate (1 volume) and ethanol (2.5 volumes) at -20 °C for 1 h. After centrifuge (at 4°C, 14000 rpm, >30 min), the supernatant was carefully removed followed by twice washing with 70% ethanol (ice cold). The air-dried pellet was resuspended and purified by 10% denaturing polyacrylamide gel electrophoresis (dPAGE, 400V, 2 h). The gel was stained in 1x SYBR gold dye (ThermoFisher) and then imaged under a Bio-Rad Chemi-Doc MP imaging system. The intact RNA precursors (80-nt) were extracted from the gel and ethanol precipitated. The RNA precipitant was stored at -20 °C until further use.

In each selection, the RNA library was resuspended in 20 μ L of selection buffer (50 mM MES, pH 6, 100 mM Na⁺, 2 mM EDTA•2Na⁺) at room temperature for 2 h. After incubation, the reaction was quenched with 1x RNA loading dye (NEB) at 65°C for 10 min. The RNA loading dye (1x) contains 47.5% formamide, 0.01% SDS, 0.01% bromophenol blue, 0.005% Xylene Cyanol, and 0.5 mM EDTA. The RNA cleavage products (~67 to ~73-nt) were carefully isolated by aligning with ssRNA ladder on 10% dPAGE. The cleavage products were extracted by crush/soaking the gel slices and were ethanol precipitated. Next, the cleaved RNAs (10 μ L) were

annealed with primer 3 (100 pmol) by incubating at 65°C for 5 min. After chilling on ice, 0.5 mM dNTPs, 10 mM DTT, and 10 U/ μ L ProtoScript[®] II reverse transcriptase were added resulting in a total of 20 μ L. The cDNA synthesis reaction was performed under 42°C for 1 h followed by inactivation at 80°C for 5 min. The sequence of primer 3 restores the lost 3'-fragments after the cleavage reaction. The reverse transcribed product was directly monitored using real-time PCR. As optimized in Figure 5.14B, the volume of cDNA product was kept $\leq 1/20$ of the PCR reaction volume to eliminate the interference of residues from reverse transcription. In each round, the fractional cycles ($C_{1/2}$) at which reaction fluorescence reaches half of maximal (F_{\max}) was used for PCR amplification (95°C for 2 min, 95°C for 20 s, 59°C for 20 s, and 72°C for 30 s). The optimized cycle# and template length were confirmed with 2% agarose gel (as shown in Figure 5.14C). Two rounds of PCR (primer 1 and 2) were performed to produce sufficient dsDNA template which is purified by isopropanol precipitation. After resuspended in water, ~ 200 pmol dsDNA was used for the next round of selection.

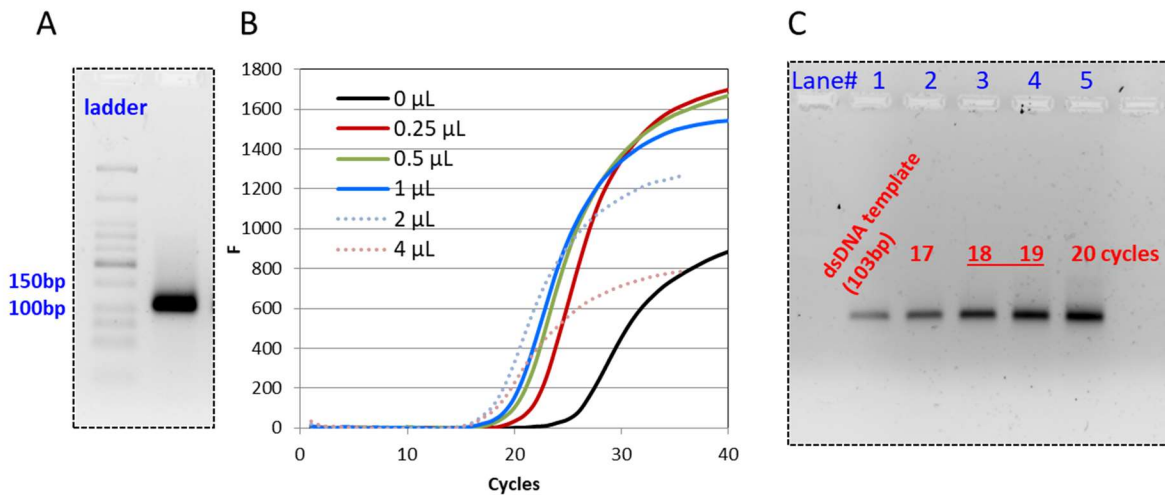


Figure 5.14 (A) The extended dsDNA template use for *in vitro* transcription with a length of 103 bps. (B) Real-time PCR for optimizing the cDNA volume used in PCR reaction. The volume of cDNA was kept

$\leq 1/20$ of the PCR reaction volume to eliminate the interference of residues from reverse transcription. (C) The optimized cycle# and template length were confirmed with 2% agarose gel in each round of selection.

5.4.3 Sequencing sample preparation

To prepare the sample for deep sequencing, PCR1 was performed to generate the full-length library. Next, PCR2 was performed to introduce specific index sequences into the library for the Illumina sequencing technology. Instead of primer 1 and 2, the forward primer (S505) and the reverse primer (N702) were used with their sequences listed in Table 8. The PCR product was then purified with 2% agarose gel (120 V, 50 min). A gel/PCR DNA fragment extraction kit (IBI Scientific) was used to extract the DNA library from the gel. Finally, the purified DNA sample was eluted in 20 μL of Milli-Q water. The DNA concentration measured with a NanoDrop spectrophotometer was ~ 38.1 ng/ μL . The sample was shipped to McMaster University for deep sequencing.

5.4.4 Characterization of cleavage activity

After sequence analysis, single-stranded DNA templates (Table 8) encoded promising sequences were extended by PCR and *in vitro* transcribed into RNA sequences. The 80-nt RNA products were further purified by 10% dPAGE and ethanol precipitated. The purified ribozyme can be resuspended in water for activity assays. For cleavage reactions performed in 50% formamide, 5 μL pure formamide ($\geq 99\%$) and 50 mM Tris•HCl buffer (pH 7.5) was added to a total of 10 μL reaction volume. Except for the metal dependency assays, a final concentration of 1 mM EDTA•2Na⁺ was added in all reactions. After incubation, the self-cleavage reaction of Rn2 was quenched by cooling at -20°C . The reaction products were then visualized and analyzed on 10% dPAGE. Kinetic data were fit with the first-order equation, $\%P_{cleavage,t} = \%P_{max}(1 -$

$e^{-K_{obs}t}$), where $\%P_{max}$ is the maximum cleavage yield at the end of the reaction and K_{ob} is the cleavage rate constant.

References

1. Kruger, K.; Grabowski, P. J.; Zaug, A. J.; Sands, J.; Gottschling, D. E.; Cech, T. R., Self-splicing RNA: autoexcision and autocyclization of the ribosomal RNA intervening sequence of *Tetrahymena*. *Cell* **1982**, *31* (1), 147-157.
2. Guerrier-Takada, C.; Gardiner, K.; Marsh, T.; Pace, N.; Altman, S., The RNA moiety of ribonuclease P is the catalytic subunit of the enzyme. *Cell* **1983**, *35* (3), 849-857.
3. Robertson, M. P.; Joyce, G. F., The origins of the RNA world. *Cold Spring Harbor Perspectives in Biology* **2012**, *4* (5), a003608.
4. Fedor, M. J.; Williamson, J. R., The catalytic diversity of RNAs. *Nature Reviews Molecular Cell Biology* **2005**, *6* (5), 399-412.
5. Breaker, R. R.; Joyce, G. F., A DNA enzyme that cleaves RNA. *Chemistry & Biology* **1994**, *1* (4), 223-229.
6. Schlosser, K.; Li, Y., Biologically inspired synthetic enzymes made from DNA. *Chemistry & Biology* **2009**, *16* (3), 311-322.
7. Silverman, S. K., DNA as a versatile chemical component for catalysis, encoding, and stereocontrol. *Angewandte Chemie International Edition* **2010**, *49* (40), 7180-7201.
8. Zhou, W.; Saran, R.; Liu, J., Metal sensing by DNA. *Chemical Reviews* **2017**, *117* (12), 8272-8325.
9. Tritz, R.; Habita, C.; Robbins, J. M.; Gomez, G. G.; Kruse, C. A., Catalytic nucleic acid enzymes for the study and development of therapies in the central nervous system. *Gene Therapy & Molecular Biology* **2005**, *9*, 89.

10. Aguirre, S. D.; Ali, M. M.; Kanda, P.; Li, Y., Detection of bacteria using fluorogenic DNAzymes. *Journal of Visualized Experiments: JoVE* **2012**, 28 (63), 3961.
11. Lu, Y.; Liu, J., Functional DNA nanotechnology: emerging applications of DNAzymes and aptamers. *Current Opinion in Biotechnology* **2006**, 17 (6), 580-588.
12. Bevilacqua, P. C.; Yajima, R., Nucleobase catalysis in ribozyme mechanism. *Current Opinion in Chemical Biology* **2006**, 10 (5), 455-464.
13. Thaplyal, P.; Bevilacqua, P. C., Experimental approaches for measuring pKa's in RNA and DNA. *Methods in Enzymology* **2014**, 549, 189-219.
14. Weinberg, C. E.; Weinberg, Z.; Hammann, C., Novel ribozymes: discovery, catalytic mechanisms, and the quest to understand biological function. *Nucleic Acids Research* **2019**, 47 (18), 9480-9494.
15. Silverman, S. K., Catalytic DNA: scope, applications, and biochemistry of deoxyribozymes. *Trends in Biochemical Sciences* **2016**, 41 (7), 595-609.
16. Wong, J. P.; Christopher, M. E.; Salazar, A. M.; Sun, L.-Q.; Viswanathan, S.; Wang, M.; Saravolac, E. G.; Cairns, M. J., Broad-spectrum and virus-specific nucleic acid-based antivirals against influenza. *Frontiers in Bioscience (Scholar Edition)* **2010**, 2, 791-800.
17. Willner, I.; Shlyahovsky, B.; Zayats, M.; Willner, B., DNAzymes for sensing, nanobiotechnology and logic gate applications. *Chemical Society Reviews* **2008**, 37 (6), 1153-1165.
18. Li, Y.; Breaker, R. R., Kinetics of RNA degradation by specific base catalysis of transesterification involving the 2'-hydroxyl group. *Journal of the American Chemical Society* **1999**, 121 (23), 5364-5372.
19. Liu, J.; Cao, Z.; Lu, Y., Functional nucleic acid sensors. *Chemical Reviews* **2009**, 109 (5), 1948-1998.

20. Wang, F.; Lu, C.-H.; Willner, I., From cascaded catalytic nucleic acids to enzyme–DNA nanostructures: controlling reactivity, sensing, logic operations, and assembly of complex structures. *Chemical Reviews* **2014**, *114* (5), 2881-2941.
21. Doudna, J. A.; Cech, T. R., The chemical repertoire of natural ribozymes. *Nature* **2002**, *418* (6894), 222-228.
22. Goldman, A. D.; Kacar, B., Cofactors are remnants of life's origin and early evolution. *Journal of Molecular Evolution* **2021**, *89* (3), 127-133.
23. Hirao, I.; Ellington, A. D., Re-creating the RNA world. *Current Biology* **1995**, *5* (9), 1017-1022.
24. and, D. S. W.; Szostak, J. W., In Vitro Selection of Functional Nucleic Acids. *Annual Review of Biochemistry* **1999**, *68* (1), 611-647.
25. Lincoln, T. A.; Joyce, G. F., Self-Sustained Replication of an RNA Enzyme. *Science* **2009**, *323* (5918), 1229-1232.
26. Robertson, Michael P.; Joyce, Gerald F., Highly Efficient Self-Replicating RNA Enzymes. *Chemistry & Biology* **2014**, *21* (2), 238-245.
27. Cojocar, R.; Unrau, P. J., Processive RNA polymerization and promoter recognition in an RNA World. *Science* **2021**, *371* (6535), 1225-1232.
28. Prody, G. A.; Bakos, J. T.; Buzayan, J. M.; Schneider, I. R.; Bruening, G., Autolytic processing of dimeric plant virus satellite RNA. *Science* **1986**, *231* (4745), 1577-1580.
29. Ferré-D'Amaré, A. R.; Scott, W. G., Small self-cleaving ribozymes. *Cold Spring Harb Perspect Biology* **2010**, *2* (10), a003574.
30. Ren, A.; Micura, R.; Patel, D. J., Structure-based mechanistic insights into catalysis by small self-cleaving ribozymes. *Current Opinion in Chemical Biology* **2017**, *41*, 71-83.

31. Ward, W. L.; Plakos, K.; DeRose, V. J., Nucleic acid catalysis: Metals, nucleobases, and other cofactors. *Chemical Reviews* **2014**, *114* (8), 4318-4342.
32. Cochrane, J. C.; Strobel, S. A., Catalytic Strategies of Self-Cleaving Ribozymes. *Accounts of Chemical Research* **2008**, *41* (8), 1027-1035.
33. Martick, M.; Scott, W. G., Tertiary Contacts Distant from the Active Site Prime a Ribozyme for Catalysis. *Cell* **2006**, *126* (2), 309-320.
34. Chen, J.-H.; Yajima, R.; Chadalavada, D. M.; Chase, E.; Bevilacqua, P. C.; Golden, B. L., A 1.9 Å Crystal Structure of the HDV Ribozyme Precleavage Suggests both Lewis Acid and General Acid Mechanisms Contribute to Phosphodiester Cleavage. *Biochemistry* **2010**, *49* (31), 6508-6518.
35. Winkler, W. C.; Nahvi, A.; Roth, A.; Collins, J. A.; Breaker, R. R., Control of gene expression by a natural metabolite-responsive ribozyme. *Nature* **2004**, *428* (6980), 281-286.
36. Sullenger, B. A.; Gilboa, E., Emerging clinical applications of RNA. *Nature* **2002**, *418* (6894), 252-258.
37. Rossi, J. J., Ribozyme therapy for HIV infection. *Advanced Drug Delivery Reviews* **2000**, *44* (1), 71-78.
38. Pavco, P. A.; Bouhana, K. S.; Gallegos, A. M.; Agrawal, A.; Blanchard, K. S.; Grimm, S. L.; Jensen, K. L.; Andrews, L. E.; Wincott, F. E.; Pitot, P. A.; Tressler, R. J.; Cushman, C.; Reynolds, M. A.; Parry, T. J., Antitumor and Antimetastatic Activity of Ribozymes Targeting the Messenger RNA of Vascular Endothelial Growth Factor Receptors. *Clinical Cancer Research* **2000**, *6* (5), 2094-2103.

39. Huang, X.; Zhao, Y.; Pu, Q.; Liu, G.; Peng, Y.; Wang, F.; Chen, G.; Sun, M.; Du, F.; Dong, J.; Cui, X.; Tang, Z.; Mo, X., Intracellular selection of trans-cleaving hammerhead ribozymes. *Nucleic Acids Research* **2019**, *47* (5), 2514-2522.
40. Balke, D.; Wichert, C.; Appel, B.; Müller, S., Generation and selection of ribozyme variants with potential application in protein engineering and synthetic biology. *Applied Microbiology and Biotechnology* **2014**, *98* (8), 3389-3399.
41. Baskerville, S.; Bartel, D. P., A ribozyme that ligates RNA to protein. *Proceedings of the National Academy of Sciences* **2002**, *99* (14), 9154-9159.
42. Sharma, A. K.; Plant, J. J.; Rangel, A. E.; Meek, K. N.; Anamisis, A. J.; Hollien, J.; Heemstra, J. M., Fluorescent RNA labeling using self-alkylating ribozymes. *ACS Chemical Biology* **2014**, *9* (8), 1680-1684.
43. Famulok, M.; Hartig, J. S.; Mayer, G., Functional aptamers and aptazymes in biotechnology, diagnostics, and therapy. *Chemical Reviews* **2007**, *107* (9), 3715-3743.
44. Wieland, M.; Hartig, J. S., Improved aptazyme design and in vivo screening enable riboswitching in bacteria. *Angewandte Chemie International Edition* **2008**, *47* (14), 2604-2607.
45. Penchovsky, R.; Breaker, R. R., Computational design and experimental validation of oligonucleotide-sensing allosteric ribozymes. *Nature Biotechnology* **2005**, *23* (11), 1424-1433.
46. Tang, W.; Hu, J. H.; Liu, D. R., Aptazyme-embedded guide RNAs enable ligand-responsive genome editing and transcriptional activation. *Nature Communications* **2017**, *8* (1), 15939.
47. Pan, T.; Uhlenbeck, O. C., In vitro selection of RNAs that undergo autolytic cleavage with Pb(II). *Biochemistry* **1992**, *31* (16), 3887-3895.

48. Saran, R.; Liu, J., A comparison of two classic Pb^{2+} -dependent RNA-cleaving DNazymes. *Inorganic Chemistry Frontiers* **2016**, *3*, 494-501.
49. Santoro, S. W.; Joyce, G. F., A general purpose RNA-cleaving DNA enzyme. *Proceedings of the National Academy of Sciences* **1997**, *94* (9), 4262-4266.
50. Schlosser, K.; Gu, J.; Sule, L.; Li, Y. F., Sequence-function relationships provide new insight into the cleavage site selectivity of the 8-17 RNA-cleaving deoxyribozyme. *Nucleic Acids Research* **2008**, *36* (5), 1472-1481.
51. Huanhuan, F.; Xiaobing, Z.; Yi, L., Recent advances in DNzyme-based gene silencing. *Science China Chemistry* **2017**, *60* (5), 591-601.
52. Zhou, W. H.; Ding, J. S.; Liu, J. W., Theranostic DNazymes. *Theranostics* **2017**, *7* (4), 1010-1025.
53. Young, D. D.; Lively, M. O.; Deiters, A., Activation and deactivation of DNzyme and antisense function with light for the photochemical regulation of gene expression in mammalian cells. *Journal of the American Chemical Society* **2010**, *132* (17), 6183-6193.
54. Wang, Y. J.; Liu, E. K.; Lam, C. H.; Perrin, D. M., A densely modified M^{2+} -independent DNzyme that cleaves RNA efficiently with multiple catalytic turnover. *Chemical Science* **2018**, *9* (7), 1813-1821.
55. Schubert, S.; GuÈl, D. C.; Grunert, H. P.; Zeichhardt, H.; Erdmann, V. A.; Kurreck, J., RNA cleaving '10-23' DNazymes with enhanced stability and activity. *Nucleic Acids Research* **2003**, *31* (20), 5982-5992.
56. Vester, B.; Lundberg, L. B.; Sørensen, M. D.; Babu, B. R.; Douthwaite, S.; Wengel, J., LNazymes: incorporation of LNA-type monomers into DNazymes markedly increases RNA cleavage. *Journal of the American Chemical Society* **2002**, *124* (46), 13682-13683.

57. Fokina, A. A.; Meschaninova, M. I.; Durfort, T.; Venyaminova, A. G.; François, J.-C., Targeting insulin-like growth factor I with 10–23 DNAzymes: 2'-O-methyl modifications in the catalytic core enhance mRNA cleavage. *Biochemistry* **2012**, *51* (11), 2181-2191.
58. Wang, Y.; Nguyen, K.; Spitale, R. C.; Chaput, J. C., A biologically stable DNAzyme that efficiently silences gene expression in cells. *Nature Chemistry* **2021**, *13* (4), 319-326.
59. Nguyen, K.; Wang, Y.; England, W. E.; Chaput, J. C.; Spitale, R. C., Allele-Specific RNA Knockdown with a Biologically Stable and Catalytically Efficient XNAzyme. *Journal of the American Chemical Society* **2021**, *143* (12), 4519-4523.
60. Li, J.; Zheng, W.; Kwon, A. H.; Lu, Y., In vitro selection and characterization of a highly efficient Zn(II)-dependent RNA-cleaving deoxyribozyme. *Nucleic Acids Research* **2000**, *28* (2), 481-488.
61. Brown, A. K.; Li, J.; Pavot, C. M. B.; Lu, Y., A Lead-Dependent DNAzyme with a Two-Step Mechanism. *Biochemistry* **2003**, *42* (23), 7152-7161.
62. Li, J.; Lu, Y., A highly sensitive and selective catalytic DNA biosensor for lead ions. *Journal of the American Chemical Society* **2000**, *122* (42), 10466-10467.
63. Liu, J.; Brown, A. K.; Meng, X.; Cropek, D. M.; Istok, J. D.; Watson, D. B.; Lu, Y., A catalytic beacon sensor for uranium with parts-per-trillion sensitivity and millionfold selectivity. *Proceedings of the National Academy of Sciences* **2007**, *104* (7), 2056-2061.
64. Cepeda-Plaza, M.; Null, E. L.; Lu, Y., Metal ion as both a cofactor and a probe of metal-binding sites in a uranyl-specific DNAzyme: a uranyl photocleavage study. *Nucleic Acids Research* **2013**, *41* (20), 9361-9370.
65. Zhou, W.; Saran, R.; Chen, Q.; Ding, J.; Liu, J., A new Na⁺-dependent RNA-cleaving DNAzyme with over 1000-fold rate acceleration by ethanol. *ChemBioChem* **2016**, *17* (2), 159-163.

66. Zhou, W.; Saran, R.; Huang, P.-J. J.; Ding, J.; Liu, J., An exceptionally selective DNA cooperatively binding two Ca^{2+} ions. *ChemBioChem* **2017**, *18* (6), 518–522.
67. Huang, P.-J. J.; Lin, J.; Cao, J.; Vazin, M.; Liu, J., Ultrasensitive DNzyme beacon for lanthanides and metal speciation. *Analytical Chemistry* **2014**, *86* (3), 1816-1821.
68. Huang, P.-J. J.; Vazin, M.; Matuszek, Z.; Liu, J., A new heavy lanthanide-dependent DNzyme displaying strong metal cooperativity and unrescuable phosphorothioate effect. *Nucleic Acids Research* **2015**, *43* (1), 461-469.
69. Huang, P.-J. J.; Vazin, M.; Liu, J., In vitro selection of a DNzyme cooperatively binding two lanthanide ions for RNA cleavage. *Biochemistry* **2016**, *55* (17), 2518–2525.
70. Huang, P.-J. J.; Liu, J., Rational evolution of Cd^{2+} -specific DNzymes with phosphorothioate modified cleavage junction and Cd^{2+} sensing. *Nucleic Acids Research* **2015**, *43* (12), 6125-6133.
71. Huang, P.-J. J.; Liu, J., An ultrasensitive light-up Cu^{2+} biosensor using a new DNzyme cleaving a phosphorothioate-modified substrate. *Analytical Chemistry* **2016**, *88* (6), 3341–3347.
72. Torabi, S.-F.; Wu, P.; McGhee, C. E.; Chen, L.; Hwang, K.; Zheng, N.; Cheng, J.; Lu, Y., In vitro selection of a sodium-specific DNzyme and its application in intracellular sensing. *Proceedings of the National Academy of Sciences* **2015**, *112* (19), 5903-5908.
73. Zhou, W.; Zhang, Y.; Huang, P.-J. J.; Ding, J.; Liu, J., A DNzyme requiring two different metal ions at two distinct sites. *Nucleic Acids Research* **2016**, *44* (1), 354-363.
74. Saran, R.; Liu, J., A silver DNzyme. *Analytical Chemistry* **2016**, *88* (7), 4014–4020.
75. Saran, R.; Kleinke, K.; Zhou, W.; Yu, T.; Liu, J., A silver-specific DNzyme with a new silver aptamer and salt-promoted activity. *Biochemistry* **2017**, *56* (14), 1955-1962.

76. Stoltenburg, R.; Reinemann, C.; Strehlitz, B., FluMag-SELEX as an advantageous method for DNA aptamer selection. *Analytical and Bioanalytical Chemistry* **2005**, *383* (1), 83-91.
77. Silverman, S. K., In vitro selection, characterization, and application of deoxyribozymes that cleave RNA. *Nucleic Acids Research* **2005**, *33* (19), 6151-6163.
78. Silverman, S. K., Catalytic DNA (deoxyribozymes) for synthetic applications-current abilities and future prospects. *Chemical Communications* **2008**, (30), 3467-3485.
79. Chiuman, W.; Li, Y., Efficient signaling platforms built from a small catalytic DNA and doubly labeled fluorogenic substrates. *Nucleic Acids Research* **2006**, *35* (2), 401-405.
80. Liu, J.; Lu, Y., Stimuli-responsive disassembly of nanoparticle aggregates for light-up colorimetric sensing. *Journal of the American Chemical Society* **2005**, *127* (36), 12677-12683.
81. Xiao, Y.; Rowe, A. A.; Plaxco, K. W., Electrochemical Detection of Parts-Per-Billion Lead via an Electrode-Bound DNAzyme Assembly. *Journal of the American Chemical Society* **2007**, *129* (2), 262-263.
82. Shamsi, M. H.; Kraatz, H.-B., Interactions of Metal Ions with DNA and Some Applications. *Journal of Inorganic and Organometallic Polymers and Materials* **2013**, *23* (1), 4-23.
83. Pechlaner, M.; Sigel, R. K. O., Characterization of Metal Ion-Nucleic Acid Interactions in Solution. In *Interplay between Metal Ions and Nucleic Acids*, Sigel, A.; Sigel, H.; Sigel, R. K. O., Eds. Springer Netherlands: Dordrecht, **2012**; pp 1-42.
84. Tan, Z.-J.; Chen, S.-J., Nucleic Acid Helix Stability: Effects of Salt Concentration, Cation Valence and Size, and Chain Length. *Biophysical Journal* **2006**, *90* (4), 1175-1190.
85. Cole, P. E.; Yang, S. K.; Crothers, D. M., Conformational changes of transfer ribonucleic acid. Equilibrium phase diagrams. *Biochemistry* **1972**, *11* (23), 4358-4368.
86. Draper, D. E., A guide to ions and RNA structure. *RNA* **2004**, *10* (3), 335-43.

87. Cate, J. H.; Gooding, A. R.; Podell, E.; Zhou, K.; Golden, B. L.; Kundrot, C. E.; Cech, T. R.; Doudna, J. A., Crystal Structure of a Group I Ribozyme Domain: Principles of RNA Packing. *Science* **1996**, *273* (5282), 1678-1685.
88. Tinoco, I.; Kieft, J. S., The ion core in RNA folding. *Nature Structural Biology* **1997**, *4* (7), 509-512.
89. Eichhorn, G. L.; Shin, Y. A., Interaction of metal ions with polynucleotides and related compounds. XII. The relative effect of various metal ions on DNA helicity. *Journal of the American Chemical Society* **1968**, *90* (26), 7323-8.
90. Sigel, R. K. O.; Sigel, H., A Stability Concept for Metal Ion Coordination to Single-Stranded Nucleic Acids and Affinities of Individual Sites. *Accounts of Chemical Research* **2010**, *43* (7), 974-984.
91. Nishiyabu, R.; Hashimoto, N.; Cho, T.; Watanabe, K.; Yasunaga, T.; Endo, A.; Kaneko, K.; Niidome, T.; Murata, M.; Adachi, C.; Katayama, Y.; Hashizume, M.; Kimizuka, N., Nanoparticles of Adaptive Supramolecular Networks Self-Assembled from Nucleotides and Lanthanide Ions. *Journal of the American Chemical Society* **2009**, *131* (6), 2151-2158.
92. Gross, D. S.; Simpkins, H., Evidence for two-site binding in the terbium(III)-nucleic acid interaction. *Journal of Biological Chemistry* **1981**, *256* (18), 9593-9598.
93. Kazakov, S. A.; Hecht, S. M., Nucleic Acid–Metal Ion Interactions. In *Encyclopedia of Inorganic and Bioinorganic Chemistry* **2006** (<https://doi.org/10.1002/0470862106.ia166>).
94. Miyake, Y.; Togashi, H.; Tashiro, M.; Yamaguchi, H.; Oda, S.; Kudo, M.; Tanaka, Y.; Kondo, Y.; Sawa, R.; Fujimoto, T.; Machinami, T.; Ono, A., Mercury(II)-Mediated Formation of Thymine–Hg(II)–Thymine Base Pairs in DNA Duplexes. *Journal of the American Chemical Society* **2006**, *128* (7), 2172-2173.

95. Lane, A. N.; Chaires, J. B.; Gray, R. D.; Trent, J. O., Stability and kinetics of G-quadruplex structures. *Nucleic Acids Research* **2008**, *36* (17), 5482-5515.
96. Hud, N. V.; Smith, F. W.; Anet, F. A. L.; Feigon, J., The Selectivity for K⁺ versus Na⁺ in DNA Quadruplexes Is Dominated by Relative Free Energies of Hydration: A Thermodynamic Analysis by ¹H NMR. *Biochemistry* **1996**, *35* (48), 15383-15390.
97. Li, Y.; Sen, D., A catalytic DNA for porphyrin metallation. *Nature Structural Biology* **1996**, *3* (9), 743-747.
98. Travascio, P.; Li, Y.; Sen, D., DNA-enhanced peroxidase activity of a DNA aptamer-hemin complex. *Chemistry & Biology* **1998**, *5* (9), 505-517.
99. Kim, H.-K.; Liu, J.; Li, J.; Nagraj, N.; Li, M.; Pavot, C. M. B.; Lu, Y., Metal-Dependent Global Folding and Activity of the 8-17 DNAzyme Studied by Fluorescence Resonance Energy Transfer. *Journal of the American Chemical Society* **2007**, *129* (21), 6896-6902.
100. Liu, Y.; Sen, D., A Contact Photo-Cross-linking Investigation of the Active Site of the 8-17 Deoxyribozyme. *Journal of Molecular Biology* **2008**, *381* (4), 845-859.
101. Liu, Y.; Sen, D., Local Rather than Global Folding Enables the Lead-dependent Activity of the 8-17 Deoxyribozyme: Evidence from Contact Photo-crosslinking. *Journal of Molecular Biology* **2010**, *395* (2), 234-241.
102. Kim, H.-K.; Rasnik, I.; Liu, J.; Ha, T.; Lu, Y., Dissecting metal ion-dependent folding and catalysis of a single DNAzyme. *Nature Chemical Biology* **2007**, *3* (12), 763-768.
103. Roychowdhury-Saha, M.; Burke, D. H., Distinct reaction pathway promoted by non-divalent-metal cations in a tertiary stabilized hammerhead ribozyme. *RNA* **2007**, *13* (6), 841-8.

104. He, Y.; Lu, Y., Metal-ion-dependent folding of a uranyl-specific DNAzyme: insight into function from fluorescence resonance energy transfer studies. *Chemistry* **2011**, *17* (49), 13732-13742.
105. Saran, R.; Yao, L.; Hoang, P.; Liu, J., Folding of the silver aptamer in a DNAzyme probed by 2-aminopurine fluorescence. *Biochimie* **2018**, *145*, 145-150.
106. Dallas, A.; Vlassov, A. V.; Kazakov, S. A., Principles of Nucleic Acid Cleavage by Metal Ions. In *Artificial Nucleases*, Zenkova, M. A., Ed. Springer Berlin Heidelberg: Berlin, Heidelberg, **2004**; pp 61-88.
107. Forconi, M.; Herschlag, D., Chapter 5 - Metal Ion-Based RNA Cleavage as a Structural Probe. In *Methods in Enzymology*, Academic Press: **2009**; Vol. 468, pp 91-106.
108. Zhou, W.; Liu, J., Multi-metal-dependent nucleic acid enzymes. *Metallomics* **2017**, *10* (1), 30-48.
109. Saran, R.; Huang, Z.; Liu, J., Phosphorothioate nucleic acids for probing metal binding, biosensing and nanotechnology. *Coordination Chemistry Reviews* **2021**, *428*, 213624.
110. Vazin, M.; Huang, P.-J. J.; Matuszek, Z. a.; Liu, J., Biochemical characterization of a lanthanide-dependent DNAzyme with normal and phosphorothioate-modified substrates. *Biochemistry* **2015**, *54* (39), 6132-6138.
111. Thaplyal, P.; Ganguly, A.; Golden, B. L.; Hammes-Schiffer, S.; Bevilacqua, P. C., Thio Effects and an Unconventional Metal Ion Rescue in the Genomic Hepatitis Delta Virus Ribozyme. *Biochemistry* **2013**, *52* (37), 6499-6514.
112. Thaplyal, P.; Ganguly, A.; Hammes-Schiffer, S.; Bevilacqua, P. C., Inverse Thio Effects in the Hepatitis Delta Virus Ribozyme Reveal that the Reaction Pathway Is Controlled by Metal Ion Charge Density. *Biochemistry* **2015**, *54* (12), 2160-2175.

113. He, Y.; Zhou, Y.; Chen, D.; Liu, J., Global Folding of a Na⁺-Specific DNAzyme Studied by FRET. *ChemBioChem* **2019**, *20* (3), 385-393.
114. Liu, H. H.; Yu, X.; Chen, Y. Q.; Zhang, J.; Wu, B. X.; Zheng, L. N.; Haruehanroengra, P.; Wang, R.; Li, S. H.; Lin, J. Z.; Li, J. X.; Sheng, J.; Huang, Z.; Ma, J. B.; Gan, J. H., Crystal structure of an RNA-cleaving DNAzyme. *Nature Communications* **2017**, *8* (1), 1-10.
115. Ponce-Salvatierra, A.; Wawrzyniak-Turek, K.; Steuerwald, U.; Höbartner, C.; Pena, V., Crystal structure of a DNA catalyst. *Nature* **2016**, *529* (7585), 231-234.
116. Cepeda-Plaza, M.; McGhee, C. E.; Lu, Y., Evidence of a General Acid–Base Catalysis Mechanism in the 8–17 DNAzyme. *Biochemistry* **2018**, *57* (9), 1517-1522.
117. Cortés-Guajardo, C.; Rojas-Hernández, F.; Paillao-Bustos, R.; Cepeda-Plaza, M., Hydrated metal ion as a general acid in the catalytic mechanism of the 8–17 DNAzyme. *Organic & Biomolecular Chemistry* **2021** (DOI: 10.1039/D1OB00366F).
118. Ekesan, Ş.; York, D. M., Dynamical ensemble of the active state and transition state mimic for the RNA-cleaving 8–17 DNAzyme in solution. *Nucleic Acids Research* **2019**, *47* (19), 10282-10295.
119. Schnabl, J.; Sigel, R. K. O., Controlling ribozyme activity by metal ions. *Current Opinion in Chemical Biology* **2010**, *14* (2), 269-275.
120. Young, K. J.; Gill, F.; Grasby, J. A., Metal Ions Play a Passive Role in the Hairpin Ribozyme Catalysed Reaction. *Nucleic Acids Research* **1997**, *25* (19), 3760-3760.
121. Hampel, A.; Cowan, J. A., A unique mechanism for RNA catalysis: the role of metal cofactors in hairpin ribozyme cleavage. *Chemistry & Biology* **1997**, *4* (7), 513-517.

122. Murray, J. B.; Seyhan, A. A.; Walter, N. G.; Burke, J. M.; Scott, W. G., The hammerhead, hairpin and VS ribozymes are catalytically proficient in monovalent cations alone. *Chemistry & Biology* **1998**, *5* (10), 587-595.
123. Perrotta, A. T.; Been, M. D., HDV Ribozyme Activity in Monovalent Cations. *Biochemistry* **2006**, *45* (38), 11357-11365.
124. Hanna, R.; Doudna, J. A., Metal ions in ribozyme folding and catalysis. *Current Opinion in Chemical Biology* **2000**, *4* (2), 166-170.
125. Geyer, C. R.; Sen, D., Evidence for the metal-cofactor independence of an RNA phosphodiester-cleaving DNA enzyme. *Chemistry & Biology* **1997**, *4* (8), 579-593.
126. Jaitovich, A.; Bertorello, A. M., Intracellular sodium sensing: SIK1 network, hormone action and high blood pressure. *Biochimica et Biophysica Acta (BBA) - Molecular Basis of Disease* **2010**, *1802* (12), 1140-1149.
127. Zhou, W.; Ding, J.; Liu, J., A highly specific sodium aptamer probed by 2-aminopurine for robust Na⁺ sensing. *Nucleic Acids Research* **2016**, *44* (21), 10377-10385.
128. He, Y.; Chen, D.; Huang, P.-J. J.; Zhou, Y.; Ma, L.; Xu, K.; Yang, R.; Liu, J., Misfolding of a DNAzyme for ultrahigh sodium selectivity over potassium. *Nucleic Acids Research* **2018**, *46* (19), 10262-10271.
129. Yu, T.; Zhou, W.; Liu, J., An RNA-Cleaving Catalytic DNA Accelerated by Freezing. *ChemBioChem* **2018**, *19* (10), 1012-1017.
130. Gao, G.; Cao, Y.; Liu, W.; Li, D.; Zhou, W.; Liu, J., Fluorescent sensors for sodium ions. *Analytical Methods* **2017**, *9* (38), 5570-5579.
131. Yin, J.; Hu, Y.; Yoon, J., Fluorescent probes and bioimaging: alkali metals, alkaline earth metals and pH. *Chemical Society Reviews* **2015**, *44* (14), 4619-4644.

132. Qu, H.; Csordas, A. T.; Wang, J.; Oh, S. S.; Eisenstein, M. S.; Soh, H. T., Rapid and Label-Free Strategy to Isolate Aptamers for Metal Ions. *ACS Nano* **2016**, *10* (8), 7558-7565.
133. Santoro, S. W.; Joyce, G. F.; Sakthivel, K.; Gramatikova, S.; Barbas, C. F., RNA cleavage by a DNA enzyme with extended chemical functionality. *Journal of the American Chemical Society* **2000**, *122* (11), 2433-2439.
134. Carmi, N.; Balkhi, S. R.; Breaker, R. R., Cleaving dna with dna. *Proceedings of the National Academy of Sciences* **1998**, *95* (5), 2233-2237.
135. Hollenstein, M.; Hipolito, C.; Lam, C.; Dietrich, D.; Perrin, D. M., A highly selective DNzyme sensor for mercuric ions. *Angewandte Chemie* **2008**, *120* (23), 4418-4422.
136. Ono, A.; Cao, S.; Togashi, H.; Tashiro, M.; Fujimoto, T.; Machinami, T.; Oda, S.; Miyake, Y.; Okamoto, I.; Tanaka, Y., Specific interactions between silver (I) ions and cytosine–cytosine pairs in DNA duplexes. *Chemical Communications* **2008**, (39), 4825-4827.
137. Ueyama, H.; Takagi, M.; Takenaka, S., A novel potassium sensing in aqueous media with a synthetic oligonucleotide derivative. Fluorescence resonance energy transfer associated with guanine quartet– potassium ion complex formation. *Journal of the American Chemical Society* **2002**, *124* (48), 14286-14287.
138. Hoang, M.; Huang, P.-J. J.; Liu, J., G-quadruplex DNA for fluorescent and colorimetric detection of thallium (I). *ACS Sensors* **2016**, *1* (2), 137-143.
139. Torabi, S.-F.; Lu, Y., Identification of the same Na⁺-specific DNzyme motif from two in vitro selections under different conditions. *Journal of Molecular Evolution* **2015**, *81* (5), 225-234.
140. Zhou, W.; Ding, J.; Liu, J., A Selective Na⁺ Aptamer Dissected by Sensitized Tb³⁺ Luminescence. *ChemBioChem* **2016**, *17* (16), 1563-1570.

141. Gong, B.; Chen, J.-H.; Bevilacqua, P. C.; Golden, B. L.; Carey, P. R., Competition between $\text{Co}(\text{NH}_3)_6^{3+}$ and Inner Sphere Mg^{2+} Ions in the HDV Ribozyme. *Biochemistry* **2009**, *48* (50), 11961-11970.
142. Zuker, M., Mfold web server for nucleic acid folding and hybridization prediction. *Nucleic Acids Research* **2003**, *31* (13), 3406-3415.
143. Cruz, R. P.; Withers, J. B.; Li, Y., Dinucleotide junction cleavage versatility of 8-17 deoxyribozyme. *Chemistry & Biology* **2004**, *11* (1), 57-67.
144. Schlosser, K.; Li, Y., A Versatile Endoribonuclease Mimic Made of DNA: Characteristics and Applications of the 8–17 RNA-Cleaving DNAzyme. *ChemBioChem* **2010**, *11* (7), 866-879.
145. Zhou, W.; Vazin, M.; Yu, T.; Ding, J.; Liu, J., In vitro selection of chromium-dependent DNAzymes for sensing chromium (III) and chromium (VI). *Chemistry-A European Journal* **2016**, *22* (28), 9835-9840.
146. Branzoi, I.; Iordoc, M.; Branzoi, F.; Vasilescu-Mirea, R.; Sbarcea, G., Influence of diamond-like carbon coating on the corrosion resistance of the NITINOL shape memory alloy. *Surface and Interface Analysis* **2010**, *42* (6-7), 502-509.
147. Mir, A.; Chen, J.; Robinson, K.; Lendy, E.; Goodman, J.; Neau, D.; Golden, B. L., Two divalent metal ions and conformational changes play roles in the hammerhead ribozyme cleavage reaction. *Biochemistry* **2015**, *54* (41), 6369-6381.
148. Mir, A.; Golden, B. L., Two active site divalent ions in the crystal structure of the hammerhead ribozyme bound to a transition state analogue. *Biochemistry* **2016**, *55* (4), 633-636.

149. Ren, A.; Vušurović, N.; Gebetsberger, J.; Gao, P.; Juen, M.; Kreutz, C.; Micura, R.; Patel, D. J., Pistol ribozyme adopts a pseudoknot fold facilitating site-specific in-line cleavage. *Nature Chemical Biology* **2016**, *12* (9), 702-708.
150. Nguyen, L. A.; Wang, J.; Steitz, T. A., Crystal structure of Pistol, a class of self-cleaving ribozyme. *Proceedings of the National Academy of Sciences* **2017**, *114* (5), 1021-1026.
151. Gaines, C. S.; York, D. M., Ribozyme catalysis with a twist: active state of the twister ribozyme in solution predicted from molecular simulation. *Journal of the American Chemical Society* **2016**, *138* (9), 3058-3065.
152. Golden, B. L., Two distinct catalytic strategies in the hepatitis delta virus ribozyme cleavage reaction. *Biochemistry* **2011**, *50* (44), 9424-9433.
153. Zhou, W.; Saran, R.; Ding, J.; Liu, J., Two completely different mechanisms for highly specific Na⁺ recognition by DNAzymes. *ChemBioChem* **2017**, *18* (18), 1828-1835.
154. Ma, L.; Liu, J., An in vitro-selected DNAzyme mutant highly specific for Na⁺ under slightly acidic conditions. *ChemBioChem* **2019**, *20* (4), 537-542.
155. Chen, J.; Ganguly, A.; Miswan, Z.; Hammes-Schiffer, S.; Bevilacqua, P. C.; Golden, B. L., Identification of the catalytic Mg²⁺ ion in the hepatitis delta virus ribozyme. *Biochemistry* **2013**, *52* (3), 557-567.
156. Košutić, M.; Neuner, S.; Ren, A.; Flür, S.; Wunderlich, C.; Mairhofer, E.; Vušurović, N.; Seikowski, J.; Breuker, K.; Höbartner, C.; Patel, D. J.; Kreutz, C.; Micura, R., A Mini-Twister Variant and Impact of Residues/Cations on the Phosphodiester Cleavage of this Ribozyme Class. *Angewandte Chemie International Edition* **2015**, *54* (50), 15128-15133.
157. Bevilacqua, P. C., Mechanistic considerations for general acid–base catalysis by RNA: Revisiting the mechanism of the hairpin ribozyme. *Biochemistry* **2003**, *42* (8), 2259-2265.

158. Frankel, E. A.; Bevilacqua, P. C., Complexity in pH-Dependent Ribozyme Kinetics: Dark p K a Shifts and Wavy Rate–pH Profiles. *Biochemistry* **2018**, *57* (5), 483-488.
159. Huang, P.-J. J.; Liu, J., Sensing parts-per-trillion Cd²⁺, Hg²⁺, and Pb²⁺ collectively and individually using phosphorothioate DNAzymes. *Analytical Chemistry* **2014**, *86* (12), 5999-6005.
160. Huang, P.-J. J.; Moon, W. J.; Liu, J., Instantaneous iodine-assisted DNAzyme cleavage of phosphorothioate RNA. *Biochemistry* **2018**, *58* (5), 422-429.
161. Kapinos, L. E.; Operschall, B. P.; Larsen, E.; Sigel, H., Understanding the acid–base properties of adenosine: the intrinsic basicities of N1, N3 and N7. *Chemistry-A European Journal* **2011**, *17* (29), 8156.
162. Jones, A. C.; Neely, R. K., 2-aminopurine as a fluorescent probe of DNA conformation and the DNA–enzyme interface. *Quarterly Reviews of Biophysics* **2015**, *48* (2), 244-279.
163. Ballin, J. D.; Bharill, S.; Fialcowitz-White, E. J.; Gryczynski, I.; Gryczynski, Z.; Wilson, G. M., Site-specific variations in RNA folding thermodynamics visualized by 2-aminopurine fluorescence. *Biochemistry* **2007**, *46* (49), 13948-13960.
164. Wang, S.; Karbstein, K.; Peracchi, A.; Beigelman, L.; Herschlag, D., Identification of the hammerhead ribozyme metal ion binding site responsible for rescue of the deleterious effect of a cleavage site phosphorothioate. *Biochemistry* **1999**, *38* (43), 14363-14378.
165. Koizumi, M.; Ohtsuka, E., Effects of phosphorothioate and 2-amino groups in hammerhead ribozymes on cleavage rates and magnesium binding. *Biochemistry* **1991**, *30* (21), 5145-5150.
166. Lindell, M.; Romby, P.; Wagner, E. G. H., Lead (II) as a probe for investigating RNA structure in vivo. *RNA* **2002**, *8* (4), 534-541.

167. Werner, C.; Krebs, B.; Keith, G.; Dirheimer, G., Specific cleavages of pure tRNAs by plumbous ions. *Biochimica et Biophysica Acta (BBA)-Nucleic Acids and Protein Synthesis* **1976**, *432* (2), 161-175.
168. Brown, R.; Dewan, J.; Klug, A., Crystallographic and biochemical investigation of the lead (II)-catalyzed hydrolysis of yeast phenylalanine tRNA. *Biochemistry* **1985**, *24* (18), 4785-4801.
169. Pan, T.; Uhlenbeck, O. C., A small metalloribozyme with a two-step mechanism. *Nature* **1992**, *358* (6387), 560-563.
170. Pan, T.; Dichtl, B.; Uhlenbeck, O. C., Properties of an in vitro selected Pb^{2+} cleavage motif. *Biochemistry* **1994**, *33* (32), 9561-9565.
171. Wedekind, J. E.; McKay, D. B., Crystal structure of a lead-dependent ribozyme revealing metal binding sites relevant to catalysis. *Nature Structural Biology* **1999**, *6* (3), 261-268.
172. Wedekind, J. E.; McKay, D. B., Crystal structure of the leadzyme at 1.8 Å resolution: Metal ion binding and the implications for catalytic mechanism and allo site ion regulation. *Biochemistry* **2003**, *42* (32), 9554-9563.
173. Ohmichi, T.; Sugimoto, N., Role of Nd^{3+} and Pb^{2+} on the RNA cleavage reaction by a small ribozyme. *Biochemistry* **1997**, *36* (12), 3514-3521.
174. Sugimoto, N.; Ohmichi, T., Site-specific cleavage reaction catalyzed by leadzyme is enhanced by combined effect of lead and rare earth ions. *FEBS Letters* **1996**, *393* (1), 97-100.
175. Saran, R.; Chen, Q.; Liu, J., Searching for a DNAzyme version of the leadzyme. *Journal of Molecular Evolution* **2015**, *81* (5), 235-244.
176. Moon, W. J.; Huang, P.-J. J.; Liu, J., Probing Metal-Dependent Phosphate Binding for the Catalysis of the 17E DNAzyme. *Biochemistry* **2021**, *60* (24), 1909–1918.

177. Huang, P.-J. J.; Vazin, M.; Liu, J., In Vitro Selection of a New Lanthanide-Dependent DNAzyme for Ratiometric Sensing Lanthanides. *Analytical Chemistry* **2014**, *86* (19), 9993-9999.
178. Brown, A. K.; Liu, J.; He, Y.; Lu, Y., Biochemical Characterization of a Uranyl Ion-Specific DNAzyme. *ChemBioChem* **2009**, *10* (3), 486-492.
179. Ma, L.; Kartik, S.; Liu, B.; Liu, J., From general base to general acid catalysis in a sodium-specific DNAzyme by a guanine-to-adenine mutation. *Nucleic Acids Research* **2019**, *47* (15), 8154-8162.
180. Ma, L.; Liu, J., Catalytic Nucleic Acids: Biochemistry, Chemical Biology, Biosensors, and Nanotechnology. *iScience* **2020**, *23* (1), 100815.
181. Lake, R. J.; Yang, Z.; Zhang, J.; Lu, Y., DNAzymes as Activity-Based Sensors for Metal Ions: Recent Applications, Demonstrated Advantages, Current Challenges, and Future Directions. *Accounts of Chemical Research* **2019**, *52* (12), 3275-3286.
182. Ma, L.; Liu, J., An In Vitro Selected DNAzyme Mutant Highly Specific for Na⁺ in Slightly Acidic Conditions. *ChemBioChem* **2019**, *20* (4), 537-542.
183. Micura, R.; Höbartner, C., Fundamental studies of functional nucleic acids: aptamers, riboswitches, ribozymes and DNAzymes. *Chemical Society Reviews* **2020**, *49* (20), 7331-7353.
184. Furukawa, K.; Ramesh, A.; Zhou, Z.; Weinberg, Z.; Vallery, T.; Winkler, W. C.; Breaker, R. R., Bacterial riboswitches cooperatively bind Ni (II) or Co (II) ions and control expression of heavy metal transporters. *Molecular Cell* **2015**, *57* (6), 1088-1098.
185. Regulski, E. E.; Moy, R. H.; Weinberg, Z.; Barrick, J. E.; Yao, Z.; Ruzzo, W. L.; Breaker, R. R., A widespread riboswitch candidate that controls bacterial genes involved in molybdenum cofactor and tungsten cofactor metabolism. *Molecular Microbiology* **2008**, *68* (4), 918-932.

186. Baker, J. L.; Sudarsan, N.; Weinberg, Z.; Roth, A.; Stockbridge, R. B.; Breaker, R. R., Widespread Genetic Switches and Toxicity Resistance Proteins for Fluoride. *Science* **2012**, *335* (6065), 233-235.
187. Sarkar, G.; Kapelner, S.; Sommer, S. S., Formamide can dramatically improve the specificity of PCR. *Nucleic Acids Research* **1990**, *18* (24), 7465.
188. Smith, J. B.; Dinter-Gottlieb, G., Antigenomic Hepatitis delta virus ribozymes self-cleave in 18 M formamide. *Nucleic Acids Research* **1991**, *19* (6), 1285-1289.
189. Rosenstein, S. P.; Been, M. D., Self-cleavage of hepatitis delta virus genomic strand RNA is enhanced under partially denaturing conditions. *Biochemistry* **1990**, *29* (35), 8011-6.
190. Belinsky, M. G.; Dinter-Gottlieb, G., Non-ribozyme sequences enhance self-cleavage of ribozymes derived from Hepatitis delta virus. *Nucleic Acids Research* **1991**, *19* (3), 559-564.
191. Misra, V. K.; Draper, D. E., On the role of magnesium ions in RNA stability. *Biopolymers: Original Research on Biomolecules* **1998**, *48* (2-3), 113-135.
192. Nakano, S.-i.; Chadalavada, D. M.; Bevilacqua, P. C., General Acid-Base Catalysis in the Mechanism of a Hepatitis Delta Virus Ribozyme. *Science* **2000**, *287* (5457), 1493-1497.
193. O'Rear, J. L.; Wang, S.; Feig, A. L.; Beigelman, L.; Uhlenbeck, O. C.; Herschlag, D., Comparison of the hammerhead cleavage reactions stimulated by monovalent and divalent cations. *RNA* **2001**, *7* (4), 537-545.
194. Duhamel, J.; Liu, D. M.; Evilia, C.; Fleysh, N.; Dinter-Gottlieb, G.; Lu, P., Secondary structure content of the HDV ribozyme in 95% formamide. *Nucleic Acids Research* **1996**, *24* (20), 3911-3917.

195. Nakano, S.-i.; Kitagawa, Y.; Miyoshi, D.; Sugimoto, N., Hammerhead ribozyme activity and oligonucleotide duplex stability in mixed solutions of water and organic compounds. *FEBS Open Bio* **2014**, *4*, 643-650.
196. Nakano, S. i.; Kitagawa, Y.; Yamashita, H.; Miyoshi, D.; Sugimoto, N., Effects of cosolvents on the folding and catalytic activities of the hammerhead ribozyme. *ChemBioChem* **2015**, *16* (12), 1803-1810.
197. Nakano, S.-i.; Karimata, H.; Ohmichi, T.; Kawakami, J.; Sugimoto, N., The effect of molecular crowding with nucleotide length and cosolute structure on DNA duplex stability. *Journal of the American Chemical Society* **2004**, *126* (44), 14330-14331.
198. Nakano, S.-i.; Yamaguchi, D.; Tateishi-Karimata, H.; Miyoshi, D.; Sugimoto, N., Hydration changes upon DNA folding studied by osmotic stress experiments. *Biophysical Journal* **2012**, *102* (12), 2808-2817.
199. Hammann, C.; Westhof, E., Searching genomes for ribozymes and riboswitches. *Genome Biology* **2007**, *8* (4), 1-11.
200. Hutchins, C. J.; Rathjen, P. D.; Forster, A. C.; Symons, R. H., Self-cleavage of plus and minus RNA transcripts of avocado sunblotch viroid. *Nucleic Acids Research* **1986**, *14* (9), 3627-3640.
201. Hammann, C.; Luptak, A.; Perreault, J.; De La Peña, M., The ubiquitous hammerhead ribozyme. *RNA* **2012**, *18* (5), 871-885.
202. de la Peña, M.; García-Robles, I., Ubiquitous presence of the hammerhead ribozyme motif along the tree of life. *RNA* **2010**, *16* (10), 1943-1950.
203. De La Peña, M.; García-Robles, I., Intronic hammerhead ribozymes are ultraconserved in the human genome. *EMBO Reports* **2010**, *11* (9), 711-716.

204. Altschul, S. F.; Madden, T. L.; Schäffer, A. A.; Zhang, J.; Zhang, Z.; Miller, W.; Lipman, D. J., Gapped BLAST and PSI-BLAST: a new generation of protein database search programs. *Nucleic Acids Research* **1997**, *25* (17), 3389-3402.